Synaptotagmins ensure speed and efficiency of inhibitory neurotransmitter release

by

Chong Chen

March, 2018

A thesis presented to the
Graduate School
of the
Institute of Science and Technology Austria, Klosterneuburg, Austria
in partial fulfilment of the requirements
for the degree of
Doctor of Philosophy

The dissertation of Chong Chen, titled “Synaptotagmins ensure speed and efficiency of inhibitory neurotransmitter release”, is approved by:

Supervisor: Peter Jonas, IST Austria, Klosterneuburg, Austria

Signature: _____

Committee Member: Ryuichi Shigemoto, IST Austria, Klosterneuburg, Austria

Signature: _____

Committee Member: Samuel M. Young Jr., University of Iowa, Iowa City, USA

Signature: _____

Exam Chair: Johann Danzl, IST Austria, Klosterneuburg, Austria

Signature: _____

I hereby declare that this dissertation is my own work and that it does not contain other people's work without this being so stated; this thesis does not contain my previous work without this being stated, and the bibliography contains all the literature that I used in writing the dissertation.

I declare that this is a true copy of my thesis, including any final revisions, as approved by my thesis committee, and that this thesis has not been submitted for a higher degree to any other university or institution.

I certify that any republication of materials presented in this thesis has been approved by the relevant publishers and co-authors.

Signature: _____

March 28, 2017

Abstract

Neuronal networks in the brain consist of two main types of neuron, glutamatergic principal neurons and GABAergic interneurons. Although these interneurons only represent 10–20% of the whole population, they mediate feedback and feedforward inhibition and are involved in the generation of high-frequency network oscillations. A hallmark functional property of GABAergic interneurons, especially of the parvalbumin−expressing (PV^+) subtypes, is the speed of signaling at their output synapse across species and brain regions. Several molecular and subcellular factors may underlie the submillisecond signaling at GABAergic synapses. Such as the selective use of P/Q type Ca^{2+} channels and the tight coupling between Ca^{2+} channels and Ca^{2+} sensors of exocytosis. However, whether the molecular identity of the release sensor contributes to these signaling properties remains unclear. Besides, these interneurons are mainly show depression in response to train of stimuli. How could they keep sufficient release to control the activity of postsynaptic principal neurons during high network activity, is largely elusive.

For my Ph.D. work, we firstly examined the Ca^{2+} sensor of exocytosis at the GABAergic basket cell (BC) to Purkinje cell (PC) synapse in the cerebellum. Immunolabeling suggested that BC terminals selectively expressed synaptotagmin 2 (Syt2), whereas synaptotagmin 1 (Syt1) was enriched in excitatory terminals. Genetic elimination of Syt2 reduced action potential-evoked release to ~10% compared to the wild-type control, identifying Syt2 as the major Ca^{2+} sensor at BC−PC synapses. Differential adenovirus-mediated rescue revealed Syt2 triggered release with shorter latency and higher temporal precision, and mediated faster vesicle pool replenishment than Syt1. Furthermore, deletion of Syt2 severely reduced and delayed disynaptic inhibition following parallel fiber stimulation. Thus, the selective use of Syt2 as the release sensor at BC–PC synapse ensures fast feedforward inhibition in cerebellar microcircuits.

Additionally, we tested the function of another synaptotagmin member, Syt7, for inhibitory synaptic transmission at the BC–PC synapse. Syt7 is thought to be a Ca^{2+} sensor that mediates asynchronous transmitter release and facilitation at synapses. However, it is strongly expressed in fast-spiking, PV^+ GABAergic interneurons and the output synapses of these neurons produce only minimal asynchronous release

and show depression rather than facilitation. How could Syt7, a facilitation sensor, contribute to the depressed inhibitory synaptic transmission needs to be further investigated and understood. Our results indicated that at the BC–PC synapse, Syt7 contributes to asynchronous release, pool replenishment and facilitation. In combination, these three effects ensure efficient transmitter release during high-frequency activity and guarantee frequency independence of inhibition.

Taken together, our results confirmed that Syt2, which has the fastest kinetic properties among all synaptotagmin members, is mainly used by the inhibitory BC-PC synapse for synaptic transmission, contributing to the speed and temporal precision of transmitter release. Furthermore, we showed that Syt7, another highly expressed synaptotagmin member in the output synapses of cerebellar BCs, is used for ensuring efficient inhibitor synaptic transmission during high activity.

Acknowledgments

Time flies, especially when you're happy! I still clearly remember the first time when I was visiting Jonas lab four years ago: I was so excited and nervous. After that visit, I told myself that I really want to join this group, a group led by a predominant scientist, who is rigorous and strict to science. I also clearly remember how happy I was when I got the offer from IST Austria. Suddenly, I realize that four years have passed peacefully and the time has came to leave Jonas lab, from where I have not only learned how to conduct research but also earned a full memory of an enjoyable life. In the past four years, tremendous invaluable supports have been given to me from family members, the supervisor and other colleagues.

First of all, I want to show my appreciation to my family members, especially my wife Yanbo Song, and my daughter Anlan Chen. In order to support my career, Yanbo gave up her job. I know how difficult it was for her to make this decision, considering she was so dedicated to her job. I thank her for staying in Austria with me the last four years. Without her, I would not have so much enjoyable time here. And thanks for Anlan, my lovely daughter. Thanks for choosing us. She is so cute, bringing us much fun and motivating me to move further. Thanks to my mother and Yanbo's mother, for helping us to look after the baby.

Then, I would like to express my sincere gratitude to my supervisor Prof. Peter Jonas. He is a great scientist and a wonderful leader. He is knowledgeable and always gives useful suggestions for the projects, and finds ways to encourages us when we are frustrated by the experiments. It has actually been a great honor to work with him and I feel happy of having the chance to join in his lab. We finished two quite competitive projects together and still have one ongoing project. From Prof. Jonas one can find all the characteristics that a successful scientist must have for doing science, which is critical for us, the young generation.

Finally, I want to show my appreciation to all members in Jonas lab. In chronological order: Itaru Arai, who taught me the virus injection and showed me how to do the paired recording. Hua Hu, a great colleague, gave me quite useful suggestions for patching and encouraged me when I was frustrated about patching at the beginning. Caro, a nice labmate, who always discusses literature with me and organizes events for the lab members. Rajiv, a nice and warm-hearted guy. Xiaomin

Zhang, with whom I always talk about career. She also shared a lot of food with me. Ben Suter, a quite clever and nice office mate, who is trying to provide help all the time. Magdalena, another office mate, who brings so much fun to us. And also, Florian, Eva, Alois, David, Claudia, Olena… Besides the lab members, some people at IST Austria also helped me a lot. Ruslan, Stephan, Shamsi, Zuzka, Pepa. Thanks to all of you and it has been a great pleasure to meet all of you here at IST Austria.

About the Author

Chong Chen completed his bachelor degree of Medicine at Wenzhou Medical University in China. He then joined the Second Affiliated Hospital of Wenzhou Medical University as an anaesthesiologist for three years. During those three years, he treated more than 1000 patients in the operation room.

Before joining IST Austria in September 2014, he earned his Master degree of Medicine from Shanghai Jiaotong University in China. His main research interests included the role of inhibitory interneuron in anaesthesia and the effect of general anaesthetics on intelligence development of neonatal patients. He worked on the project “The effect of sevoflurane on adult neurogenesis in hippocampus of neonatal mice” and published the results on the journal *ASN Neuro.*

During his Ph.D. studies, Chong worked on the research project “Ca^{2+} channel–release sensor coupling at a central GABAergic synapse” in Jonas group. He got two papers published on the journal Cell Reports. He presented his research in Gordon Research Conference (Inhibition in the CNS), Austrian Neuroscience Meeting (ANA) in 2017, and Society of Neuroscience (SfN) in 2017. Besides, he also worked as a teaching assistant in 2017 for Prof. Peter Jonas.

With all the excellent work during his Ph.D., Chong was awarded the Outstanding Self–financed Chinese Students Abroad from China scholarship Council in 2018.

List of Publications Appearing in Thesis

Chen, C., Arai, I., Satterfield, R., Young, S.M. Jr., and Jonas, P. (2017a). Synaptotagmin 2 is the fast Ca^{2+} sensor at a central inhibitory synapse. Cell Rep. *18*, 723–736.

Chen C, Satterfield R, Young SM, and Jonas P. (2017b). Triple function of synaptotagmin 7 ensures efficiency of high-frequency transmission at central GABAergic synapses. Cell Rep. *21,* 2082–2089.

Contents

List of Figures

List of Tables

List of Symbols/Abbreviations

AP	Action potential
ATP	Adenosine triphosphate
BC	Basket cell
BGH	Bovine growth hormone
CA1	Cornu ammonis region 1
CNQX	6-cyano-7-nitroquinoxaline-2,3-dione
CV	Coefficient of variation
D-AP5	D-2-amino-5-phosphonopentanoic
EGFP	Enhanced Green Fluorescent Protein
EGTA	Ethylene glycol-bis(β-aminoethyl ether)-N,N,N',N'-tetraacetic acid
GABA	γ–aminobutyric acid
GCL	Granule cell layer
HdAd	Helper-dependent adenovirus
HEPES	4-(2-hydroxyethyl)-1-piperazineethanesulfonic acid
IPSC	Inhibitory postsynaptic current
ML	Molecular layer
mIPSC	Miniature inhibitory postsynaptic current
NGS	Normal goat serum
NRP	Non-recycling pool
PBS	Phosphate-buffered solution
PC	Purkinje cell
PCL	Purkinje cell layer
PV^+	Parvalbumin-positive
RIM	Rab3-interacting molecule
RIM-BP	Rab3-interacting molecule binding protein
RP	Recycling pool
RRP	Readily releasable pool
SEM	Standard Error of the Mean
SM	Sec1/Munc 18-like
SNARE	Soluble NSF attachment receptor
SV	Synaptic vesicles

Syt	Synaptotagmin
TCR	Time course of release
TTX	Tetrodotoxin
TPMPA	(1,2,5,6-Tetrahydropyridin-4-yl)-methylphosphinic acid
VGAT	Vesicular GABA Transporter
VGLUT1	Vesicular glutamate transporter 1
Ω	Ohm
τ	Time constant
	Spearman’s rank correlation coefficient

Chapter 1. General introduction

1.1 Synaptic transmission

About 100 years ago, Otto Loewi (1873–1961), a professor of pharmacology in Vienna, devised a crucial experiment which provides the first reliable evidence for the existence of chemical transmission in a synapse, opening the era for synaptic transmission investigation. After that, Bernard Katz (1911–2003), working on the neuromuscular junction, established the fundamental pathway of synaptic transmission: an action potential arrives at a presynaptic nerve terminal and gates Ca^{2+} channels; inflowing Ca^{2+} then triggers the fusion of synaptic vesicles with the plasma membrane, releasing neurotransmitter; the released neurotransmitter subsequently produces a postsynaptic signal by binding the postsynaptic receptor (Katz, 1969). Katz initiated a series of elegant electrophysiological experiments that characterized the process of synaptic transmission in exquisite detail. These studies revealed that Ca^{2+} triggers release in a highly cooperative manner (Dodge and Rahamimoff, 1967) within a few hundred milliseconds, which is not much slower than the opening of a voltage-gated ion channel (Sabatini and Regehr, 1966). What underlying molecular mechanism ensures the fast neurotransmitter release at a synapse, however, remained a mystery until molecular biology allowed mechanistic dissection of vesicle fusion and its control by Ca^{2+} (Südhof and Rothman, 2009).

After several decades work on molecular identities mediating transmitter release, dozens of proteins have been revealed, and a molecular framework for neurotransmitter release has been built by neuroscientists (Südhof, 2013). RIM (Rab3-interacting molecule), RIM-BP (Rab3-interacting molecule binding protein) and Munc 13 mediates the docking and priming of synaptic vesicles at the active zone and recruits Ca^{2+} channels to docked and primed vesicles (Kaeser et al., 2011). Synaptotagmin (Syt), known as the Ca^{2+} sensor, is an evolutionarily conserved transmembrane protein with two cytoplasmic C2 domains (Perin et al., 1990, 1991) that binds Ca^{2+}, triggers the synaptic vesicle fusion with the plasma membrane, releasing neurotransmitter (Gepper et al., 1994). Complexin is a universal cofactor for synaptotagmin in Ca^{2+}-triggered vesicles fusion. The loss of function of complexin induces a decrease in Ca^{2+} triggering of release, an increase in the spontaneous miniature release, and a decrease in the size of the RRP (readily releasable pool) (Reim et al., 2001; Cao et al., 2013). Membrane fusion is mediated by SNARE

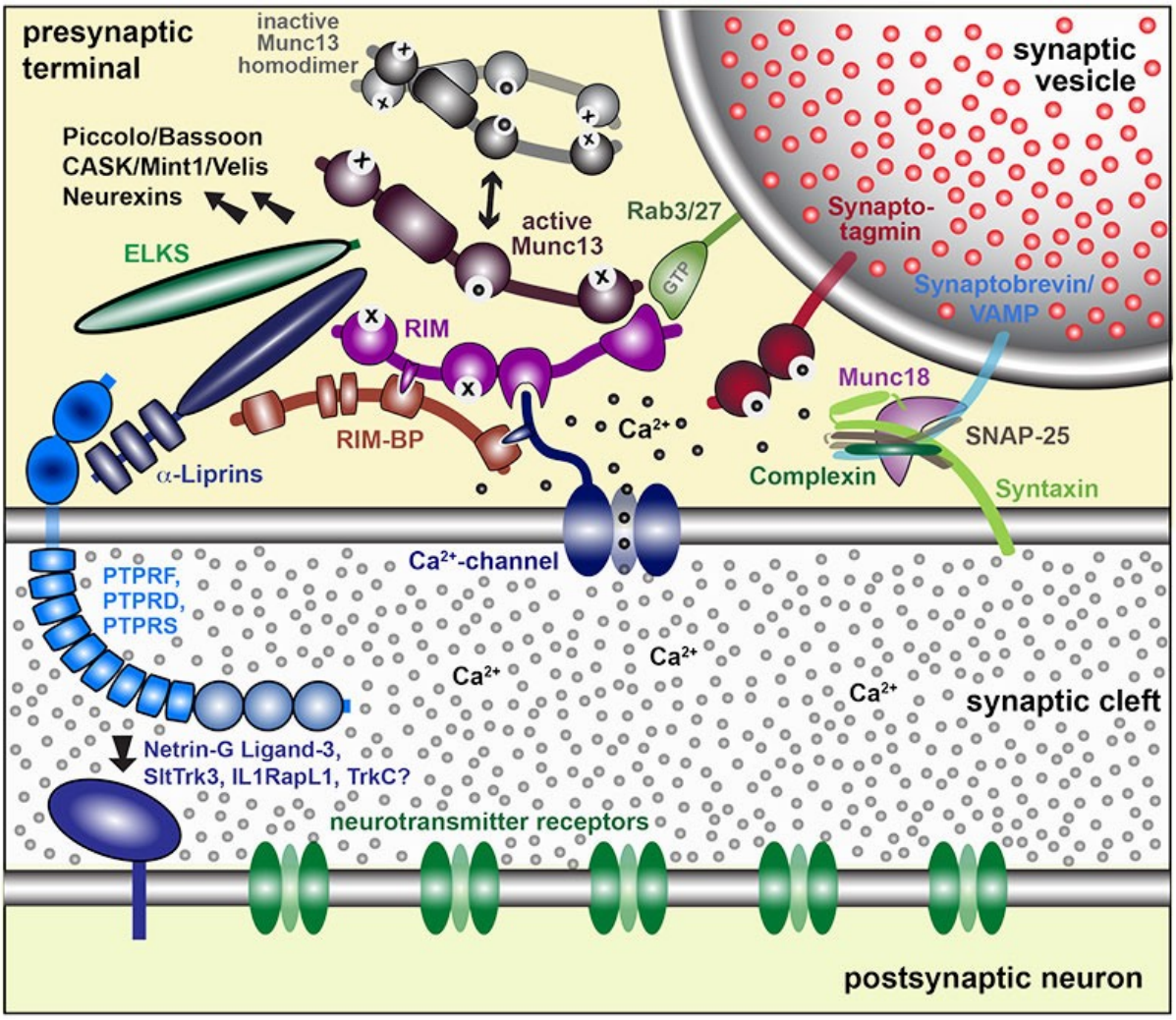

Figure 1-1. Organization of the presynaptic release machinery

Schematic of the molecular machinery mediating Ca^{2+}-triggered vesicle fusion. The drawing depicts a segment of a docked synaptic vesicle on the top right and the presynaptic active zone in the middle. On the right, the core fusion machine composed of the SNARE/SM protein complex is shown; this machine comprises the SNARE proteins synaptobrevin/ VAMP, syntaxin-1, and SNAP-25 and the SM protein Munc18-1. The Ca^{2+} sensor synaptotagmin is depicted in the middle; and it functions using complexin (bound to the SNARE complex) as an assistant. The active zone protein complex containing RIM, Munc13, and RIM-BP and a Ca^{2+} channel in the presynaptic plasma membrane is shown on the left. Some regulator proteins, like bassoon and piccolo are also shown. (Adapted from Südhof, 2012)

proteins (soluble NSF attachment receptor proteins) and SM proteins (Sec1/

Munc18−like proteins) that undergo a cycle of association and dissociation during fusion reaction (Südhof and Rothman, 2009). SNARE proteins embedded in the two fusing membranes form a trans-complex in an N- to C-terminal direction (Hanson et al., 1997). Zippering of trans-SNARE complex forces the fusing membranes into close proximity, destabilizing their hydrophilic surfaces. Together with the action of SM protein, assembly of the full trans-SNARE complex opens the fusion pore (Südhof, 2013). These proteins constitute the general release machinery (Südhof, 2013). Additionally, bassoon (Mukherjee et al., 2010; Davydova et al., 2014), piccolo (Mukherjee et al., 2010), and mover (Korber et al., 2015) have been shown as regulators for neurotransmitter release (**Figure1-1**).

After neurotransmitter release from SV (synaptic vesicles) by fusion with the plasma membrane (exocytosis), the signaling molecules diffuse across the gap between the pre- and postsynaptic neuronal membranes leading to the activation or inhibition of the postsynaptic compartment. The SV components are subsequently retrieved from the plasma membrane of the presynaptic neuron (endocytosis) and are then turned into a new fusion-competent SV (Südhof, 2004). The classical model for vesicle retrieval involves invagination of vesicles from clathrin-coated membrane pits (clathrin-mediated endocytosis) or budding from an endosomal structure formed after bulk endocytosis (**Figure 1-2**; Heuser and Reese, 1973). But this process is thought to occur slowly with a time constant of tens of seconds to minutes (Mueller et al., 2004; Wu et al., 2007). The balance between exocytosis and endocytosis is vital to sustain synaptic transmission and maintain nerve terminal size. However, this classical endocytosis is unlikely fast enough to account for the rapid and continuous rate of transmitter release observed at many synapses in the nervous system (Smith et al., 2008). Crucially, two more types of rapid endocytosis have been identified in nerve terminals: one with a time constant of about 1-2 s (von Gersdorff and Matthews, 1994), and the other is even faster, termed “kiss and run” (Ceccarelli et al., 1973) in which a single vesicle is endocytosed rapidly before full collapse has occurred, preventing loss of vesicle identity. However, the endocytotic pathways that retrieve synaptic vesicles after fusion are still poorly understood (Kononenko and Haucke, 2015). In addition, research suggested that the exocytosis and endocytosis are not totally separated processes, they couple with each other in a Ca^{2+}-dependent way (Wu et al., 2014). Several proteins mediating exocytosis, such as the Ca^{2+}

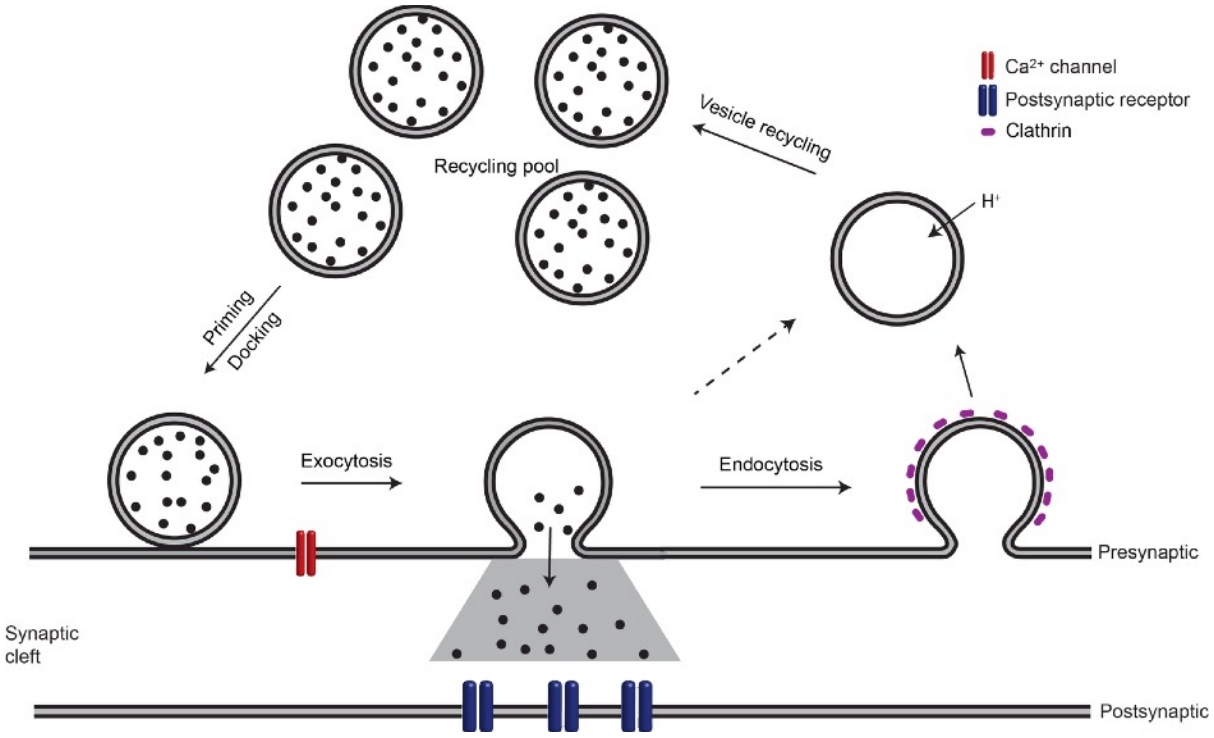

Figure 1-2. Synaptic vesicles recycling pathway

Docked and primed synaptic vesicles constitute the readily releasable pool. Following the Ca^{2+} influx they undergo exocytosis and release neurotransmitter into the synaptic cleft, where these molecules diffuse and bind to postsynaptic receptors, inducing voltage change of a postsynaptic cell. To maintain the availability of release sites for subsequent fusion reactions, release sites have to undergo clearance. Endocytosis of synaptic vesicle membranes, including transmembrane synaptic vesicle cargo proteins, preferentially occurs within the periactive zone surrounding the active zone area. Synaptic vesicle endocytosis is predominantly mediated by the classical clathrin- and dynamin-dependent pathway. Following cathrin uncoating and concomitant neurotransmitter uptake, synaptic vesicles return to the recycling pool.

sensor Syt1, Syt7 and complexin, have also been shown to affect synaptic vesicles retrieval in an activity-dependent way (Zhang et al., 1994; Haucke and De Camilli, 1999; Li et al., 2017).

1.2 Short-term plasticity

Synaptic transmission is a dynamic process. It is well established that synapses are

regulated by their past activity on time scales of milliseconds to days and longer (Zuker and Regehr, 2002). A dynamic enhancement of such synaptic transmission has been recognized for over 70 years (Feng, 1941; Eccles et al., 1941). Virtually all types of synapses are regulated by a variety of short-lived and long-lasting processes, some of which lead to a decrease in synaptic strength and others that lead to synaptic enhancement (Zucker and Regehr, 2002). At synapses where depression is prominent, the second of two closely spaced stimuli evokes a response that is much smaller than that evoked by the first, and this reduction in synaptic strength lasts hundreds of milliseconds to seconds. Sustained stimulation produces longer-lasting depression that recovers slowly (tens of seconds to minutes). At some synapses, facilitation is observed, and the second of two closely spaced stimuli evokes a larger response than the first, provided the stimuli are delivered within hundreds of milliseconds to seconds of each other (Regehr, 2012; Jackman, et al., 2017).

Ca^{2+} plays a prominent role in many use-dependent forms of plasticity (Burnashev and Rozov, 2005; Neher and Sakaba, 2008). When an action potential invades a presynaptic terminal, Ca^{2+} flows into through voltage-gated Ca^{2+} channels (VGCCs), reaching the local concentration (Ca_{local}) of about 10–100 μM at the release site near Ca^{2+} channels (Schneggenburger and Neher, 2005). Then Ca^{2+} binds to multiple low-affinity sites of the Ca^{2+} sensor, synaptotagmin, triggering the fusion of synaptic vesicle, releasing the neurotransmitter (Jahn et al., 2003). Ca_{local} is short-lived, and is highly sensitive to the distance between open Ca^{2+} channels and Ca^{2+} sensors (Eggerman and Jonas, 2012), due to capture by Ca^{2+}-binding proteins, called Ca^{2+} buffer, in the presynaptic bouton (Roberts, 1993). Ca^{2+} buffers with rapid kinetics are particularly effective at intercepting Ca^{2+} before it reaches the release sites, thereby decreasing the release probability (Roberts, 1993). After Ca^{2+} channels closed, the spatial gradient of Ca^{2+} collapses as the calcium diffuses and binds to Ca^{2+} buffers within the presynaptic terminal (Fogelson and Zucker, 1985; Simon and Llinás, 1985). The remaining Ca^{2+}, known as residual calcium (Ca_{res}), is then gradually extruded from the presynaptic terminal by Ca^{2+} pumps (Neher and Augustine, 1992). Ca_{res} levels are much lower, only about hundreds of nanomolar, and longer-lived,. They play an important role in short-term plasticity.

The properties of vesicles within a presynaptic terminal are another important

factor of short-term plasticity. Based on the terminology used by Betz (Rizzoli and Betz, 2005), the vesicles associated with each active zone could be divided into the recycling pool (RP) that is released with sustained high-frequency activation, and the non-recycling pool (NRP) which is difficult to be evoked for release. The readily releasable pool (RRP) is immediately release-competent vesicles when the presynaptic terminal is activated. The size of the RRP could be measured by extracellularly applying hypertonic sucrose solution (Rosenmund and Stevens, 1996), or by sustained elevation of presynaptic calcium produced by either depolarizing the presynaptic terminal or uncaging Ca^{2+} (Schneggenburger et al., 2002; Rizzoli and Betz, 2005). The RRP consists of only a small fraction of the vesicles within a presynaptic terminal. At some synapses, the RRP can be divided into fast and slow vesicle pools, based on their propensity to release (Wu and Borst, 1999; Sakaba and Never, 2001). Measurements of RRP size are often used to clarify the mechanisms of short-term plasticity, but the utility is limited due to the uncertain interpretation of RRP size and the methods used to estimate it (Regehr, 2012).

Some other factors, like the inactivation of Na^{+} and Ca^{2+} channels, the saturation or desensitization of postsynaptic receptors, feedback via autoreceptors and changes of H^{+} and Ca^{2+} concentration in the cleft have also been implicated in short-term plasticity (Kushmerick et al., 2004; Smith et al., 2004; Palmer et al., 2003).

1.3 Fast signaling of inhibitory synapse

There are around 100 billion neurons in the human brain, which can be classified into two main types: glutamatergic principal neurons and GABAergic interneurons (GABA, γ–aminobutyric acid). Across all cortical circuits, almost 80 to 90% of the neuronal population are glutamatergic, whereas GABAergic neurons constitute the remaining 10 to 20% (Hu et al., 2014). In terms of cell numbers, GABAergic interneurons are definitely a minority. But these minority interneurons are critical for development of the neocortex (Butt et al., 2017) and keeping normal function of the mature brain, by controlling the activity of the majority principal neurons in the entire brain. If function of GABAergic interneurons breaks down, excitation will take over, leading to seizures and failure of high brain functions (Westbrook et al., 2013).

GABAergic interneurons play a key role in controlling the activity of neuronal

microcircuits, balancing excitation and inhibition. These neurons mediate feedback and feedforward inhibition and are involved in the generation of high-frequency network oscillations (Wang and Buzsáki, 1996; Hu et al., 2014). But, GABAergic interneurons are highly diverse. Twenty-one different classes of interneurons have been found just in the CA1 region of the hippocampus (Klausberger et al., 2008), and it's likely that an even larger number of types can be dissected in the neocortex (DeFelipe et al., 2013). These diverse interneurons can be distinguished based on three sets of criteria: (a) morphological properties of these cells, especially the selective target of the axon; (b) expression of molecular markers, like neuropeptides (somatostatin, cholecystokinin and neuropeptide-Y) and Ca^{2+}-binding proteins (calretinin, calbindin and parvalbumin); (c) functional characteristics, particularly the action potential phenotype (Rudy et al., 2001). In last few decades, several types of interneuron, especially the fast-spiking PV^{+} interneurons were widely investigated, due to several technical advantages. First, the selective expression of the Ca^{2+}-binding protein PV allows unequivocal post hoc labeling by highly specific antibodies (Celio, 1986; Eggermann and Jonas, 2012); Second, both the short action potential duration and the fast spiking action potential phenotype make it easy to identify these cells under experimental conditions. Third, the high selectivity of the promoter of PV gene can be used to genetically target these cells by enhanced colorful fluorescent proteins and optogenetic methods (Cardin et al., 2009; Sohal et al., 2009). Finally, the specific developmental trajectory of cortical PV^{+} interneurons, which are born in the medial ganglion eminence and depend on specific sets of transcription factors, could be exploited for labeling (Tricoire et al., 2011; Bartolini et al., 2013).

After two decades of work on PV^{+} interneuron, combining subcellular patch-clamp recording, simultaneous multiple-cell recording, optogenetics, *in vivo* measurement and computational approaches, the understanding about PV^{+} interneuron becomes more and more extensive in molecular, cellular, network and behavior levels (Hu et al., 2014). A hallmark functional property of PV^{+} interneuron is the speed of signaling at their output synapse across brain regions and species (Kraushaar and Jonas, 2000; Hefft and Jonas, 2005; Caillard et al., 2000; Sakaba, 2008; Arai and Jonas, 2014). Several molecular and subcellular factors have been identified as contributing to submillisecond signaling at the GABAergic inhibitory

synapse. For instance, the expression of Kv3 channel, which shortens the action potential by its high activation threshold and fast deactivation (Martina et al., 1998). The selective use of P/Q type Ca^{2+} channels, which activate and deactivate very rapidly, in presynaptic terminals (Li et al., 2007; Hefft and Jonas, 2005; Arai and Jonas, 2014). The tight coupling (nanodomain coupling) between Ca^{2+} channels and Ca^{2+} sensors of exocytosis will contribute by reducing the diffusional time delay of Ca^{2+} (Eggermann et al., 2012; Chen et al., 2015). Besides that, the activation and deactivation kinetics of the Ca^{2+} sensors (presumably synaptotagmins) of exocytosis, which is probably the first step for Ca^{2+} binding to trigger release, could be important for the speed of synaptic transmission (Chapman, 2002; Südhof, 2002; Koh and Bellen, 2003; Xu et al., 2007; Kochubey et al., 2016). However, the molecular identity of the Ca^{2+} sensor for inhibitory synaptic transmission has not been clearly determined yet.

Besides, fast-spiking PV^{+} interneurons in different brain regions generate APs at high frequency. For example, PV^{+} interneurons in the cerebellum fire APs with a frequency of up to 100 Hz during active movement (Jelitai et al., 2016), and PV^{+} interneurons in the hippocampal CA1 region generate high-frequency trains of spikes during sharp-wave ripples (Lapray et al., 2012). Under these conditions, PV^{+} interneurons need to generate stable and reliable inhibitory output signals. Considering PV^{+} interneurons mainly show short-term depression in response to train of stimuli (Hefft and Jonas, 2005; Arai and Joans, 2014), the sustained release during the activity, especially during the later phase, would be critical for keeping their ability to control the activity of postsynaptic cells. However, the underlying molecular mechanism for sustained release during activity still largely elusive.

1.4 Cerebellum and the cerebellar basket cell

The cerebellum constitutes only 10% of the total volume of the brain but contains more than one-half of its neurons in human (Herculano-Houzel, 2010). The cerebellum comprises a series of highly regular repeating units, each of which contains the same basic microcircuit (Cattani et al., 2016). Different regions of the cerebellum receive projections from different parts of the brain and spinal cord, and project to different motor systems (Adrian, 1943; Lisberger et al., 2013). The symptoms of cerebellar damage in humans and experimental animals give the clear

impression that the cerebellum participates in the control of movement. Four distinctive symptoms are manifested in patients with cerebellum disorders: hypotonia, astasia–abasia, ataxia and terminal tremor (Bastian et al., 1996; Lisberger et al., 2013).

The cellular organization of the cerebellar microcircuit is striking, neurons in the cerebellar cortex are organized into three layers: granule cell layer (GCL), Purkinje cell layer (PCL) and the molecular layer (ML) (**Figure 1-3**). GCL, located deepest, is

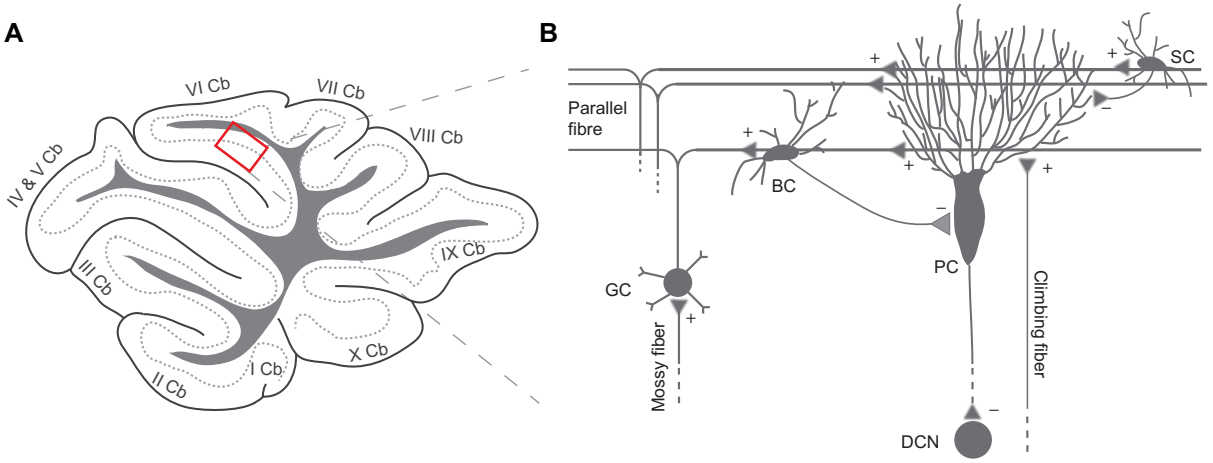

Figure 1-3. The neuronal circuits in cerebellum

(A). Schematic of sagittal cerebellar slice preparation.
(B). Cell types and their connections in cerebellar cortex. GC (granule cells), PC(purkinje cell), BC(basket cell), SC(stellate cell), DCN(deep cerebellar nuclear); + and – indicate excitatory and inhibitory synapses respectively.

the input layer. It contains a vast number of granule cells. This layer also contains a few larger Golgi interneurons and in some cerebellar regions, some other neurons, such as Lugaro, unipolar brush cells and chandelier cells. PCL, in the middle, is the output layer of cerebellar cortex. This layer consists of a single sheet of Purkinje cell bodies. The fan-like dendrites of Purkinje cells extend upward into the molecular layer where they receive input from climbing fibers, as well as the excitatory input from GCL and inhibitory input from ML. PCL is the sole output of cerebellar cortex, projecting to deep nuclei in the underlying white matter or the vestibular nuclei in the brain stem. ML located outmost is an important processing layer of the cerebellar cortex. It contains the cell body and dendrites of two types of inhibitory interneurons,

the basket cell and stellate cell. It also contains the extensive dendrites of Purkinje cells, as well as the axons of the granule cells, called parallel fibers.

The molecular layer interneurons of the cerebellar cortex have been historically divided into the basket and stellate cells (Eccles et al., 1967). They receive excitatory input from parallel fibers and inhibitory input from other interneurons and exert GABAergic inhibition on PCs (Palay and Chan-Palay, 1974; Hausser and Clarck, 1997). Basket cells are usually found in the inner third of the molecular layer and their somas are close or within the PC layer. They are characterized by the basket−like structures that their axonal arborizations envelop PCs soma (Eccles et al., 1967; Palay and Chan-Palay, 1974). The stellate cells are usually located in the outer two-thirds of the molecular layer, and the inhibitory inputs of stellate cells directly innervate the dendrites of PCs. The stellate-type dendritic inhibition is predicted to specifically counterbalance the parallel fiber excitation in local regions of the PC dendrites (Jaeger and Bower, 1999), resulting in no direct influence on PC spiking output (Santamaria et al., 2007). In contrast, basket-type somatic inhibition is powerful and rapid (Donato et al., 2008; Sakaba, 2008), and results in a direct influence on PC spiking output by inhibition of the soma and initial segment of PCs.

All cells in the three layers constitute a quite simple neuronal circuit: GCs receive excitatory input from mossy fibers, inhibitory input from Golgi cells and PCs, give output to PCs, stellate cells and BCs; PCs receive excitatory input from climbing fiber and parallel fiber, inhibitory input from stellate cell and BCs, give output to the deep nuclei cells, GCs and collaterally inhibit other PCs; Stellate cells and BCs receive excitatory input from parallel fiber, inhibitory input from Golgi cells and other stellate cells and BCs (**Figure 1-3**).

1.5 Goals of the project

We are interested in the fast signaling output of PV^+ interneurons. To investigate the underlying mechanism which ensures fast and efficient neurotransmitter release of PV^+ interneurons, we use the cerebellar BC–PC synapse as our working model. This is an ideal synapse for biophysically investigating inhibitory synaptic transmission. First, this synapse shows high connectivity and strictly perisomatic location (Arai and Jonas, 2014), enabling us to examine the time course of release with microsecond temporal precision. Second, in comparison to hippocampus and neocortex,

interneuron diversity is more limited, making it easier to dissect the functional contribution of potential proteins by comparison of wild-type and knockout synapses. Third, this synapse is amenable to genetic manipulation (such as virus injection), because of the superficial location of the cerebellar microcircuits.

Our goals are trying to 1) identify which synaptotagmin isoform is mainly used by the cerebellar BC–PC synapse; 2) How it contributes to the fast signaling property of inhibitory synaptic transmission of the BC output synapse; 3) the function of other synaptotagmins, especially Syt7, for inhibitory synaptic transmission of the cerebellar BCs.

Chapter 2. Synaptotagmin 2 is the fast Ca^{2+} sensor at a central inhibitory synapse (Chen et al., 2017a)

2.1 Introduction

17 synaptotagmins have been found in mammalian brain, among them, eight members (Syt1, 2, 3, 5, 6, 7, 9, and 10; Chapman, 2002; Südhof, 2002) bind Ca^{2+}, and three of Ca^{2+}-binding members mediate fast release with different kinetic properties (Syt1, Syt2, and Syt9; Xu et al., 2007; Kochubey et al., 2016). Which of these synaptotagmins are involved in transmitter release at GABAergic synapses remains elusive. Genetic labelling and immunohistochemistry experiments indicated the expression of Syt2 in GABAergic interneurons, most likely PV^+ subtypes (Pang et al., 2006a; Fox and Sanes, 2007; Sommeijer and Levelt, 2012). Additionally, genetic elimination of Syt1 reduced release to ~50% of control value at output synapse of fast-spiking, PV^+ interneurons in the hippocampus, suggesting that multiple synaptotagmins, probably Syt1 and Syt2, work in concert (Kerr et al., 2008).

How different synaptotagmin isoforms shape the time course of transmitter release is controversial. Recombinant expression of different synaptotagmin isoforms in cultured neurons suggested marked kinetic differences among Syt1, Syt2, and Syt9, with Syt2-mediated release has the fastest and Syt9-mediated release has the slowest onset and decay (Xu et al., 2007). However, expression of different synaptotagmin isoforms in the calyx of Held revealed no significant differences in release kinetics between Syt2 and Syt1 (Kochubey et al., 2016). Furthermore, Syt2 mediated slower vesicle fusion kinetics than Syt1 in chromaffin cells (Nagy et al., 2006) and showed slower kinetics in comparison to Syt1 in liposome binding-unbinding assays (Hui et al., 2005). Thus, how the differential expression of synaptotagmin isoforms (Mittelsteadt et al., 2009) relates to the speed of synaptic transmission has not been defined.

Here, combining electrophysiological, immunohistochemistrical, genetical and viral exogenous gene expression methods, we are trying to investigate which synaptotagmin isoform is mainly used by inhibitory interneurons, and how it contributes to the fast signaling output synapses.

2.2 Methods

Animal experiments

Experiments on C57BL/6 wild-type and mutant mice were performed in strict accordance with institutional, national, and European guidelines for animal experimentation and were approved by the Bundesministerium für Wissenschaft, Forschung und Wirtschaft of Austria (A. Haslinger, Vienna; BMWF-66.018/0008-II/3b/2010; BMWF-66.018/0010-WF/V/3b/2015).

Immunohistochemistry

Brains of 14- to 16-day-old mice were dissected out, fixed in 4% paraformaldehyde and 1% sucrose for ~2 h, and transferred to 30% sucrose in phosphate-buffered solution (PBS; ~10 h) for cryoprotection. 50 µm-thick slices were cut from the cerebellar vermis using a cryostat (HM560; Thermo-Scientific). After washing with 0.01 M PBS, slices were incubated with 10% normal goat serum (NGS) for 1 h and subsequently with primary monoclonal antibodies against Syt1 (IgG2b, mab48, 1:500, developmental studies hybridoma bank, DSHB), Syt2 (IgG2a, znp1, 1:500, zebrafish international resource center, ZIRC; Fox and Sanes, 2007), or both in PBS containing 5% NGS and 0.3% Triton X-100 overnight. After washing, slices were incubated with isotype-specific secondary antibodies (goat anti-mouse IgG2b for mab48 and goat anti-mouse IgG2a for znp1, 1:1000 for both; Invitrogen) with PBS containing 3% NGS and 0.3% TritonX-100 overnight. After washing, slices were embedded in Prolong Antifade and examined under a TCS SP5 II confocal microscope (Leica Microsystems). Syt2 immunolabeling was completely absent in $Syt2^{-/-}$ mice (Figure S1C). For double labeling for VGAT or VGLUT1, rabbit polyclonal antibodies (#131003 and #135303; Synaptic Systems) were used.

Confocal stacks were analyzed using the open-source software Fiji ("Fiji is just ImageJ"). For analyzing puncta in different layers of the cerebellum, regions of interest were randomly defined using the "Freehand Selection" feature of Fiji. Threshold was automatically adjusted using the "Triangle" method for both channels. Puncta number and area was analyzed using the "Analyze Particles" function.

Cerebellar slice preparation

C57BL/6 Syt2 knockout mice ($Syt2^{-/-}$), in which exons 2–7 of the Syt2 gene were deleted, were kindly provided by T.C. Südhof, Stanford University (Pang et al., 2006a). All experiments were performed on littermate offspring from heterozygous

matings, with knockout mice being homozygous for the deletion allele ($Syt2^{-/-}$) and wild-type animals homozygous for the wild-type allele ($Syt2^{+/+}$). Slices were cut from the cerebellum of 14- to 16-day-old mice of either sex. In all experiments, genotypes were determined by polymerase chain reaction analysis. After decapitation, the brain was rapidly dissected out and immersed in ice-cold slicing solution containing: 87 mM NaCl, 25 mM $NaHCO_3$, 2.5 mM KCl, 1.25 mM NaH_2PO_4, 10 mM D-glucose, 75 mM sucrose, 0.5 mM $CaCl_2$, and 7 mM $MgCl_2$, (pH 7.4 in 95% O_2 / 5% CO_2, 325 mOsm). Parasagittal 250-µm-thick cerebellar slices from the vermis region were cut using a custom-built or a VT1200 vibratome (Leica Microsystems). After ~20 min incubation at ~35ºC, the slices were stored at room temperature. Slices were used for maximally 5 hours after dissection. Experiments were performed at 21–24°C.

Electrophysiology

During experiments, slices were superfused with a physiological extracellular solution containing: 125 mM NaCl, 2.5 mM KCl, 25 mM $NaHCO_3$, 1.25 mM NaH_2PO_4, 25 mM D-glucose, 2 mM $CaCl_2$, and 1 mM $MgCl_2$ (pH 7.4 in 95% O_2 / 5% CO_2, ~325 mOsm). Paired recordings from synaptically connected BCs and PCs were performed as described previously (Caillard et al., 2000; Sakaba, 2008; Christie et al., 2011; Eggermann and Jonas, 2012; Arai and Jonas, 2014). Intracellular solution used for the presynaptic BCs contained: 125 mM K-gluconate, 20 mM KCl, 0.1 mM EGTA, 10 mM phosphocreatine, 2 mM $MgCl_2$, 2 mM ATP, 0.4 mM GTP, 10 mM HEPES (pH adjusted to 7.28 with KOH, ~310 mOsm); 0.2% biocytin was added in a subset of recordings. The presynaptic pipette resistance was 8–15 MΩ. BCs were recorded under current-clamp conditions. A holding current of ~−50 pA was injected to maintain the membrane potential at ~−65 mV and to avoid spontaneous AP generation. To evoke presynaptic APs, single pulses or trains of either 10 pulses at 50 Hz or 50 pulses at 100 Hz (400 pA, 4 ms) were injected into the presynaptic BC every 4 s or 20 s, respectively.

Intracellular solution for postsynaptic PCs contained: 140 mM KCl, 10 mM EGTA, 2 mM $MgCl_2$, 2 mM ATP, 10 mM HEPES, and 2 mM QX-314 (pH adjusted to 7.28 with KOH, ~313 mOsm). To achieve the lowest possible postsynaptic series resistance, leaded glass (PG10165-4, WPI) was used to fabricate large tip-sized recording pipettes. The postsynaptic pipette resistance was 0.8–1.5 MΩ, resulting in

a series resistance of 3–8 MΩ. Experiments in which series resistance changed by > 2 MΩ were discarded. PCs were recorded in the voltage-clamp configuration with a holding potential of −70 mV. For monitoring series and input resistance, 5-mV, 100−ms hyperpolarizing test pulses were applied after the IPSCs had decayed to baseline.

For recording of mIPSCs (**Figure 2-5**), synaptic events were examined in pharmacological isolation in the presence of 1 µM TTX, 10 µM CNQX, and 20 µM D-AP5 at −70 mV. For feedforward inhibition experiments (**Figure 2-12**; **Figure 2-13**), slices were cut in frontal plane to preserve parallel fibers (Mittmann et al., 2005). Parallel fibers were stimulated with glass pipettes (~ 1 MΩ) containing extracellular solution placed at a distance > 100 µm from the recorded PC to avoid direct stimulation of interneuron axons. The stimulus electrode was placed in the center or outer half of the molecular layer. Electrical stimuli (5–8 V amplitude, 100 µs duration) were delivered using a stimulus isolation unit. PCs were recorded in the whole-cell configuration using patch pipettes similar to those in paired recordings. Membrane potential was set to −50 mV to record both EPSCs and IPSCs in the same trace and to either −60 mV or 0 mV to examine EPSCs and IPSCs in isolation. The electrode solution contained: 130 mM K-methanesulfonate, 2 mM KCl, 10 mM EGTA, 2 mM $MgCl_2$, 2 mM Na_2ATP, 10 mM HEPES, and 5 mM QX-314 (pH adjusted to 7.27 with KOH). In a subset of experiments, the selective $GABA_A$ receptor antagonist SR-95531 (10 µM, Biotrend) was used to block IPSCs.

Production of adenoviral expression vectors

Synaptotagmin cDNA (*Mus musculus* isoforms 1 and 2) was codon-optimized for expression in mouse (GeneArt) and then cloned into the EcoRI and NotI sites of the synapsin expression cassette (Montesinos et al., 2011). This cassette included the 470 bp human synapsin (hsyn) promoter, the minute virus of mice (mvm) intron, and the bovine growth hormone (BGH) polyA. Subsequently, the expression cassette was cloned into the AscI site of pdelta28E4, a gift from Dr. Phil Ng (Palmer and Ng, 2003), using InFusion (Clontech). This version of pdelta28E4 was modified to also contain a separate neurospecific EGFP expression cassette driven by the 470 bp hsyn promoter. The final HdAd plasmids allow for expression of synaptotagmin isoforms independently of EGFP as dual expression recombinant Ad vectors, similar

to the strategy previously used with 2nd generation rAd vectors (Young and Neher, 2009; Chen et al., 2013).

Production of HdAd was carried out as previously described (Palmer and Ng, 2003). Briefly, HdAds were produced by first digesting the pHdAd with PmeI to linearize and expose the ends of the 5' and 3' inverted terminal repeats. Transfection of the pHdAd was performed using 116 producer cells, a modified HEK293 line expressing high levels of Cre recombinase, and a 4-kbp adenoviral genome fragment that encodes for the E1A/E1B gene, necessary for rAd to replicate (Palmer and Ng, 2003). Standard protocols for recombinant HdAd were followed (Palmer and Ng, 2003) with slight modifications. HdAd was serially amplified in 5 consecutive passages from 3–60 mm tissue culture dishes followed by 1–15 cm and finally 30−15 cm dishes. Each successive passage was performed after cytopathic effect (CPE) occurred and cell lysates were subjected to 3 freeze/thaw cycles to lyse cells and thereby release the viral particles. HdAd was stored at −80°C in storage buffer containing 10 mM HEPES, 250 mM sucrose, and 1 mM $MgCl_2$ at pH 7.4. Viral particle concentration (ml^{-1}) was calculated (Palmer and Ng, 2003) as follows: Viral particles/ml = (A260) x (dilution factor) x (1.1×10^{12}) x (36) / (size of the vector in kb). Virus titers were similar for HdAd-Syt1 and HdAd-Syt2: 4.39×10^{12} vp ml^{-1} and 3.98×10^{12} vp ml^{-1}, respectively.

Virus injection

$Syt2^{-/-}$ mice, at postnatal day (P) 3 to 6, were anesthetized using isoflurane (5% for induction and ~3% during the injection procedure) (Forane®, Abbott) combined with meloxicam (1 mg kg^{-1}, Boehringer) for analgesia. Meloxicam was given 2 hours before surgery for pre-operative analgesia and repeated twice 24 h after the previous injection for post-operative analgesia. After sufficient sedation, mice were put on a stereotaxic apparatus and head-fixed with ear bars. The skin was cut, the skull was exposed, and a small hole was made with a needle in the region over the cerebellum. 1 µl adenovirus (~10^9 vp $µl^{-1}$) was injected into the vermis of the cerebellum at a depth of ~600 µm from the endocranium. After virus injection, pups were returned to their home cages for recovery. Recordings were made at P14 to 16. Infected cerebellar BCs were identified by EGFP fluorescence. For electrophysiology, epifluorescence illumination was used. For analysis of rescue

efficiency and documentation, cells were examined using a TCS SP5 II confocal microscope.

To address the expression level of synaptotagmin protein after viral infection, we examined both EGFP fluorescence and Syt1 or Syt2 immunoreactivity. Expression levels probed with this approach were very similar. This is consistent with previous results, which demonstrated that the expression level probed with a Myc tag and a anti-Myc antibody was the same for different synaptotagmins (Kochubey et al., 2016).

Data acquisition and analysis

Data were acquired with a Multiclamp 700B amplifier (Axon Instruments), low-pass filtered at 10 kHz, and sampled at 20 or 50 kHz using a CED power1401 interface (Cambridge Electronic Design). Stimulus generation and data acquisition were performed using custom-made software (FPulse versions 3.19 and 3.33, Ulrich Fröbe, University of Freiburg) running under Igor Pro 6.22 (WaveMetrics). Data were analyzed using Stimfit 0.14.9 (www.stimfit.org), Igor Pro 6.22, R 3.3.0 (the R project for statistical computing), and Mathematica 10.3 (Wolfram Research). Synaptic latency of monosynaptic IPSCs was measured from the peak of the presynaptic AP to the IPSC onset. Latency of disynaptic IPSCs (**Figure 2-12E**) was measured from the peak of the EPSC at −60 mV to that of the IPSC at 0 mV. IPSC decay time constant was determined by fitting the decay phase of an average IPSC trace. To quantify multiple-pulse depression, traces were averaged and the amplitude of each IPSC in a train was measured from the baseline directly preceding the rising phase. mIPSCs were detected using a template matching algorithm and verified by visual inspection (Pernía-Andrade et al., 2012; Goswami et al., 2012). Synchronous and asynchronous release was quantified by a deconvolution algorithm based on Fourier transformation, using trains of 10 APs at 50 Hz as stimuli (Hefft and Jonas, 2005). Synchronous release was measured 0–5 ms after each AP. Asynchronous release during the train was quantified 15–20 ms after each AP, and asynchronous release after the train was quantified > 20 ms after end of the train. For display purposes, the TCR was filtered at 2 kHz (**Figure 2-4D** and 2-4E).

Latency and half-duration of the TCR following a single AP were quantified by a deconvolution algorithm in which the TCR function was represented by a Gaussian

or a gamma distribution. Unitary IPSCs recorded in 2 mM extracellular Ca^{2+} concentration were aligned to the peak of the presynaptic AP and averaged. Quantal IPSCs recorded in 0.7 mM extracellular Ca^{2+} and 2.3 mM Mg^{2+} were aligned to the 50% rising point and also averaged. The TCR function was convolved with the quantal IPSC waveform, using ListConvolve of Mathematica. Amplitude and shape of the time course of release function were adjusted to minimize the sum of squared differences between predicted and measured unitary IPSC.

For analysis of vesicular pool size and refilling rate, IPSC amplitudes during a 100-Hz train of 50 stimuli were examined. IPSC values were normalized by $IPSC_1$, averaged across cells, and cumulatively plotted against stimulus number. The last ten data points were fit by linear regression. The size of the RRP was determined from intersection of the regression line with the ordinate, whereas refilling rate was determined from the slope (Neher, 2015). The RRP estimate represents “pool decrement” rather than absolute pool size; the true pool size will be larger than the estimate (Neher, 2015). Release probability was quantified as the ratio of normalized $IPSC_1$ over pool size. For obtaining absolute numbers of RRP size and refilling rate, estimated values were multiplied by the quantal content of $IPSC_1$. Quantal size was estimated by nonstationary fluctuation analysis. Variance was plotted against mean for all IPSCs in the train, and analyzed by linear regression. Quantal size was determined from the slope of the fit line (Scheuss et al., 2002; Sakaba, 2008).

Statistics and conventions

All values were reported as mean ± SEM. Statistical significance was tested using a Kruskal-Wallis and two-sided Wilcoxon rank sum test in R. Differences with $P < 0.05$ were considered significant. In figures, *, **, and *** indicate $P < 0.05$, $P < 0.01$, and $P < 0.001$, respectively. In experiments with parallel fiber stimulation, stimulation artifacts were blanked for display purposes.

Data included in this paper are based on recordings from a total of 137 BC–PC paired recordings (32 for experiments on $Syt2^{+/+}$, 28 for $Syt2^{-/-}$, 37 for HdAd-Syt2 rescue, and 40 for HdAd-Syt1 rescue) and 48 PC recordings (25 for mIPSC and 23 for disynaptic inhibition experiments).

2.3 Results

Differential expression of Syt1 and Syt2 between excitatory and inhibitory presynaptic terminals in cerebellum

Previous expression analysis showed that several synaptotagmin isoforms are expressed in the cerebellum, with strongest expression of Syt1 and Syt2 (Mittelsteadt et al., 2009). To determine the molecular identity of the Ca^{2+} sensor at cerebellar BC–PC synapses, we examined synaptotagmin immunoreactivity in BC terminals, using specific antibodies against either Syt1 or Syt2 (Fox and Sanes, 2007; Kochubey et al., 2016; **Figure 2-1**). Although Syt1 immunoreactivity was abundant in both the granule cell layer and the molecular layer, putative presynaptic BC terminals surrounding PC somata were completely devoid of fluorescent labeling (**Figure 2-1A** and 1B). In contrast, putative BC terminals were strongly immunopositive for Syt2 (**Figure 2-1A** and 1B). Syt2 labeling was completely eliminated in the $Syt2^{-/-}$ mice, demonstrating the specificity of the antibody (**Figure 2-2**). Double labeling with antibodies against Syt1 and Syt2 revealed that, despite the abundant expression of both isoforms in the cerebellum, colocalization of immunoreactivities was minimal, indicating expression in non-overlapping populations of synapses (**Figure 2-1B**). Double labeling with antibodies against one of the synaptotagmins and the vesicular GABA transporter (VGAT) or vesicular glutamate transporter (VGLUT1) demonstrated that in the cerebellum Syt1 was exclusively expressed at excitatory synapses (**Figure 2-2B; see Figure 2-1C**), whereas Syt2 was largely confined to inhibitory synapses (**Figure 2-1D**). These results suggest that Syt2 may constitute the main Ca^{2+} sensor for fast transmitter release at inhibitory BC–PC synapses.

Syt2 deletion severely reduces action potential-evoked release at BC–PC synapses

To directly test the hypothesis that Syt2 is the Ca^{2+} sensor of exocytosis at BC–PC synapses, we studied the effects of genetic elimination. To achieve this, we compared the properties of unitary inhibitory postsynaptic currents (IPSCs) between wild-type ($Syt2^{+/+}$) and Syt2-deficient ($Syt2^{-/-}$) BC–PC synapses in 14- to 16-day-old mice (**Figure 2-3**; **Table 1**). Genetic elimination of Syt2 reduced the peak amplitude of evoked IPSCs at BC–PC synapses to 16.4% of the wild-type control value

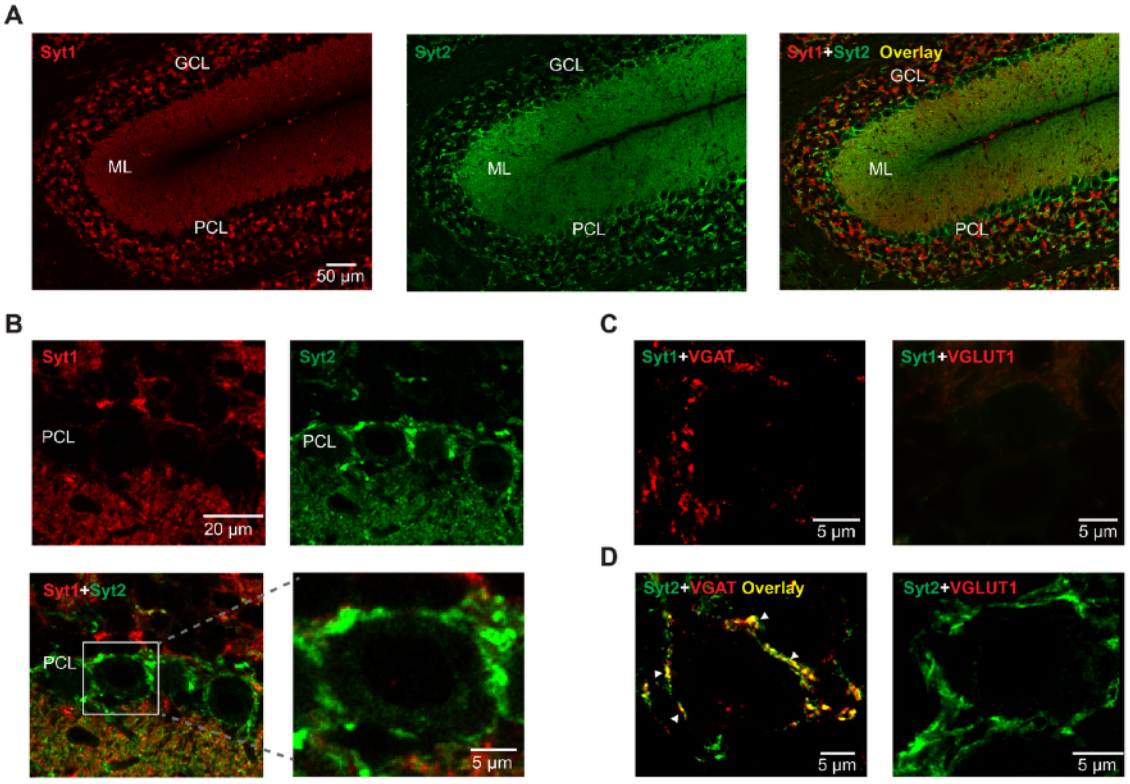

Figure 2-1. Differential expression of Syt1 and Syt2 between excitatory and inhibitory presynaptic terminals in cerebellum

(A) Light-micrographs of cerebellar cortex, showing immunolabeling for synaptotagmin 1 (Syt1, left), synaptotagmin 2 (Syt2, center), and overlay (right) from a wild-type mouse; single confocal sections.
(B) Similar to (A), but at higher magnification. Note that putative BC terminals surrounding PC somata are only immunoreactive for Syt2, but not for Syt1.
(C) Colocalization of Syt1 and VGAT (left) and VGLUT1 (right). Note the absence of Syt1 immunoreactivity in inhibitory terminals surrounding PCs.
(D) Similar colocalization analysis as shown in (C), but for Syt2. Note high Syt2 immunoreactivity in putative BC terminals (arrowheads).
ML: molecular layer. PCL: Purkinje cell layer; GCL: granule cell layer.

(925.1 ± 99.2 pA in $Syt2^{+/+}$ synapses; 151.9 ± 44.2 pA in $Syt2^{-/-}$ synapses, 12 pairs in both cases; $P < 0.0001$; **Figure 2-3A–C**). In parallel, genetic elimination of Syt2 markedly increased the proportion of failures, from 0.9 ± 0.6% in $Syt2^{+/+}$ mice to 47.4 ± 7.7% in $Syt2^{-/-}$ mice ($P < 0.0001$; **Figure 2-3C**), confirming a presynaptic

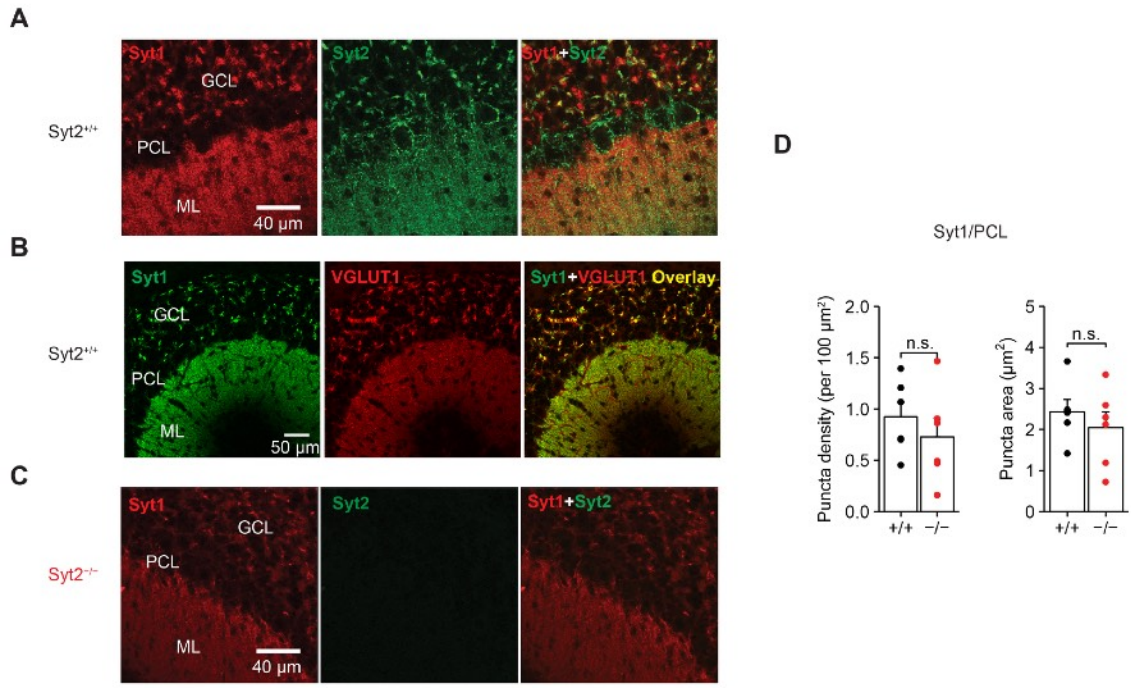

Figure 2-2. Syt1 expression in cerebellar synapses of Syt2$^{+/+}$ and Syt2$^{-/-}$ mice

(A) Light-micrographs of cerebellar cortex, showing immunolabeling for synaptotagmin Syt1 1 (Syt1, left), Syt2 synaptotagmin 2 (Syt2, center), and overlay (right).

(B) Light-micrographs of cerebellar cortex, showing immunolabeling for synaptotagmin 1 (Syt1, left), vesicular glutamate transporter immunoreactivity (VGLUT1, center), and overlay (right). Both (A) and (B) were obtained from Syt2$^{+/+}$ mice; single confocal sections.

(C) Similar analysis as in (A), but for Syt2$^{-/-}$ mouse.

(D) Summary bar graphs of puncta density (left) and puncta cross-sectional area (right) in the Purkinje cell layer (PCL). Bars represent mean ± SEM, circles indicate data from individual experiments. Note that both puncta density and area are very similar in Syt2$^{+/+}$ and Syt2$^{-/-}$ mice, suggesting lack of compensatory

change. These results identify Syt2 as the main functional Ca^{2+} sensor for synchronous transmitter release at inhibitory BC–PC synapses.

To reveal the mechanisms by which genetic elimination of Syt2 reduces the amplitude of evoked IPSCs, we further examined the coefficient of variation (CV) and the skewness of IPSC peak amplitudes. Syt2 deletion increased the CV, from 0.49 ± 0.03 to 1.28 ± 0.17 (12 pairs in both cases; $P < 0.0001$; **Figure 2-3D**). Furthermore, genetic elimination of Syt2 increased the skewness, from 0.50 ± 0.14 in

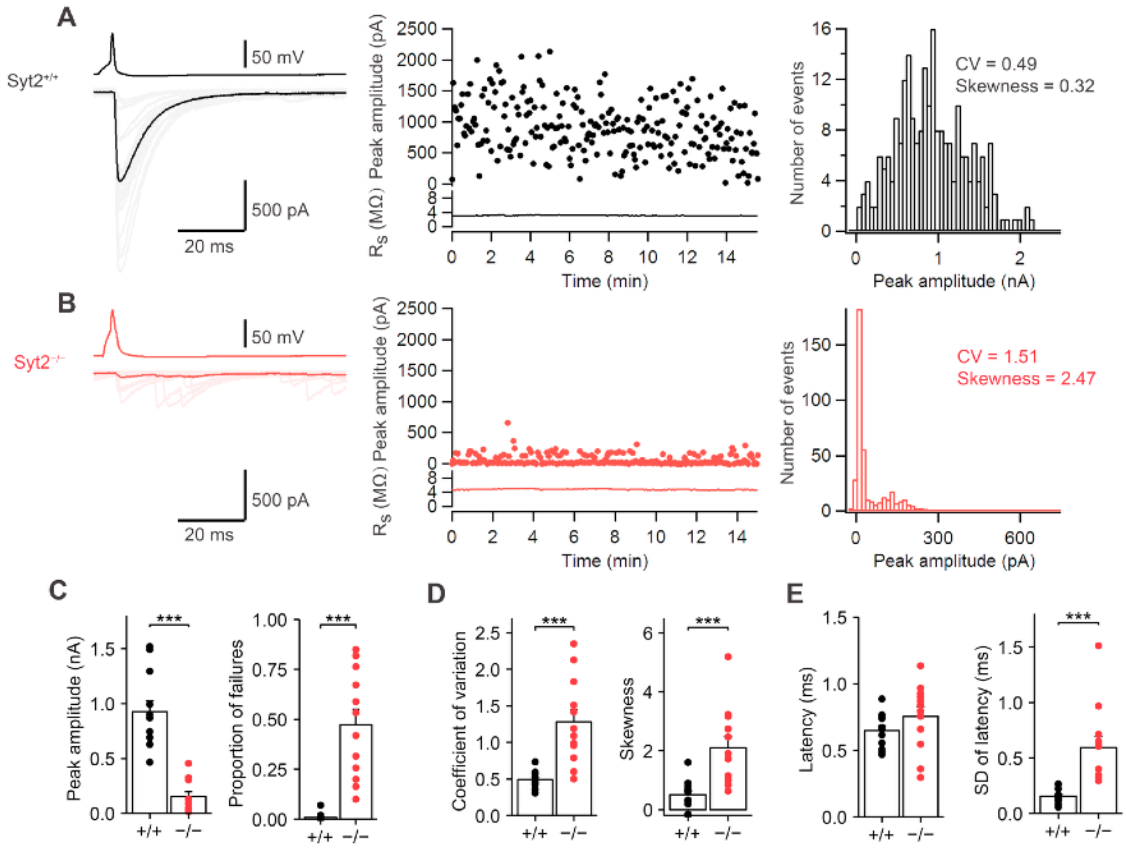

Figure 2-3. Genetic elimination of Syt2 severely reduces transmitter release at the BC–PC synapse

(A) Left, presynaptic AP (black), individual evoked IPSCs (gray), and average IPSC (black) recorded from a $Syt2^{+/+}$ synapse. Center, plot of IPSC peak amplitude and postsynaptic series resistance (R_S) against experimental time. Right, peak amplitude histogram from the same pair, obtained from 235 unitary IPSCs. The number of failures was 2 in this experiment.

(B) Similar experiment as shown in (A) but recorded from a $Syt2^{-/-}$ synapse (red, light red, and red). Histogram shown on the right was obtained from 400 unitary IPSCs. The number of failures was 279.

(C–E) Genetic elimination of Syt2 reduces release probability. Summary bar graph of peak amplitude (C, left), proportion of failures (C, right), coefficient of variation (CV, D, left), skewness (D, right), latency (E, left), and standard deviation of latency (E, right) for $Syt2^{+/+}$ (black) and $Syt2^{-/-}$ synapses (red). Bars represent mean ± SEM, points indicate data from individual experiments. Data from 12 pairs ($Syt2^{+/+}$) and 12 pairs ($Syt2^{-/-}$).

$Syt2^{+/+}$ mice to 2.10 ± 0.38 in $Syt2^{-/-}$ mice ($P < 0.0001$; **Figure 2-3D**). Taken together, these results suggest that Syt2 deletion reduces release probability without

Table 2-1. Functional properties of synaptic transmission at cerebellar BC–PC synapses in $Syt2^{+/+}$ and $Syt2^{-/-}$ mice.

Parameter	$Syt2^{+/+}$	$Syt2^{-/-}$	P
Latency	0.65 ± 0.04 ms (12)	0.75 ± 0.07 ms (12)	0.1135
SD latency	0.15 ± 0.02 ms (12)	0.59 ± 0.10 ms (12)	<0.0001
20–80% rise time	0.60 ± 0.05 ms (12)	0.64 ± 0.05 ms (12)	0.5137
IPSC peal amplitude	925.1 ± 99.2 pA (12)	151.9 ± 44.2 pA (12)	<0.0001
IPSC decay time constant	9.19 ± 0.51 (12)	9.53 ± 1.08 ms (12)	0.6707
Proportion of failures	0.91 ± 0.58% (12)	47.4 ± 7.7% (12)	<0.0001
Paired-pulse ratio $IPSC_2/IPSC_1$	1.06 ± 0.05 (11)	1.79 ± 0.16 (16)	0.0003
$IPSC_{10}/IPSC_1$	0.61 ± 0.02 (11)	2.79 ± 0.46 (16)	<0.0001
Miniature IPSC frequency	3.75 ± 0.42 Hz (12)	9.64 ± 1.74 Hz (13)	0.0008
Miniature IPSC amplitude	110 ± 11.0 pA (12)	141.7 ± 12.0 pA (12)	0.0868

Mean ± SEM (n, number of experiments).

changing the number of release sites (Kerr et al., 2008). Finally, we quantified the latency and its standard deviation, a measure of temporal precision of transmitter release. Whereas latency was not significantly different (0.65 ± 0.04 ms in $Syt2^{+/+}$; 0.75 ± 0.07 ms in $Syt2^{-/-}$; P = 0.11; **Figure 2-3E**), standard deviation of latency markedly increased, from 0.15 ± 0.02 ms to 0.59 ± 0.10 ms (P < 0.0001; **Figure 2-3E**). Thus, the residual component in $Syt2^{-/-}$ mice appeared more asynchronous. Compensatory increases in the expression of Syt1 were not detected in $Syt2^{-/-}$ mice (**Figure 2-2C** and 2-2D), suggesting that the residual component was

mediated by a different Ca^{2+} sensor. In conclusion, deletion of the Syt2 gene resulted in a massive reduction of synchronous transmitter release at cerebellar BC–PC synapses, caused by a reduction in release probability.

Effects of Syt2 deletion on short-term dynamics and asynchronous release

Next, we studied the effects of genetic elimination of Syt2 on IPSCs evoked by trains of presynaptic stimuli (**Figure 2-4**). In $Syt2^{+/+}$ synapses, trains of 10 presynaptic action potentials (APs) at 50 Hz induced a significant depression of IPSC peak amplitude and a minimal amount of asynchronous release during and after the stimulus train (**Figure 2-4A** and 2-4C), consistent with previous observations (Caillard et al., 2000; Sakaba, 2008; Arai and Jonas, 2014). In contrast, in $Syt2^{-/-}$ synapses, IPSC peak amplitudes showed a marked facilitation (**Figure 2-4B** and 2-4C), and the frequency of asynchronous release was increased (**Figure 2-4B**). To quantify synchronous and asynchronous release components, we analyzed release during train stimulation by deconvolution (**Figure 2-4D** and 2-4E). Synchronous release was quantified in the time interval of 5 ms following the AP, whereas asynchronous release was measured in a time window 15 to 20 ms following each presynaptic stimulus. Syt2 deletion reduced the cumulative release of the synchronous component from 34.1 ± 6.5 quanta in $Syt2^{+/+}$ mice to 11.1 ± 3.3 quanta in $Syt2^{-/-}$ mice (11 and 16 pairs, respectively; P = 0.0009; **Figure 2-4F**). In contrast, Syt2 deletion increased asynchronous release during the train from 0.14 ± 0.99 quanta in $Syt2^{+/+}$ mice to 5.62 ± 1.53 quanta in $Syt2^{-/-}$ mice (11 and 16 pairs, respectively; P = 0.0001; **Figure 2-4F**). Similarly, genetic elimination of Syt2 increased asynchronous release after the train from 0.52 ± 0.38 quanta in $Syt2^{+/+}$ mice to 3.31 ± 0.81 quanta in $Syt2^{-/-}$ mice (11 and 16 pairs, respectively; P = 0.0033; **Figure 2-4F**). These results demonstrate that Syt2 selectively mediates synchronous release, whereas asynchronous release appears to be mediated by a different sensor, e.g. Syt7 (Bacaj et al., 2013; Jackman et al., 2016).

Elevated frequency of spontaneous release in $Syt2^{-/-}$ mice

Previous studies showed that deletion of synaptotagmins increases the frequency of spontaneous release, suggesting a clamping function of synaptotagmin (Littleton et al., 1994; Pang et al., 2006b; Chicka et al., 2008; Giraudo et al., 2006; Kerr et al.,

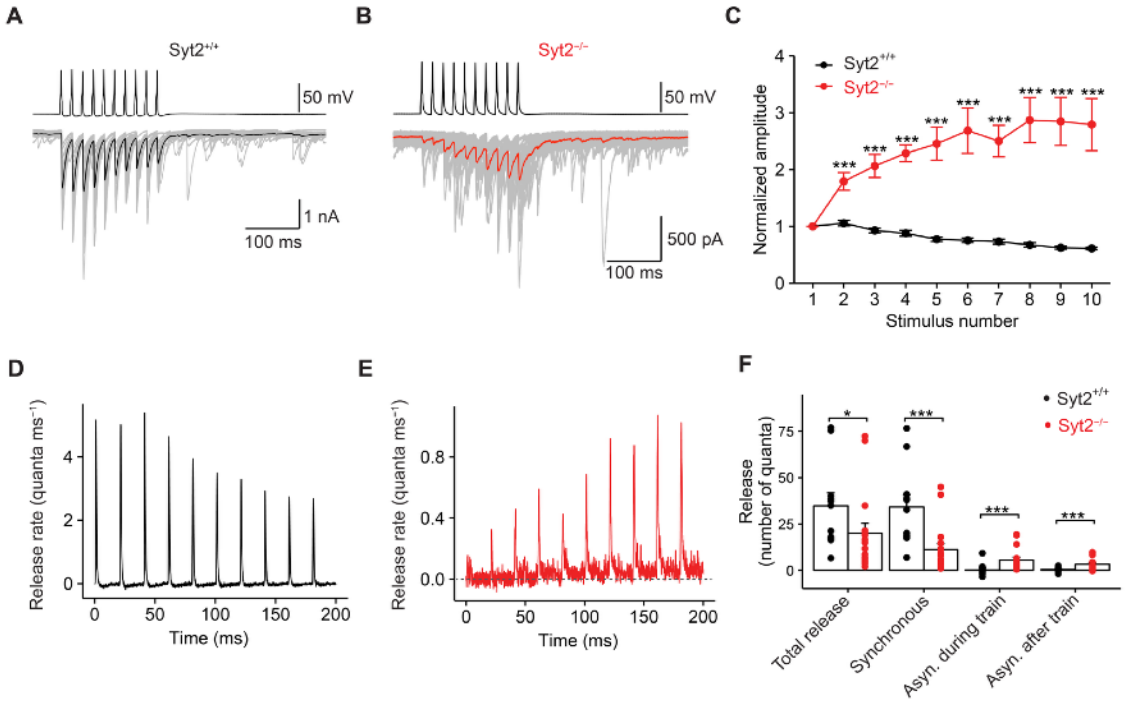

Figure 2-4. Genetic elimination of Syt2 selectively abolishes synchronous release

(A, B) Trains of 10 presynaptic APs at 50 Hz and corresponding IPSCs recorded from a $Syt2^{+/+}$ synapse (A) and a $Syt2^{-/-}$ synapse (B). 20 consecutive IPSC traces (gray) and the average trace (black and red, respectively) are shown superimposed.
(C) Plot of normalized IPSC amplitude ($IPSC_n$ / $IPSC_1$) against IPSC number (n) for $Syt2^{+/+}$ (black circles) and $Syt2^{-/-}$ synapses (red circles).
(D, E) Corresponding release rate during the AP train obtained by deconvolution for a $Syt2^{+/+}$ synapse (D) and a $Syt2^{-/-}$ synapse (E; horizontal dashed line indicates a release rate of 0).
(F) Summary bar graph of cumulative release (total release, synchronous release, asynchronous release during the train, and asynchronous release after the train). Bars represent mean ± SEM, points indicate data from individual experiments.
All data were obtained with trains of 10 APs, applied at a frequency of 50 Hz. Data in (C) and (F) are from 11 pairs ($Syt2^{+/+}$) and 16 pairs ($Syt2^{-/-}$).

2008). However, these experiments have mostly been performed in culture conditions, in which compensatory changes in connectivity or homeostatic mechanisms may occur (Liu et al., 2014). To test the clamping hypothesis in the intact circuit, we compared the frequency of miniature IPSCs (mIPSCs) in PCs

between $Syt2^{+/+}$ and $Syt2^{-/-}$ mice (**Figure 2-5**). mIPSCs were recorded in pharmacological isolation in the presence of Na^+ channel and glutamate receptor blockers (1 µM tetrodotoxin, TTX; 10 µM 6-cyano-7-nitroquinoxaline-2,3-dione, CNQX; 20 µM D-2-amino-5-phosphonopentanoic acid, D-AP5), and were detected with a template matching algorithm (Pernía-Andrade et al., 2012; **Figure 2-5A**). Genetic elimination of Syt2 resulted in a ~2.5-fold increase in the frequency of mIPSCs in PCs, from 3.75 ± 0.42 Hz in $Syt2^{+/+}$ mice (12 cells) to 9.64 ± 1.74 Hz in $Syt2^{-/-}$ mice (13 cells; P = 0.0008; **Figure 2-5B** and 2-5C). In contrast, the amplitude of mIPSCs was unchanged (110.0 ± 11.0 pA in $Syt2^{+/+}$ vs. 141.7 ± 12.0 pA in $Syt2^{-/-}$; P = 0.087; **Figure 2-5C**). These results are consistent with a clamping function of Syt2 at GABAergic synapses.

To distinguish mIPSCs generated at BC synapses from those at stellate cell synapses, we analyzed the 20–80% rise time of mIPSCs, an indicator of synaptic location. When the analysis was restricted to IPSCs with a 20–80% rise time of < 1.5 ms, likely to be generated by synapses in the inner third of the molecular layer (Roth and Häusser, 2001), Syt2 deletion resulted in a ~2.5-fold increase in the frequency of mIPSCs, from 2.54 ± 0.30 Hz to 7.28 ± 1.43 Hz (12 and 13 cells, respectively; P = 0.0005; **Figure 2-5D**). Furthermore, the amplitude of mIPSCs was unchanged (P = 0.27; **Figure 2-5D**). To rule out that changes in inhibitory connectivity confounded these observations, we labeled GABAergic synaptic sites with antibodies against VGAT, and quantified the density of immunopositive puncta in $Syt2^{+/+}$ and $Syt2^{-/-}$ mice in the PC layer (**Figure 2-5E** and 2-5F). On average, the number of VGAT-positive puncta per 100 μm^2 in single confocal sections was 2.37 in $Syt2^{+/+}$ and 2.59 in $Syt2^{-/-}$ mice (**Figure 2-5F**, left; P = 0.39). Likewise, the puncta area was not significantly different (**Figure 2-5F**, right; P = 0.41). These results support the assumption of unchanged inhibitory connectivity in $Syt2^{-/-}$ mice. Taken together, our results suggest that Syt2 acts as a fusion clamp at GABAergic BC–PC synapses (Giraudo et al., 2006).

Adenoviral rescue with Syt2 generates fast transmitter release

What is the functional significance of the selective usage of Syt2 as a Ca^{2+} sensor at cerebellar BC–PC synapses? Previous studies suggested that different synaptotagmins might differ in their activation and deactivation kinetics (Hui et al.,

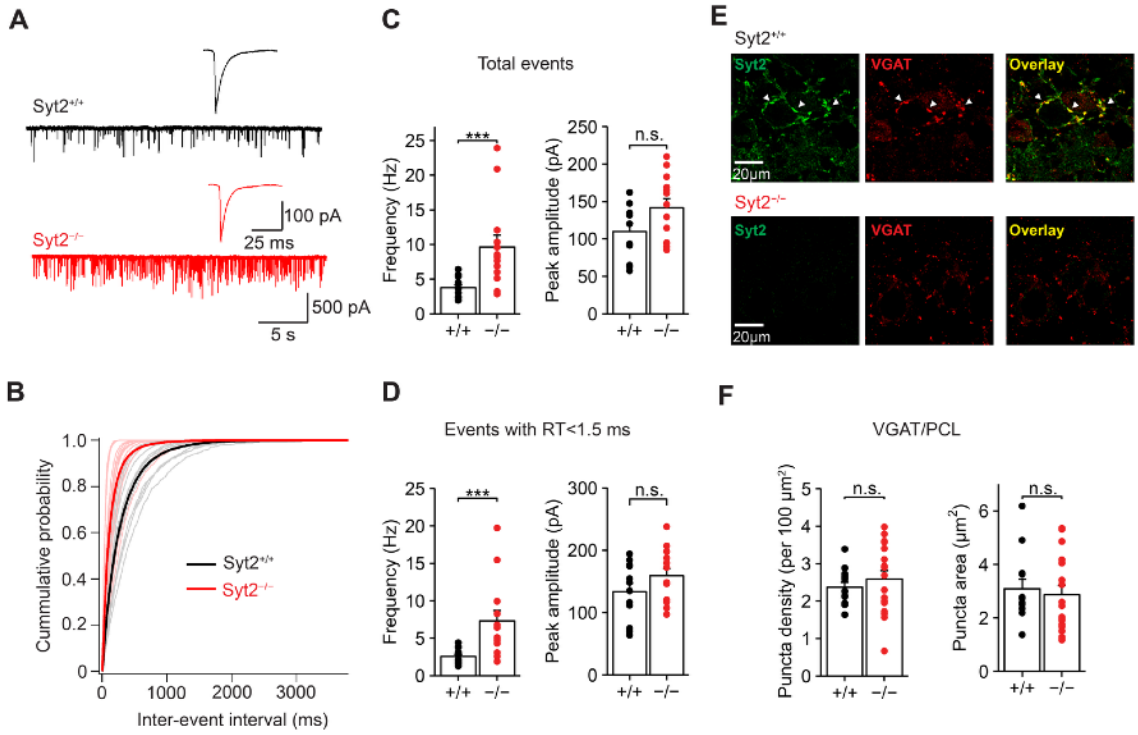

Figure 2-5. Genetic elimination of Syt2 increases mIPSC frequency

(A) Traces of mIPSCs in a PC at −70 mV $Syt2^{+/+}$ synapses (top, black traces) and $Syt2^{-/-}$ synapses (bottom, red traces). 1 µM TTX, 20 µM D-AP5, and 10 µM CNQX were added to external solution to block spontaneous AP firing and excitatory synaptic activity. Inset shows average mIPSC at expanded time scale (averages from 1073 and 2132 single events).

(B) Cumulative histograms of mIPSC inter-event interval (gray: from individual PCs of $Syt2^{+/+}$ mice; black: average of $Syt2^{+/+}$ data; light red: from individual PCs of $Syt2^{-/-}$ mice; red: average of $Syt2^{-/-}$ data).

(C) Comparison of mIPSC frequency (left) and peak amplitude (right) between $Syt2^{+/+}$ and $Syt2^{-/-}$ mice. Bars represent mean ± SEM, points indicate data from individual experiments. Data were obtained from 12 PCs ($Syt2^{+/+}$) and 13 PCs ($Syt2^{-/-}$).

(D) Similar data as shown in (C), but for mIPSCs with 20–80% rise time < 1.5 ms, presumably corresponding to synaptic events generated by BC terminals (Roth and Häusser, 2001).

(E) Confocal light-micrograph of Syt2 immunoreactivity (left), VGAT immunoreactivity (center), and overlay (right) in $Syt2^{+/+}$ (top) and $Syt2^{-/-}$ (bottom) mice; single confocal sections.

(F) Summary bar graphs of puncta density (left) and puncta cross-sectional area (right) in the PC layer. Bars represent mean ± SEM, circles indicate data from individual experiments.

2005; Xu et al., 2007). However, it is controversial whether Syt2, the isoform expressed in BC terminals, is faster than the other Ca^{2+} sensors (Nagy et al., 2006; Xu et al., 2007; Kochubey et al., 2016). To address this question, we attempted to rescue transmitter release at BC–PC synapses in $Syt2^{-/-}$ mice by viral expression of Syt2, the naturally expressed synaptotagmin isoform (**Figure 2-6**; **Figure 2-7**; **Table 2-2**). A helper-dependent adenovirus (HdAd) construct was used to express Syt2 and enhanced green fluorescent protein (EGFP) under the control of two synapsin promoters (**Figure 2-6A**). The virus was injected at postnatal day (P) 3 to 6, giving sufficient time for expression until P14 to 16 (**Figure 2-6B**). HdAd-mediated expression of Syt2 in $Syt2^{-/-}$ mice led to a complete rescue of IPSC peak amplitude (Syt2 rescue versus $Syt2^{-/-}$: $P < 0.0001$; Syt2 rescue versus $Syt2^{+/+}$: $P = 0.412$; **Figure 2-7**; **Figure 2-7A** and 2-7B). Similarly, adenovirus-mediated expression of Syt2 led to a complete rescue of all other measured synaptic parameters (**Figure 2-7C**–F).

Next, we attempted to rescue transmitter release in $Syt2^{-/-}$ mice by viral expression of Syt1, a synaptotagmin isoform naturally absent from BC–PC synapses (**Figure 2-6; Figure 2-7**; **Table 2-2**). Similar to virally expressed Syt2, HdAd-expressed Syt1 fully rescued IPSC peak amplitude (Syt1 versus $Syt2^{+/+}$; $P = 0.861$). These results indicate that Syt2 and Syt1 fully rescued the IPSC amplitude in an interchangeable manner.

To directly test whether Syt1 and Syt2 mediated transmitter release with different time course, we quantified the time course of release (TCR) using deconvolution (**Figure 2-6C**–F). Unitary IPSCs were first recorded in standard extracellular solution containing 2 mM Ca^{2+}, aligned to the peak of the presynaptic AP, and averaged to generate a unitary IPSC waveform (**Figure 2-6C** and 2-6D). Subsequently, IPSCs were recorded in extracellular solution containing 0.7 mM Ca^{2+}, aligned to the 50% rise point, and averaged to generate a quantal IPSC waveform (**Figure 2-6D**, inset). Finally, the TCR was obtained by deconvolution of the two traces (Experimental Procedures; **Figure 2-6E**). For rescue with Syt2, the latency of the TCR was 1.17 ± 0.12 ms and the half-duration was 0.78 ± 0.13 ms (11 pairs). In contrast, for rescue with Syt1, both the latency of the TCR (1.64 ± 0.11 ms) and the half-duration were significantly longer (2.00 ± 0.35 ms; 14 pairs; $P = 0.009$ and 0.006, respectively; **Figure 2-6F**). These results indicate that different synaptotagmin

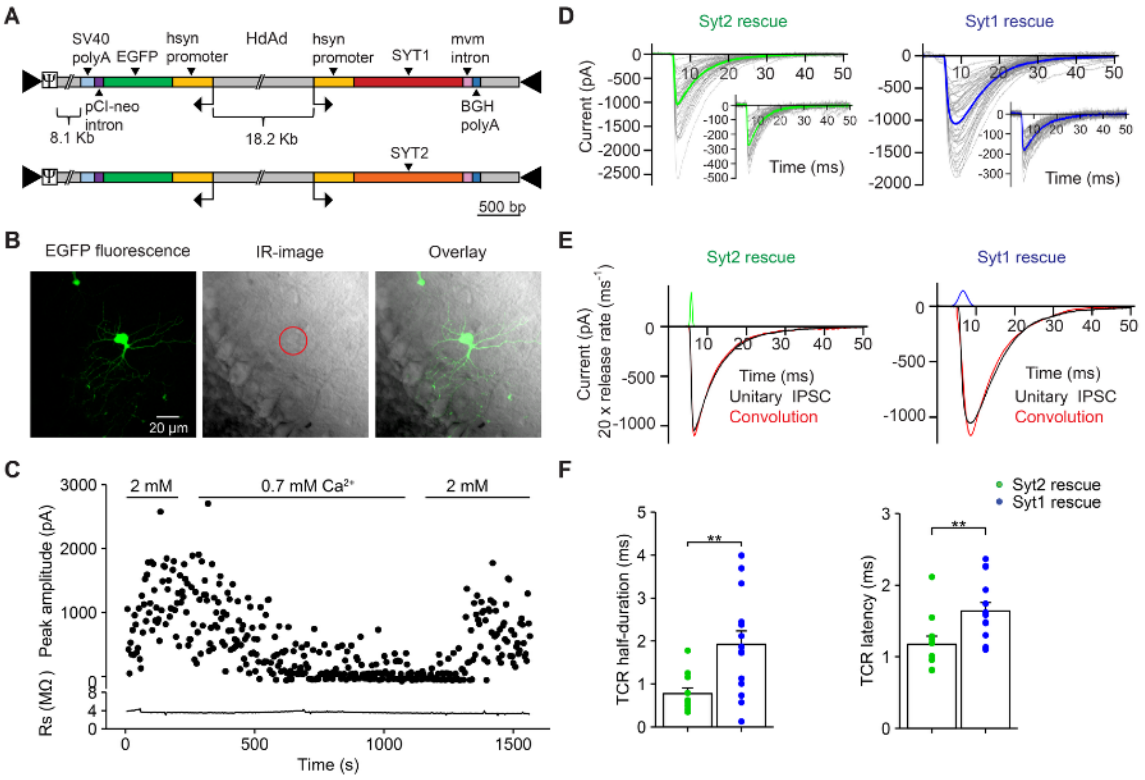

Figure 2-6. Syt2 mediates faster release than Syt1 at BC–PC synapses

(A) Schematic illustration of the helper-dependent adenovirus (HdAd) constructs used for rescue experiments. Hsyn, human synapsin promoter; mvm, minute virus of mice intron; SV40 polyA, Simian virus 40 poly A; BGH polyA, bovine growth hormone poly A.

(B) Confocal stack projection of a cerebellar BC in the molecular layer (left), infrared videomicroscopy light-micrograph (center), and overlay (right). The BC is strongly fluorescent, showing successful infection with HdAd.

(C, D) Analysis of TCR by deconvolution. To acquire unitary IPSCs evoked by single APs, recording was started in an extracellular solution containing 2 mM Ca^{2+}. To isolate quantal IPSCs, recording was continued in an extracellular solution containing 0.7 mM Ca^{2+} (C). Unitary IPSCs were aligned to the peak of the presynaptic AP and averaged (D, main graphs), and quantal IPSCs were aligned to the 50% onset point and averaged (D, insets). Left, HdAd-Syt2 rescue; right, HdAd-Syt1 rescue. Gray lines, individual traces; green and blue lines, averages.

(E) Different TCR after rescue with Syt2 and Syt1. Black, average unitary IPSC; green and blue, TCR (scaled up by a factor of 20); red, results from deconvolution. Left, HdAd-Syt2 rescue; right, HdAd-Syt1 rescue.

(F) Summary bar graph of latency (left) and half-duration of TCR (right). Bars represent mean ± SEM, points indicate data from individual experiments. Data were obtained from 11 pairs for HdAd-Syt2 rescue and 14 pairs for HdAd-Syt1 rescue.

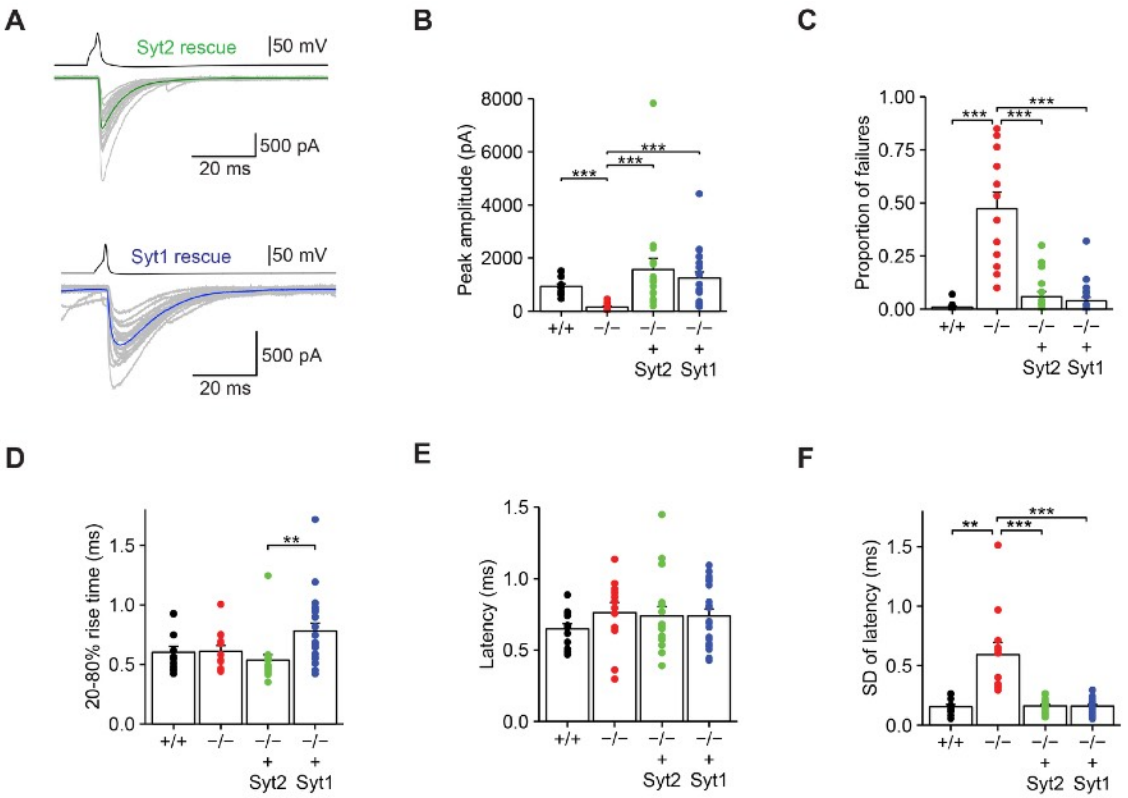

Figure 2-7. Rescue of functional properties of synaptic transmission with Similar infection and rescue levels for HdAd-Syt2 and HdAd-Syt1

(A) Original traces of unitary IPSCs after infection of the presynaptic neuron with HdAd-Syt2 (left) or HdAd-Syt1 (right). Upper traces represent presynaptic AP, lower traces show 20 consecutive IPSC traces (gray), superimposed with the average (green and blue, respectively). Note that HdAd-Syt2 and HdAd-Syt1 were equally effective in rescuing the peak amplitude of evoked IPSCs.
(B–F) Comparison of IPSC peak amplitude (B), proportion of failures (C), 20–80% rise time (D), latency (E), and standard deviation of latency (F). Black, data from $Syt2^{+/+}$ synapses; red, data from $Syt2^{-/-}$ synapses; green, HdAd-Syt2 rescue; blue, HdAd-Syt1 rescue (both on $Syt2^{-/-}$ background). Bars represent mean ± SEM, circles indicate data from individual experiments. Note that both HdAd-Syt2 and HdAd-Syt1 similarly rescued peak amplitude, proportion of failures, latency, and standard deviation of latency, but differentially rescued the 20–80% rise time.

isoforms, when expressed in GABAergic synapses in their natural context, have different kinetic properties. Syt2-mediated release shows both a shorter latency and a higher temporal precision.

Rescue with Syt2 generates faster pool refilling rates

A hallmark property of GABAergic synapses is the ability to release transmitter in a sustained manner during repetitive stimulation (Kraushaar and Jonas, 2000; Sakaba, 2008; Hu et al., 2014). To test whether the synaptotagmin isoform also controls the rate of replenishment of the vesicular pool, we applied 100-Hz trains of 50 APs and analyzed the dynamics of synaptic transmission after rescue with either Syt2 or Syt1 (**Figure 2-8**). Both HdAd-Syt2 and HdAd-Syt1 synapses showed depression during high-frequency trains of stimuli (**Figure 2-8A**). However, the ratio $IPSC_{50}$ / $IPSC_1$ was significantly larger for Syt2 rescue than for Syt1 rescue ($IPSC_{50}$ / $IPSC_1$ = 0.56 ± 0.09 for HdAd-Syt2 synapses; 0.21 ± 0.02 for HdAd-Syt1 synapses; 10 and 9 pairs, respectively; P = 0.009). In contrast, synaptic depression after Syt2 rescue was not significantly different from that in $Syt2^{+/+}$ synapses ($IPSC_{50}$ / $IPSC_1$ = 0.46 ± 0.05; 9 pairs; P = 0.54; **Figure 2-8C**). Thus, Syt2 better supported sustained synaptic transmission during high-frequency activity than Syt1.

Differences in the steady-state amplitude of IPSCs during repetitive stimulation could be generated by differences in readily releasable pool size (RRP), release probability, or replenishment rate. We therefore determined these parameters by analysis of cumulative release (Neher, 2015; **Figure 2-8D**). To determine absolute values of RRP size and refilling rate, we further measured quantal size by nonstationary fluctuation analysis (**Figure 2-10**). Cumulative IPSC amplitude was plotted against stimulus number, and the last 10 data points were fit by linear regression. The size of the RRP was then determined from the intersection of the regression line with the ordinate, and release probability was quantified as the ratio $IPSC_1$ / RRP size. Finally, the replenishment rate was measured as the slope of the regression line (**Figure 2-8D**). Comparison of HdAd-Syt2 and HdAd-Syt1 synapses revealed that the RRP size and release probability were not significantly different (RRP = 44.3 ± 7.1 vesicles and 37.6 ± 5.3 vesicles; P_r = 0.20 ± 0.02 and 0.22 ± 0.03; 10 and 9 cells; P > 0.99 and P = 0.92, respectively; **Figure 2-8F**, right and 6G, left). In contrast, the refilling rate was significantly larger in HdAd-Syt2 than HdAd-Syt1 synapses (3.91 ± 0.66 quanta ms^{-1} and 1.78 ± 0.12 quanta ms^{-1}; P = 0.008). Refilling rate of $Syt2^{+/+}$ synapses was not significantly different from Syt2 rescue, but markedly different from Syt1 rescue (P = 0.55 and 0.006, respectively; **Figure 2-8G**, right). Control experiments in the presence of 300 µM of the low-affinity

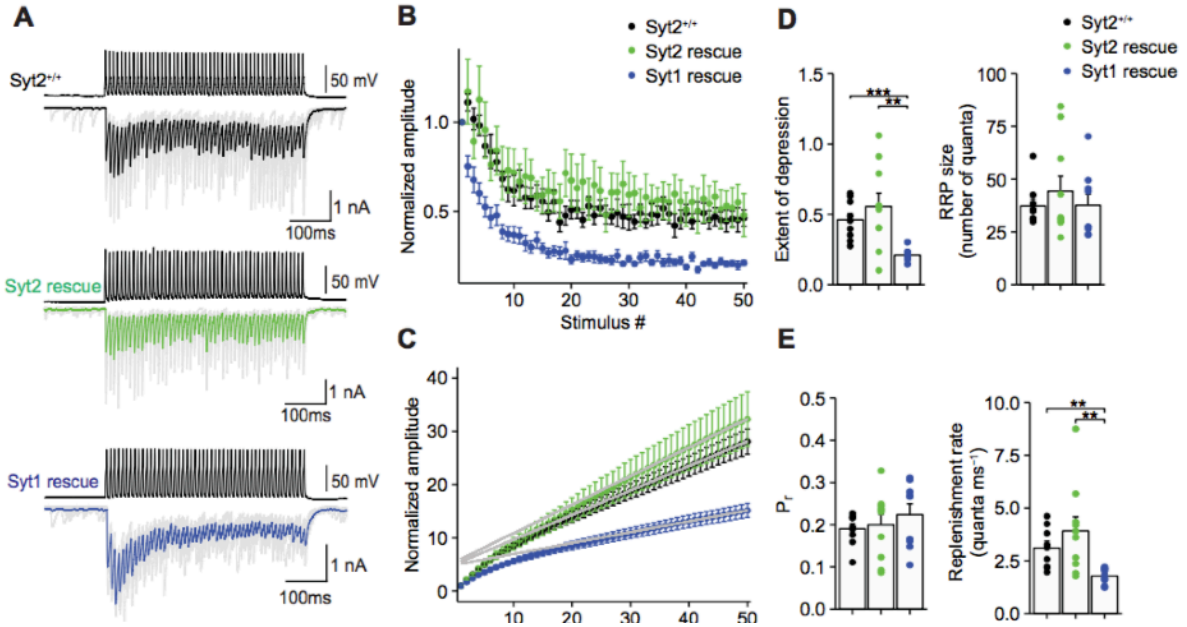

Figure 2-8. Syt2 mediates faster vesicular pool refilling during train stimulation than Syt1 at BC–PC synapses

(A) Unitary IPSCs evoked by a train of 50 APs at 100 Hz for $Syt2^{+/+}$ (top), HdAd-Syt2 rescue (center) and HdAd-Syt1 rescue (bottom; both on $Syt2^{-/-}$ background).

(B) Normalized IPSC peak amplitudes, plotted against stimulus number. Black circles, $Syt2^{+/+}$; green circles, HdAd-Syt2 rescue; blue circles, HdAd−Syt1 rescue (both on $Syt2^{-/-}$ background). Data were obtained from 9, 10, and 9 pairs. Note that depression is stronger in the HdAd-Syt1 than in HdAd-Syt2 rescue experiments.

(C) Quantitative analysis of pool size and refilling rate. IPSC peak amplitude was divided by $IPSC_1$, averaged across cells, and cumulatively plotted against stimulus number. The last ten points were fit by linear regression. Size of the RRP was determined from intersection of the regression line with the ordinate, whereas refilling rate was determined from the slope of the regression line. Release probability was quantified as the ratio of normalized $IPSC_1$ over pool size.

(D, E) Summary bar graph of steady-state depression ($IPSC_{50}$ / $IPSC_1$; D, left), RRP (D, right), release probability (P_r, E, left), and replenishment rate (E, right). Black, data from $Syt2^{+/+}$ synapses; green, HdAd-Syt2 rescue; blue, HdAd-Syt1 rescue (both on $Syt2^{-/-}$ background). Bars represent mean ± SEM, circles indicate data from individual experiments. Note that replenishment rate was ~2-fold faster with HdAd-Syt2 rescue than with HdAd-Syt1 rescue.

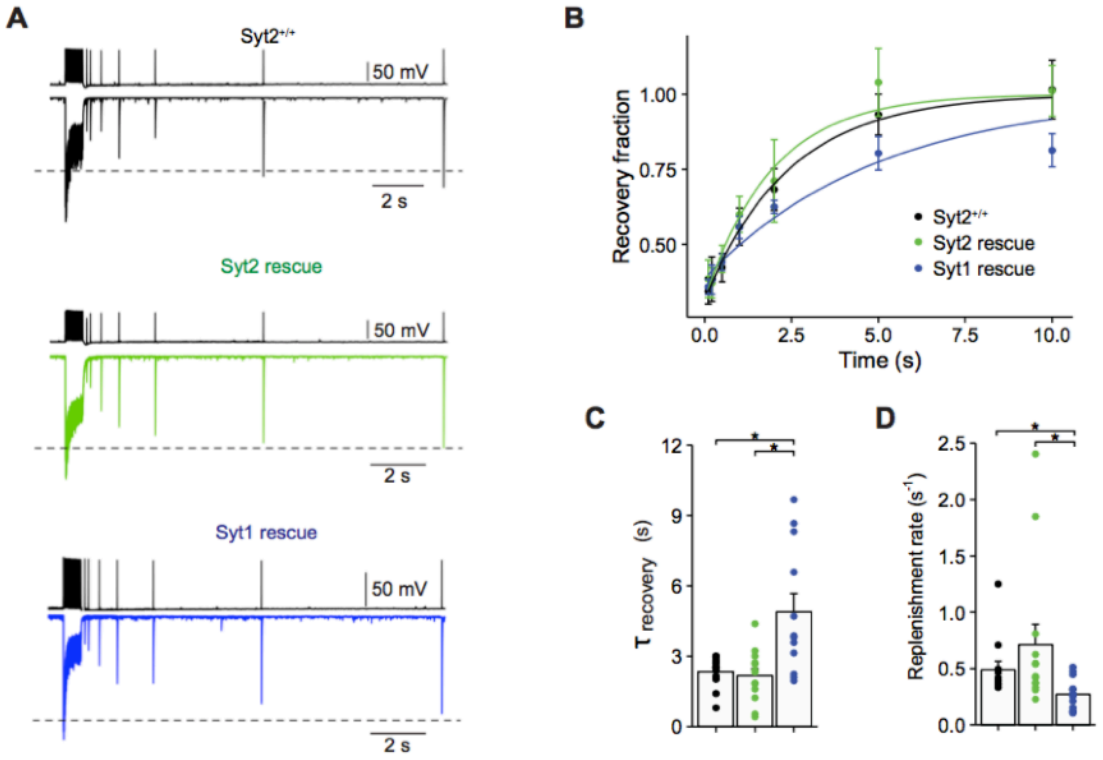

Figure 2-9. Syt2 mediates faster vesicular pool refilling after train stimulation than Syt1 at BC–PC synapses.

(A) Unitary IPSCs evoked by a train of 50 APs at 100 Hz, followed by a single test stimulus with different recovery time intervals for Syt2$^{+/+}$ synapses (top), HdAd-Syt2 rescue (center), and HdAd-Syt1 rescue (bottom; both on Syt2$^{-/-}$ background).

(B) Plot of peak amplitude of IPSC evoked by the test stimulus, normalized to the amplitude of the first IPSC in the preceding train. Black circles, Syt2$^{+/+}$ synapses; green circles, HdAd-Syt2 rescue; blue circles, HdAd-Syt1 rescue (both on Syt2$^{-/-}$ background). Continuous curves represent exponential functions fit to the data points. Note that recovery from depression is faster in the HdAd-Syt2 than in HdAd-Syt1 rescue experiments, and comparable to that in Syt2$^{+/+}$ synapses.

(C, D) Summary bar graph of recovery time constant (C) and corresponding replenishment rate (D). Time constants were 2.35 ± 0.19 s (Syt2$^{+/+}$, 12 pairs), 2.17 ± 0.31 s (HdAd-Syt2 rescue in Syt2$^{-/-}$ background; 13 pairs), and 4.89 ± 0.79 s (HdAd- Syt1 rescue in Syt2$^{-/-}$ background; 12 pairs).

competitive $GABA_A$ receptor antagonist (1,2,5,6-tetrahydropyridine-4-yl)-methylphosphinic acid (TPMPA) and the $GABA_B$ receptor antagonist CGP55845 gave similar results (**Figure 2-11**), indicating that the results of deconvolution

Table 2-2. Differential helper-dependent adenovirus-mediated rescue by Syt2 and Syt1 in Syt2$^{-/-}$ mice

Parameter	HdAd-Syt2	HdAd-Syt1	P
Latency	0.74 ± 0.06 (17)	0.74 ± 0.05 ms (21)	>0.9999
SD latency	0.16 ± 0.01 ms (17)	0.16 ± 0.01 ms (21)	>0.9999
20-80% rise time	0.534 ± 0.05 ms (17)	0.781 ± 0.065 ms (21)	0.0026
IPSC peak amplitude	1559.3 ± 426.4 pA (17)	1250.3 ± 225.2 pA (21)	0.9740
IPSC decay time	7.71 ± 0.41 ms	9.27 ± 0.55 ms	0.2700
Proportion of failure	5.91 ± 2.28% (17)	3.81 ± 1.67% (21)	>0.9999
Paired-pulse ratio $IPSC_2/IPSC_1$	1.01 ± 0.04 (10)	0.82 ± 0.05 (10)	0.0294
$IPSC_{50}/IPSC_1$	0.67 ± 008 (10)	0.39 ± 0.032 (10)	0.0030
Recovery from depression τ	2.17 ± 0.31 s (13)	4.89 ± 0.79 s (12)	0.011

All experiments were performed in Syt2$^{-/-}$ mice.

Mean ± SEM (n, number of experiments).

analysis were not confounded by desensitization of saturation of postsynaptic receptors (Jones et al., 2001; Sakaba, 2008; Arai and Jonas, 2014).

To further test whether the synaptotagmin isoform also determined the kinetics of pool refilling after a depleting train, we examined the time course of recovery from depression (**Figure 2-9**). 100-Hz train of 50 stimuli was applied to deplete the pool, followed by a single stimulus to probe the time course of refilling of the pool. Recovery from depression was faster in Syt2-rescued than in Syt1-rescued synapses (**Figure 2-9A** and 2-9C). On average, the recovery time constant was 2.17 ± 0.31 s for HdAd-Syt2 synapses and 4.89 ± 0.79 s for HdAd-Syt1 synapses

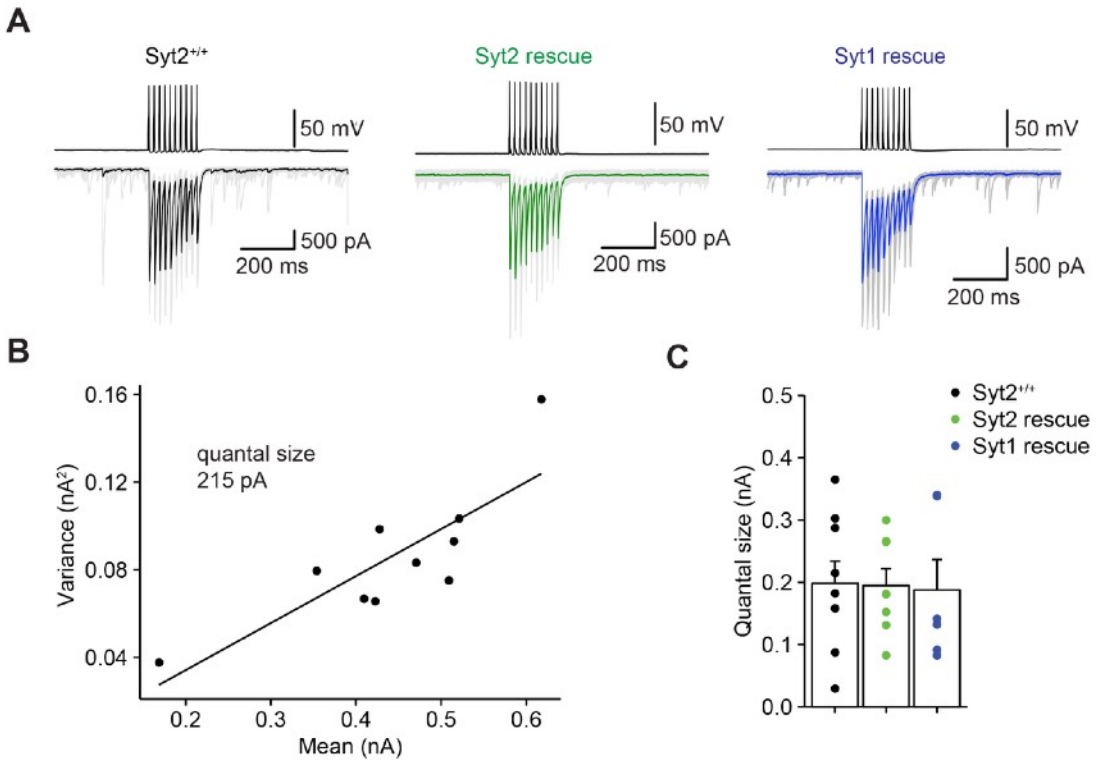

Figure 2-10. Determining quantal size at BC–PC synapses

(A) Evoked IPSCs following a 50-Hz train of ten stimuli given to the presynaptic BC. Left, $Syt2^{+/+}$; center, Syt2 rescue; right, Syt1 rescue (both in $Syt2^{-/-}$ mice).

(B) Plot of variance against mean amplitude for each IPSC evoked by train stimulation. Data from a representative experiment (from a $Syt2^{+/+}$ mouse). Data points were fit by linear regression. The line slope, corresponding to quantal size, was 215 pA. Linearity of the data is consistent with constant quantal size during train stimulation.

(C) Summary bar graph of quantal size for $Syt2^{+/+}$, HdAd-Syt2 rescue, and HdAd-Syt1 rescue (both in $Syt2^{-/-}$ mice). Data from 9, 8, and 6 pairs.

(13 and 12 pairs, respectively; P = 0.011; **Figure 9C**). Similarly, the corresponding replenishment rates were significantly larger for Syt2-rescued than in Syt1-rescued synapses (P = 0.011; **Figure 2-9D**). Recovery time constant and replenishment rate of $Syt2^{+/+}$ synapses were not significantly different from Syt2 rescue, but markedly different from Syt1 rescue (P = 0.5 and 0.02, respectively; **Figure 2-9C**). In conclusion, the synaptotagmin isoform not only controls the TCR, but also the rate of replenishment of the releasable pool, with faster refilling for Syt2, but slower refilling for Syt1.

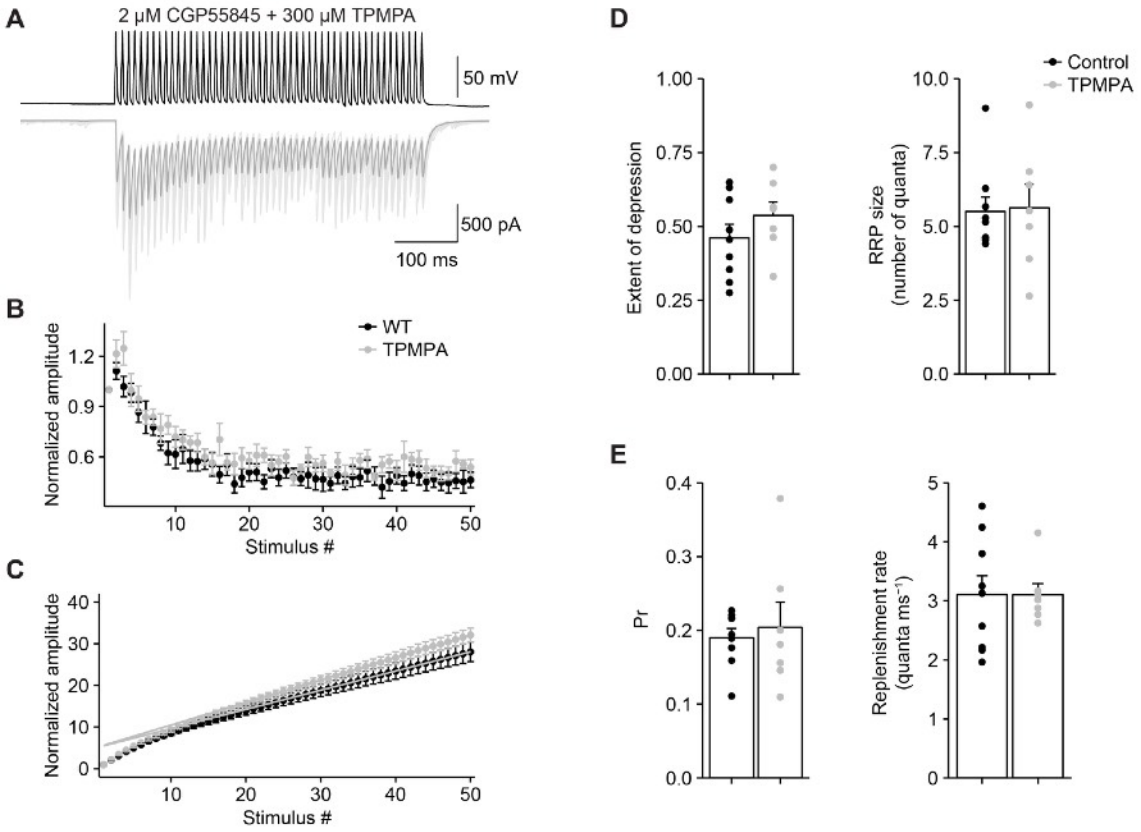

Figure 2-11. Estimates of pool size and refilling rates are not affected by postsynaptic receptor saturation or desensitization

(A) Presynaptic APs (top) and evoked IPSCs (bottom) in the presence of 300 µM of low-affinity $GABA_A$ receptor antagonist TPMPA. 2 µM CGP55845 was further added to minimize effects of TPMPA on transmitter release via presynaptic $GABA_B$ receptors. 10 consecutive individual traces (light gray) and the corresponding average trace (dark gray) are shown superimposed.

(B, C) Plot of normalized IPSC peak amplitude against stimulus number (B, non-cumulative amplitude; C, cumulative plot). Black, data in control; gray, in the presence of 300 µM TPMPA. Lines represent the results of linear regression of last ten data points. Note that the pool size, as indicated by the intersection of the regression line with the ordinate, is almost identical in the absence and presence of TPMPA.

(D, E) Summary bar graphs of the extent of depression after 50 APs (D, left), size of the readily releasable pool (RRP; D, right), release probability (P_r; E, left), and replenishment rate (E, right). Bars indicate mean ± SEM; solid circles represent data from individual experiments. Data from 9 and 7 pairs, respectively. Note that the estimates were similar for control and TPMPA (P = 0.3, 0.76, 0.76, and > 0.99). All data were obtained from wild-type synapses.

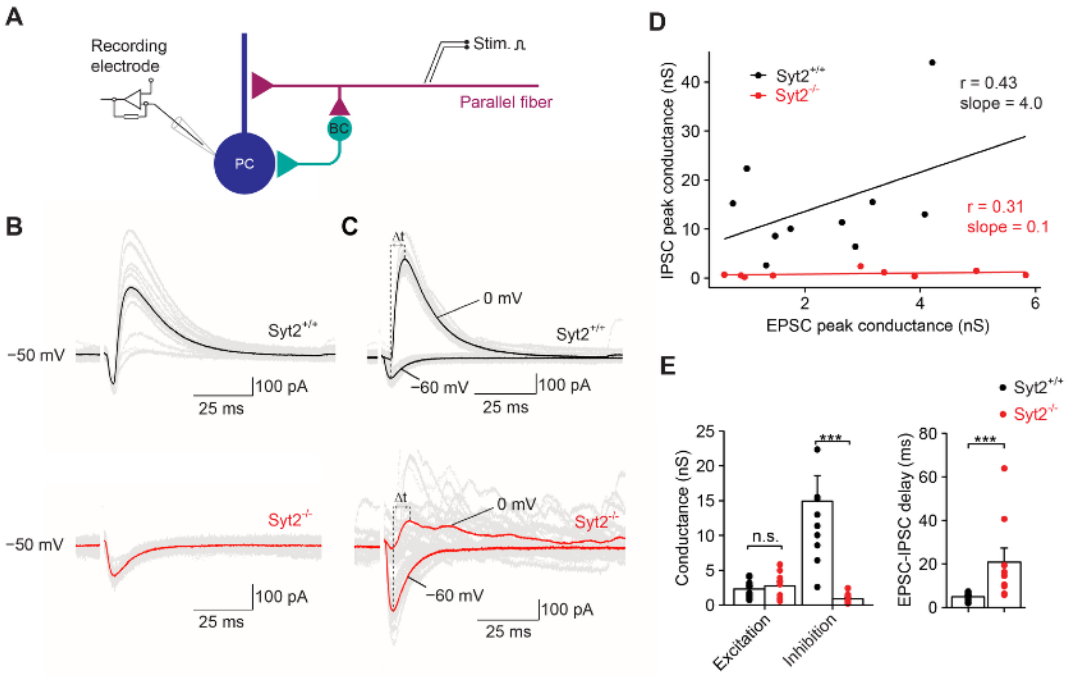

Figure 2-12. Fast feedforward inhibition in cerebellum critically depends on the presence of Syt2

(A) Schematic illustration of recording configuration for analysis of feedforward inhibition. Whole-cell recording from PC; stimulation of parallel fibers is expected to evoke both monosynaptic EPSCs and disynaptic IPSCs.

(B) Recording of mixed EPSCs and IPSCs at −50 mV. As the holding potential is between the reversal potentials for excitatory and inhibitory events, EPSCs are inwardly and IPSCs outwardly directed.

(C) Recording of EPSCs and IPSCs isolated by setting the holding potential to the reversal potential of one of the conductances (−60 mV and 0 mV, respectively). Top, $Syt2^{+/+}$; bottom, $Syt2^{-/-}$. Single traces (gray) and averages (black for $Syt2^{+/+}$ and red for $Syt2^{-/-}$).

(D) Scatter plot of inhibitory (IPSG) against excitatory peak conductance (EPSG) for $Syt2^{+/+}$ (black) and $Syt2^{-/-}$ synapses (red). Data points were fit by linear regression. Similar extracellular stimulus intensities in the two data sets.

(E) Summary bar graphs of peak conductance (left) and EPSC–IPSC delay (measured from peak to peak). Bars represent mean ± SEM, circles indicate data from individual experiments.

Syt2 is essential for feedforward inhibition in cerebellum

The present results suggest that the selective use of Syt2 at BC synapses plays a key role for the efficacy and timing of inhibitory synaptic transmission in the cerebellum, parameters which are highly relevant for feedforward inhibition. To directly test the role of Syt2 in feedforward inhibition, we measured amplitude and timing of disynaptic IPSCs evoked by extracellular parallel fiber stimulation (Mittmann et al., 2005; Bao et al., 2010; **Figure 2-12**). Monosynaptic EPSCs and

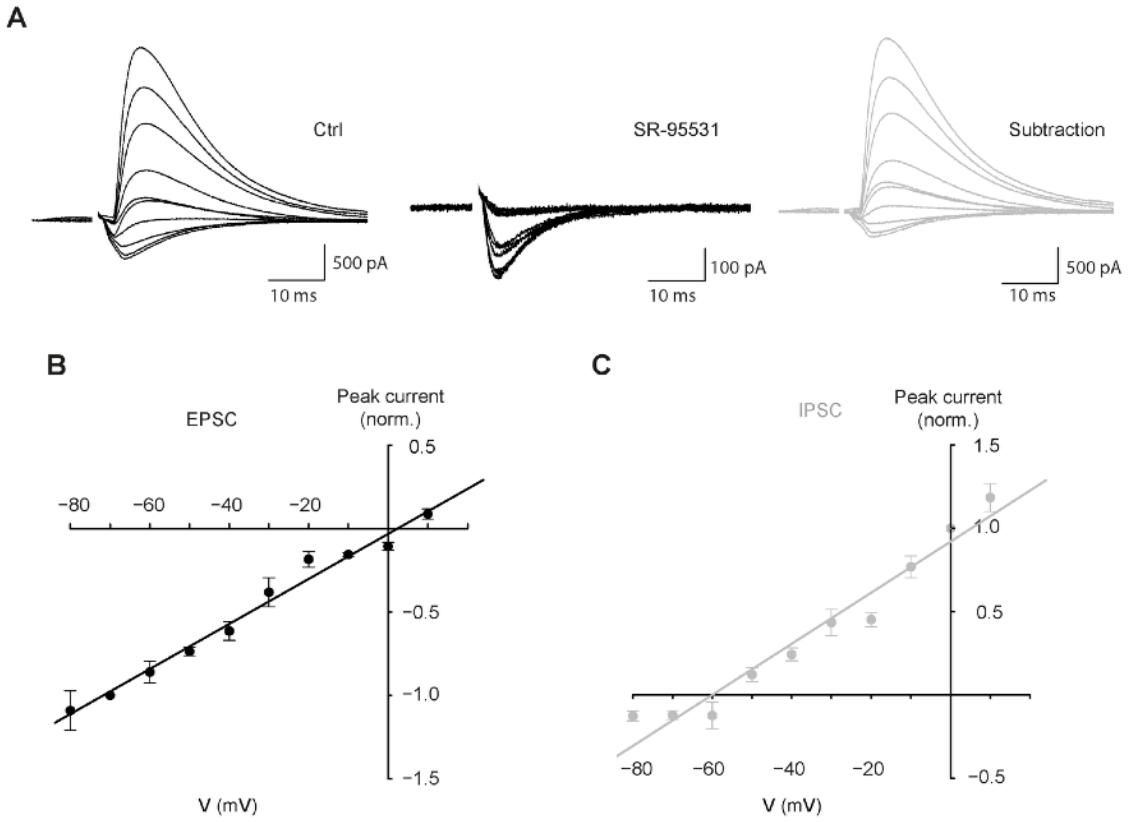

Figure 2-13. Reversal potential of monosynaptic EPSCs and disynaptic IPSCs evoked by parallel fiber stimulation

(A) Left, recording of mixed EPSCs and IPSCs; center, recording of EPSCs in the presence of 10 µM SR-95531; right, traces obtained by digital subtraction; traces were recorded at membrane potentials from −80 mV to +10 mV in 10-mV steps in a PC.
(B) Current-voltage relation for pharmacologically isolated EPSCs.
(C) Current-voltage relation for IPSCs isolated by digital subtraction. Data points indicate mean values from 4 experiments. Current amplitudes were normalized to the values at −70 mV and 0 mV, respectively. Data points were fit by linear regression, giving reversal potentials of 3.1 mV (B) and −60.0 mV (C).

disynaptic IPSCs were either measured together at a holding potential of −50 mV, where EPSCs were detected as inward currents and IPSCs as outward currents (**Figure 2-12B**), or at membrane potentials of −60 mV and 0 mV, where EPSCs and IPSCs could be studied in isolation (**Figure 2-13**). In slices from $Syt2^{+/+}$ mice, monosynaptic EPSCs were followed by large disynaptic IPSCs, confirming powerful feedforward inhibition in this circuit (Mittmann et al., 2005). In contrast, in slices from $Syt2^{-/-}$ mice, disynaptic IPSCs were markedly impaired (**Figure 2-12B** and 2-12C). Comparison of slices from $Syt2^{+/+}$ and $Syt2^{-/-}$ mice indicated that the excitatory peak conductance was the same (2.3 ± 0.4 nS versus 2.7 ± 0.6 nS; 10 and 9 cells; P = 0.84), whereas the inhibitory peak conductance was severely reduced (14.9 ± 3.7 nS versus 0.7 ± 0.2 nS; P < 0.001). Furthermore, the delay between EPSCs and IPSCs was markedly prolonged (4.9 ± 0.6 ms versus 20.8 ± 6.4 ms; P < 0.001). These results demonstrate that Syt2 plays a critical role for both efficacy and timing of feedforward inhibition in the cerebellum.

2.4 Discussion

The present results provide new insights into the mechanisms of Ca^{2+}-dependent exocytosis at the cerebellar BC–PC synapse, a major inhibitory synapse in the brain. First, we identified Syt2 as the primary Ca^{2+} sensor of exocytosis. Second, viral rescue experiments revealed that the naturally occurring sensor Syt2 mediated transmitter release with shorter latency and higher temporal precision than the alternative sensor Syt1. Finally, Syt2 mediated faster refilling of the vesicular pool during repetitive stimulation than Syt1, suggesting that Syt2 controls both exo- and endocytosis at GABAergic synapses. Thus, the use of Syt2 as a release sensor contributes to rapid signaling at this GABAergic synapse (**Figure 2-14**).

Syt2-mediated fast GABA release at inhibitory synapses

The mammalian genome encodes 16 synaptotagmins, eight of which bind Ca^{2+} (Syt1, 2, 3, 5, 6, 7, 9, and 10; Chapman, 2002; Südhof, 2002), and three of which were reported to act as fast release sensors (Syt1, 2, and 9; Xu et al., 2007; Kochubey et al., 2016). However, the functional significance of this molecular diversity is incompletely understood.

It is generally thought that Syt1 is predominant in cortical circuits, whereas

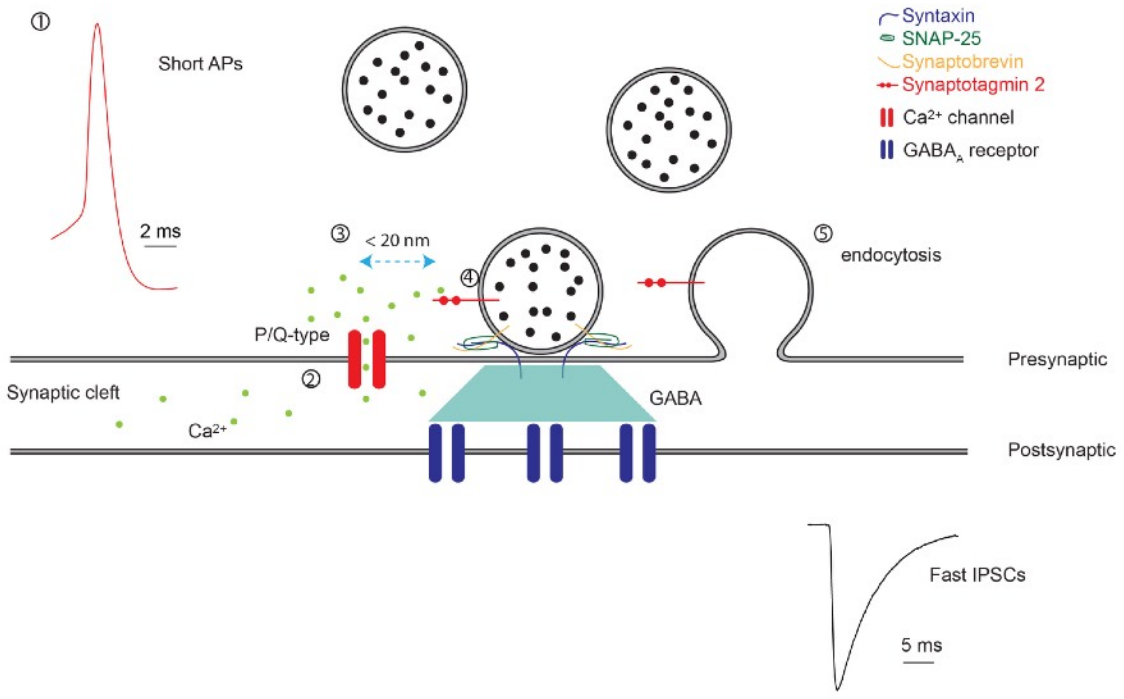

Figure 2-14. Mechanisms of fast signaling at cerebellar BC–PC synapses

Upper left, AP recorded in a presynaptic BC. Lower right, IPSCs recorded in a postsynaptic PC. Mechanisms of rapid signaling include: (1) Short duration of presynaptic AP, (2) fast gating of presynaptic P/Q-type Ca^{2+} channels (Arai and Jonas, 2014; Li et al., 2007), (3) short coupling distance between presynaptic Ca^{2+} channels and release sensor (synaptotagmin 2, red) (Arai and Jonas, 2014), (4) fast kinetics of Syt2-mediated exocytosis (present paper), and (5) fast replenishment of releasable vesicle pool due to Syt2-mediated endocytosis (present paper).

Syt2 is more prevalent in the cerebellum, brainstem, and spinal cord (Pang et al., 2006a, b; Mittelsteadt et al., 2009; Kochubey et al., 2016). However, our immunohistochemical analysis showed that Syt1 is highly expressed in the cerebellum, where it is mainly localized to excitatory synapses. This idea is supported by the disynaptic inhibition experiments, which show that Syt2 deletion suppresses inhibition, but leaves excitation unchanged (**Figure 2-12**). Thus, Syt1 and Syt2 coexist in the circuit, but are expressed in a synapse-specific manner.

It is also believed that Syt2 is more abundantly used in GABAergic interneurons. Consistent with this idea, Syt2 is highly expressed in subsets of

GABAergic hippocampal interneurons (Pang et al., 2006a; Kerr et al., 2008; Sommeijer and Levelt, 2012). Genetic deletion of Syt1 substantially reduces, but does not abolish, transmitter release (Kerr et al., 2008), suggesting that in the hippocampus Syt1 and Syt2 may work in concert. The results from immunocytochemistry, knockout, and rescue experiments convergently suggest that Syt2 is the major Ca^{2+} sensor triggering fast transmitter release at the cerebellar BC–PC synapse. Thus, both cell type (GABAergic interneurons versus glutamatergic principal neurons) and brain region (cerebellum versus other brain areas) determine which synaptotagmin isoform is used.

The molecular identity of the Ca^{2+} sensor mediating the residual release component in $Syt2^{-/-}$ synapses is presently unclear. The residual component might be generated by a compensatory upregulation of Syt1, although our immunolabeling data argue against this possibility (**Figure 2-2C** and 2-2D). Alternatively, any of the other synaptotagmins, or an entirely different Ca^{2+} sensor, may be involved. One possibility is that the residual component is mediated by Syt7 (Bacaj et al., 2013; Jackman et al., 2016). Consistent with this idea, the residual component shows profound facilitation and highly asynchronous kinetics (**Figure 2-4**). Analysis of double- or triple-knockout mice will be needed to test this hypothesis.

Syt2 controls fast exo- and endocytosis

The BC–PC synapse provides an ideal system to compare the functional properties of Syt2 with those of Syt1, the alternative Ca^{2+} sensor in synaptic transmission. As fast transmitter release at this synapse is almost completely dependent on Syt2, rescue experiments can be performed in $Syt2^{-/-}$ animals with minimal confounding effects of other synaptotagmin isoforms. Our rescue experiments revealed that Syt2 differs from Syt1 in both speed and temporal precision of transmitter release. Thus, our results corroborate the original suggestion of higher temporal precision for Syt2-mediated release (Xu et al., 2007), and extend these findings by showing that the synaptic latency is also isoform-dependent. However, they appear to be inconsistent with a recent study, which found no kinetic differences between Syt1 and Syt2 at the calyx of Held (Kochubey et al., 2016).

Differences in the shape of the Ca^{2+} transient at the sensor may explain the apparent discrepancies. In the present study, release was evoked by natural AP

waveforms. Because of the tight coupling between Ca^{2+} channels and sensors (Arai and Jonas, 2014), the Ca^{2+} transient “seen” by the sensor will be short, closely following the presynaptic Ca^{2+} current. Thus, the TCR will be shaped by the activation and deactivation rates of the sensor. In contrast, in the study by Kochubey et al. (2016), release was triggered by long voltage-pulses. Therefore, the rise in Ca^{2+} concentration will be long-lasting, and the TCR will be primarily shaped by the pool depletion and refilling; the deactivation rates of the sensor may be less relevant.

In addition to the difference in TCR, we found that synaptotagmins differentially controlled the rate of refilling of the releasable pool. Whereas the size of the RRP and the probability of release from this pool were similar for Syt2 and Syt1, the refilling rate was ~2-fold faster for Syt2 rescue. This result is consistent with several previous observations: that synaptotagmins couple to AP2 / clathrin (Zhang et al, 1994), that endocytosis at the Drosophila neuromuscular junction is suppressed by light-inactivation of synaptotagmin (Poskanzer et al., 2003), and that endocytosis at the calyx of Held is blocked by AP2 peptides (Hosoi et al., 2009). Thus, Syt2 may control both the speed of GABA release following single APs and the efficacy of release during trains of APs. Previous studies showed that the replenishment of the RRP at BC–PC synapses is dependent on intracellular Ca^{2+} concentration (Sakaba, 2008). Our results are consistent with the hypothesis that Syt2 is the molecular sensor that mediates the Ca^{2+} dependence of replenishment.

A clamping function of Syt2 at GABAergic synapses?

Whether genetic elimination of synaptotagmins increases the frequency of spontaneous release has been controversial. One potential problem is that changes in miniature release may be confounded by sprouting or homeostatic changes. Furthermore, the effects of synaptotagmin deletion on spontaneous release depend on the synaptic environment (Liu et al., 2009). Our results rigorously address this question. First, analysis of synaptic transmission is possible in the intact circuit, because of the extended survival of $Syt2^{-/-}$ mice in comparison to, e.g., $Syt1^{-/-}$ mice (Geppert et al., 1994; Kerr et al., 2008). Second, immunolabeling experiments reveal that the organization of the inhibitory microcircuits is maintained in the $Syt2^{-/-}$ mice (**Figure 2-5E** and 2-6F). Taken together, these results are consistent with a clamping function of Syt2 at BC–PC synapses (Giraudo et al., 2006). The molecular

mechanisms underlying this clamping function remain to be determined. Clamping could be achieved by an arrest of the partially zippered SNARE complex (Chicka et al., 2008). Alternatively, clamping may be generated by the competition of synaptotagmins for binding sites in the release machinery. In this model, Syt2 may prevent the access of other synaptotagmin isoforms, which may drive release at lower Ca^{2+} concentrations or even in the absence of Ca^{2+}.

Whether synaptotagmin “clamps” asynchronous release also has remained unclear. Genetic elimination of Syt1 at glutamatergic synapses was shown to selectively eliminate synchronous release, while asynchronous release was either unaffected (Geppert et al., 1994) or enhanced (Nishiki and Augustine, 2004). Differential effects on asynchronous release during and after a stimulus train have been also suggested (Maximov and Südhof, 2005). Our results show a significant enhancement of asynchronous release both during and after the train (**Figure 2-4**). This is consistent with a dual function of Syt2, which acts as both a trigger of synchronous release and a clamp of asynchronous release. Alternatively, it was proposed that synaptotagmins may operate as pure synchronizers of release (Nishiki and Augustine, 2004). However, for a pure synchronizer, the reduction in synchronous release should equate the enhancement of asynchronous release, which is not the case at BC–PC synapses. Thus, our results for Syt2 at GABAergic synapses seem inconsistent with a pure synchronizing function.

Molecular mechanisms underlying differential kinetics

Our results demonstrate that Syt2 has a kinetic advantage in terms of speed and temporal precision of synaptic transmission. What are the underlying molecular mechanisms? Syt2 has a sequence identity of ~76% with Syt1 in mice (Südhof, 2002). The C2A domain is largely conserved between Syt2 and Syt1, with only one amino acid difference in the three loops forming the putative Ca^{2+} binding site. However, the C2B domain is more divergent between isoforms, with three amino acid differences in the relevant loops (Südhof, 2002). These structural differences might explain our observations for two reasons. First, the C2B domain seems more relevant for the exocytotic Ca^{2+} sensing function than the C2A domain (Mackler et al., 2002; Nishiki and Augustine, 2004; Bacaj et al., 2013). Second, the C2B domain

is thought to represent the binding site for AP2, which might explain the effects of synaptotagmin isoform on pool replenishment.

Other regions of the synaptotagmin molecule may be also important. For example, the linker between C2A and C2B domains shows three amino acid differences between Syt1 and Syt2. Recent work suggested this linker to be critical for the function of synaptotagmins (Liu et al., 2014). In this scenario, the presence of two glycine residues in Syt2 could make the linker more flexible. Furthermore, the connector between the transmembrane segment and the C2A domain is seven amino acids shorter for Syt2 than for Syt1. This could be relevant for tight coupling between Ca^{2+} channels and synaptotagmins (Eggermann et al., 2012). Consistent with this idea, proteomic analysis revealed that Syt2, but not Syt1, is molecularly associated with Ca^{2+} channel alpha subunits (Müller et al., 2010). Finally, the C-terminus of synaptotagmins is highly divergent between the isoforms (Young and Neher, 2009). The C-terminus has been also suggested to be important for coupling, but is also for internalization of the protein from the plasma membrane (Jarousse and Kelly, 2001). Thus, both coupling distance and rate of endocytosis might be regulated by this region. Differential binding of Syt isoforms to Ca^{2+} channels or other presynaptic ion channels may also modify channel gating, and thereby affect the time course of presynaptic Ca^{2+} current, AP waveform, or both. Direct recordings from inhibitory presynaptic terminals will be needed to address these possibilities.

Relevance for microcircuit function

The selective use of Syt2 at BC output synapses may have important consequences for the function of cerebellar microcircuits. First, Syt2 may control the speed of feedforward inhibition (Mittmann et al., 2005; Bao et al., 2010). One major function of feedforward inhibition is that it narrows the time window for spiking and temporal summation (Pouille and Scanziani, 2001; Mittmann et al., 2005). Another function is shaping of the spatial activity pattern of PC activation following APs in parallel fiber beams (Mittmann et al., 2005; Bao et al., 2010). For both functions, the fast time course of inhibition is critically important. Previous studies showed that the delay of disynaptic inhibition is as short as ~1 ms at physiological temperature (Mittmann et al., 2005). We identify Syt2 as a molecular factor that contributes to this remarkable speed. Both BCs and stellate cells are thought to contribute to disynaptic inhibition.

The sensitivity of disynaptic IPSCs to Syt2 deletion (**Figure 2-12**) suggests that both BC and stellate cell output synapses use Syt2 for transmitter release. Paired recording experiments will be required to directly determine the identity of the sensor at stellate cell synapses.

Second, the selective use of Syt2 may be relevant for sustained inhibition in the intact network *in vivo*. In the awake, behaving animal, molecular layer interneurons fire APs at a frequency of ~20 Hz under resting conditions, and can be further activated by sensory stimuli (Ekerot and Jörntell, 2003). Under these conditions, depletion of the releasable pool would be expected. Therefore, the rapid replenishment of the pool mediated by Syt2 helps to maintain inhibitory output.

Finally, Syt2 may be important in synaptic diseases. In $Syt2^{-/-}$ or Syt2 mutant mice, the ataxia phenotype (Pang et al., 2006a, b) is readily explained by a failure of feedforward inhibition. Mutations in the Syt2 gene have been recently identified in humans (Herrmann et al., 2014). These mutations were primarily linked to a neuromuscular phenotype (Herrmann et al., 2014). Whether other mutations in the Syt2 gene do exist and whether these may generate a cerebellar phenotype, as predicted by the present data, remains to be determined.

Chapter 3. Triple function of synaptotagmin 7 ensures efficiency of high−frequency transmission at central GABAergic synapses (Chen et al., 2017b)

3.1 Introduction

Synaptotagmins play a key role in Ca^{2+}-dependent transmitter release (Südhof, 2002; Chapman, 2002; Koh and Bellen, 2003). The mammalian genome encodes 17 synaptotagmins, eight of which bind Ca^{2+} (Syt1, 2, 3, 5, 6, 7, 9, and 10; Südhof, 2002). Three of the synaptotagmins, Syt1, Syt2 and Syt9, have been demonstrated to operate as fast release sensors (Geppert et al., 1994; Xu et al., 2007; Kerr et al., 2008; Kochubey et al., 2016; Chen et al., 2017a). However, the function of the remaining isoforms remains unclear. Syt7 is highly expressed in the brain, but its function is controversial (Chen and Jonas, 2017). In the zebrafish neuromuscular junction and in the young calyx of Held, Syt7 promotes asynchronous release during repetitive stimulation (Wen et al., 2010; Bacaj et al., 2013; Luo and Südhof, 2017). However, in cultured hippocampal synapses, Syt7 was suggested to promote replenishment of the releasable vesicle pool (Liu et al., 2014). Finally, in hippocampal and corticothalamic synapses in slices, Syt7 was recently proposed to operate as a Ca^{2+} sensor of synaptic facilitation (Jackman et al., 2016). How these divergent functions can be reconciled remains to be determined; one possibility is that Syt7 has different functions at different synapses.

Recent results indicate that Syt7 is highly expressed in inhibitory synapses. For example, Syt7 mRNA is abundant in fast-spiking parvalbumin-expressing (PV^+) basket cells in hippocampus and cerebellum (Kerr et al., 2008; Paul et al., 2012; Földy et al., 2015). However, the GABAergic output synapses of both cerebellar and hippocampal BCs show only minimal asynchronous transmitter release during and after action potential (AP) trains (Hefft and Jonas, 2005; Eggermann and Jonas, 2012; Arai and Jonas, 2014). Furthermore, the output synapses of these neurons exhibit synaptic depression rather than facilitation during repetitive stimulation (Kraushaar and Jonas, 2000; Eggermann and Jonas, 2012). Thus, the functional properties of synaptic transmission appear inconsistent with several of the proposed functions of Syt7 (Bacaj et al., 2013; Jackman et al., 2016). Finally, both cerebellar and hippocampal BC synapses show rapid signaling properties (Hu et al., 2014). How Syt7, which shows slow Ca^{2+} binding and unbinding kinetics (Hui et al., 2005),

would contribute to rapid signaling remains unclear.

To examine the possible function of Syt7 at inhibitory synapses, we investigated the effects of deletion of the Syt7 gene in GABAergic BC–PC synapses of cerebellum (Arai and Jonas, 2014). Our results reveal a novel function of Syt7, which is to ensure efficient and temporally precise inhibitory synaptic transmission during high-frequency activity.

3.2 Methods

Experimental model and subject details

Experiments on C57BL/6 wild-type and mutant mice were performed in strict accordance with institutional, national, and European guidelines for animal experimentation and were approved by the Bundesministerium für Wissenschaft, Forschung und Wirtschaft of Austria (A. Haslinger, Vienna; BMWFW-66.018/0007-WF/II/3b/2014; BMWF-66.018/0010-WF/V/3b/2015; BMWFW-66.018/0020-WF/V/3b/2016).

Immunohistochemistry

14- to 16-day-old mice of either sex were transcardially perfused, using 4% paraformaldehyde in 100 mM phosphate buffer (PB; pH 7.35) for fixation. Brains were dissected out and post-fixed in 4% paraformaldehyde for ~24 h. 50 µm-thick slices were cut from the cerebellar vermis using a VT1200S vibratome (Leica Microsystems). After washing with 0.1 M PB, slices were incubated with 10% normal goat serum (NGS) for 1 h and subsequently with primary antibodies against Syt7 (polyclonal rabbit; Synaptic Systems, 105173; 1:200) and GAD65 (polyclonal guinea pig; Synaptic Systems, 198104; 1:500) both in PB containing 5% NGS and 0.5% Triton X-100 overnight. After washing, slices were incubated with specific secondary antibodies (Alexa Fluor 647-conjugated anti-rabbit secondary antibody; Alexa Fluor 488-conjugated anti-guinea pig secondary antibody; Thermo Fisher Scientific; 1:1000 for both) with PB containing 5% NGS and 0.3% TritonX-100 overnight. After washing, slices were embedded in Prolong Antifade and examined under a TCS SP5 II confocal microscope (Leica Microsystems).

Cerebellar slice preparation

C57BL/6 Syt7 knockout mice ($Syt7^{-/-}$), in which a stop codon was inserted in exon 4, were obtained from Jackson Labs (stock number 004950; generated by Norma Andrews; $Syt7^{tm1Nan}$; Chakrabati et al., 2003). All experiments were performed on littermate offspring from heterozygous matings, with knockout mice being homozygous for the deletion allele ($Syt7^{-/-}$) and wild-type animals homozygous for the wild-type allele ($Syt7^{+/+}$). Previous work showed that deletion of Syt7 has no detectable effects on the expression of several other synaptic proteins (Maximov et al., 2008; Bacaj et al., 2013). Slices were cut from the vermis of the cerebellum of 14- to 16-day-old mice of either sex. In all experiments, genotypes were determined by polymerase chain reaction analysis. After decapitation, the brain was rapidly dissected out and immersed in ice-cold slicing solution containing: 87 mM NaCl, 25 mM $NaHCO_3$, 2.5 mM KCl, 1.25 mM NaH_2PO_4, 10 mM D-glucose, 75 mM sucrose, 0.5 mM $CaCl_2$, and 7 mM $MgCl_2$, (pH 7.4 in 95% O_2 / 5% CO_2, ~325 mOsm). Parasagittal 300-µm-thick cerebellar slices from the vermis region were cut using a VT1200 vibratome (Leica Microsystems). In a subset of experiments (**Figure 3-8**), slices were cut from the hippocampus of 14- to 16-day-old mice, as previously described (Kraushaar and Jonas, 2000; Hefft and Jonas, 2005). After ~20 min incubation at ~35ºC, the slices were stored at room temperature. Slices were used for maximally 5 hours after dissection. Experiments were performed at 21–24°C.

Paired recordings

During experiments, slices were superfused with a physiological extracellular solution containing: 125 mM NaCl, 2.5 mM KCl, 25 mM $NaHCO_3$, 1.25 mM NaH_2PO_4, 25 mM D-glucose, 2 mM $CaCl_2$, and 1 mM $MgCl_2$ (pH 7.4 in 95% O_2 / 5% CO_2, ~325 mOsm). Paired recordings from synaptically connected BCs and PCs were performed as previously described (Caillard et al., 2000; Sakaba, 2008; Eggermann and Jonas, 2012; Arai and Jonas, 2014; Chen et al., 2017a). Intracellular solution used for the presynaptic BCs contained: 125 mM K-gluconate, 20 mM KCl, 0.1 mM EGTA, 10 mM phosphocreatine, 2 mM $MgCl_2$, 2 mM ATP, 0.4 mM GTP, and 10 mM HEPES (pH adjusted to 7.28 with KOH, ~310 mOsm); 0.2% biocytin was added in a subset of recordings. BCs were identified by the location of the soma in

the inner molecular layer close to the PC layer under experimental conditions and by the formation for basket-like arborizations and Pinceau terminations around PC somata in biocytin-labeled material (Eggermann and Jonas, 2012; Arai and Jonas, 2014; Chen et al., 2017a). The presynaptic pipette resistance was 8–10 MΩ. BCs were recorded under current-clamp conditions. A holding current of ~−50 pA was injected to maintain the membrane potential at ~−65 mV and to avoid spontaneous AP generation. To evoke presynaptic APs, single pulses or trains of 20 or 50 pulses at 10–100 Hz (400 pA, 4 ms) were injected into the presynaptic BC every 4 s or 20 s, respectively.

Intracellular solution for postsynaptic PCs contained: 140 mM KCl, 10 mM EGTA, 2 mM $MgCl_2$, 2 mM ATP, 10 mM HEPES, and 2 mM QX-314 (pH adjusted to 7.28 with KOH, ~313 mOsm). To achieve the lowest possible postsynaptic series resistance, large tip-sized patch pipettes were fabricated from leaded glass (PG10165-4, WPI) using a horizontal micropipette puller (P-97, Sutter Instrument). To reduce pipette capacitance, pipettes were coated with dental wax. The postsynaptic pipette resistance was 0.8–1.5 MΩ, resulting in a series resistance of 3–8 MΩ. Experiments in which series resistance changed by > 2 MΩ were discarded. PCs were recorded in the voltage-clamp configuration with a holding potential of –70 mV. For monitoring series and input resistance, 5-mV, 100−ms hyperpolarizing test pulses were applied after the IPSCs had decayed to baseline. For recording of miniature IPSCs (**Figure 3-3**), synaptic events were examined in pharmacological isolation in the presence of 1 µM tetrodotoxin (TTX), 10 µM 6-cyano-7-nitroquinoxaline-2,3-dione (CNQX), and 20 µM D-2-amino-5-phosphonopentanoic acid (D-AP5) at −70 mV. For cell-attached recordings (**Figure 5**), recording pipettes were filled with intracellular solution (without QX-314), and pipette potential was adjusted to keep the holding current at ~0. In a subset of experiments (**Figure 3-3**), recordings were made from hippocampal BC–GC synapses, as previously described (Kraushaar and Jonas, 2000; Hefft and Jonas, 2005).

Production and injection of adenoviral expression vectors

Synaptotagmin 7 cDNA (alpha splice variant, *Mus musculus* (NP_061271); Sugita et al., 2001) was codon-optimized for expression in mouse (GeneArt) and then cloned

into the EcoRI and NotI sites of the synapsin expression cassette (Montesinos et al., 2011; Montesinos et al., 2016; Chen et al., 2017a). This cassette included the 470 bp human synapsin (hsyn) promoter, the minute virus of mice (mvm) intron, and the bovine growth hormone (BGH) polyA. Subsequently, the expression cassette was cloned into the AscI site of pC4HSU28. This version of pC4HSU28 was modified to also contain a separate neurospecific EGFP expression cassette driven by the 470 bp hsyn promoter.

HdAds were produced by first digesting the pHdAd with PmeI to linearize and expose the ends of the 5' and 3' inverted terminal repeats. Transfection of the pHdAd was performed using 116 producer cells, a modified HEK293 line expressing high levels of Cre recombinase, and a 4-kbp adenoviral genome fragment that encodes for the E1A/E1B gene. HdAd was serially amplified in 5 consecutive passages. Each successive passage was performed after cytopathic effect (CPE) occurred and cell lysates were subjected to 3 freeze-thaw cycles to lyse cells and thereby release the viral particles. HdAd was stored at −80°C in storage buffer containing 10 mM HEPES, 250 mM sucrose, and 1 mM $MgCl_2$ at pH 7.4.

Syt7$^{-/-}$ mice, at postnatal day (P) 3 to 6, were anesthetized using isoflurane (5% for induction and ~3% during the injection procedure; Forane®, Abbott) combined with meloxicam (1 mg kg^{-1}, Boehringer) for analgesia. Meloxicam was given 2 hours before surgery for pre-operative analgesia and repeated twice 24 h after the previous injection for post-operative analgesia. After sufficient sedation, mice were put on a stereotaxic apparatus and head-fixed with ear bars. The skin was cut, the skull was exposed, and a small hole was made with a needle in the region over the cerebellum. 1 µl adenovirus (~10^9 vp) was injected into the vermis of the cerebellum at a depth of ~600 µm from the endocranium. After virus injection, pups were returned to their home cages for recovery. Recordings were made at P14 to 16. Infected cerebellar BCs were identified by EGFP fluorescence, using epifluorescence during experiments and confocal imaging for subsequent documentation.

Data acquisition and analysis

Data were acquired with a Multiclamp 700B amplifier (Axon Instruments), low-pass filtered at 10 kHz, and sampled at 20 kHz using a CED power1401 interface

(Cambridge Electronic Design). Stimulus generation and data acquisition were performed using custom-made software (FPulse version 3.33, Ulrich Fröbe, University of Freiburg) running under Igor Pro 6.22 (WaveMetrics). Data were analyzed using Stimfit 0.14.9 (https://github.com/neurodroid/stimfit; Guzman et al., 2014), R 3.4.1 (the R project for statistical computing), and Mathematica 11.0 (Wolfram Research). Synaptic latency of monosynaptic IPSCs was measured from the peak of the presynaptic AP to the IPSC onset. IPSC decay time constant was determined by fitting the decay phase of an average IPSC trace. To quantify multiple-pulse depression, traces were averaged and the amplitude of each IPSC in a train was measured from the baseline directly preceding the rising phase. Asynchronous IPSCs during train stimulation (**Figure 3-2**) and miniature IPSCs in the presence of TTX (**Figure 3-3**) were detected using a template matching algorithm and verified by visual inspection (Pernía-Andrade et al., 2012). Asynchronous release rate was quantified in a time interval 15–50 ms after the peak of each presynaptic AP.

For analysis of vesicular pool size and refilling rate, IPSC amplitudes during a 100-Hz train of 50 stimuli were examined. 100-Hz stimulation was used to maximize the extent of depression. IPSC values were normalized by $IPSC_1$, averaged across cells, and cumulatively plotted against stimulus number. The last ten data points were fit by linear regression. The size of the readily releasable pool (RRP) was determined from intersection of the regression line with the ordinate, while refilling rate was determined from the slope (Schneggenburger et al., 1999). The RRP estimate represents “pool decrement” rather than absolute pool size; the true pool size may be larger than the estimate (Neher, 2015). To obtain absolute numbers of RRP size and refilling rate, estimated values were multiplied by the quantal content of $IPSC_1$. Quantal size was determined as the mean peak amplitude of miniature IPSCs in each group (**Figure 3-3**). Control experiments in the presence of 300 µM of the low-affinity competitive $GABA_A$ receptor antagonist (1,2,5,6-tetrahydropyridine-4-yl)-methylphosphinic acid (TPMPA) and the $GABA_B$ receptor antagonist CGP55845 (both Tocris) gave similar results, indicating that the analysis of pool size and refilling rate were not confounded by desensitization or saturation of postsynaptic receptors (Jones et al., 2001; Sakaba, 2008; Arai and Jonas, 2014; Chen et al., 2017a).

Quantification and statistical analysis

All values were reported as mean ± SEM. Statistical significance was tested using nonparametric Kruskal-Wallis and two-sided Wilcoxon rank sum tests in R. Differences with $P < 0.05$ were considered significant. In figures, *, **, and *** indicate $P < 0.05$, $P < 0.01$, and $P < 0.001$, respectively. In box plots, horizontal lines represent median; boxes, quartiles; whiskers, most extreme data points ≤1.5 interquartile range from box edges; and single points, data from individual experiments. In total, data were obtained from 163 cerebellar BC–PC pairs (80 from $Syt7^{+/+}$ and 83 from $Syt7^{-/-}$), 19 PC recordings (10 from $Syt7^{+/+}$ and 9 from $Syt7^{-/-}$), and 10 hippocampal BC–GC pairs (5 from $Syt7^{+/+}$ and 5 from $Syt7^{-/-}$).

3.3 Results

We examined the functional contribution of Syt7 to transmitter release at the GABAergic basket cell (BC)–Purkinje cell (PC) synapse in the cerebellum, a synapse ideal for the biophysical analysis of GABAergic synaptic transmission (Eggermann and Jonas, 2012; Arai and Jonas, 2014; Chen et al., 2017a). As a first step, we probed the expression of Syt7 (**Figure 3-1**). Immunolabeling with Syt7 antibodies revealed that Syt7 was highly expressed throughout the cerebellum. Immunoreactivity was largely abolished in $Syt7^{-/-}$ mice, demonstrating the specificity of the labeling. Double labeling with GAD65 antibodies further suggested that Syt7 was strongly expressed in inhibitory terminals surrounding PC somata (**Figure 3-1**A). Furthermore, microarray analysis of mRNA expression in cerebellar BCs/stellate cells (Paul et al., 2012) suggested that amongst all Ca^{2+}-binding synaptotagmins, Syt7 was the most abundant isoform (**Figure 3-1B**). Thus, Syt7 is highly expressed in cerebellar BC presynaptic terminals.

To determine the functional contribution of Syt7 to GABAergic synaptic transmission, we compared cerebellar BC–PC synapses in wild-type ($Syt7^{+/+}$) and knockout mice ($Syt7^{-/-}$; Chakrabarti et al., 2003; **Figure 3-2; Table 3-1**). To evoke unitary inhibitory postsynaptic currents (IPSCs), we performed paired recordings in slices from 14- to 16-day-old mice (Eggermann and Jonas, 2012; Arai and Jonas, 2014; Chen et al., 2017a). Genetic elimination of Syt7 did not change the basic properties of synaptic transmission following single action potentials (APs) (**Figure 3-2B** and 3-2C; **Table 3-1**). For example, deletion of Syt7 did not alter the IPSC latency, the standard deviation of the latency as a measure for temporal precision of transmitter release, the 20–80% rise time, the IPSC peak amplitude, and the IPSC decay time constant ($P > 0.1$ in all cases except SD, where $P = 0.070$; 15 pairs in $Syt7^{+/+}$ and 15 pairs in $Syt7^{-/-}$ slices). Additionally, genetic elimination of Syt7 did not change the amplitude or frequency of miniature IPSCs, demonstrating Syt7 does not contribute to spontaneous release (**Figure 3-3**; **Table 3-1**). These results confirm previous suggestions that Syt7 does not contribute to synchronous transmitter release after single APs or spontaneous release in the absence of APs (Bacaj et al., 2013).

To test whether Syt7 contributes to asynchronous release during high-frequency stimulus trains (Wen et al., 2010; Bacaj et al., 2013; Luo and Südhof,

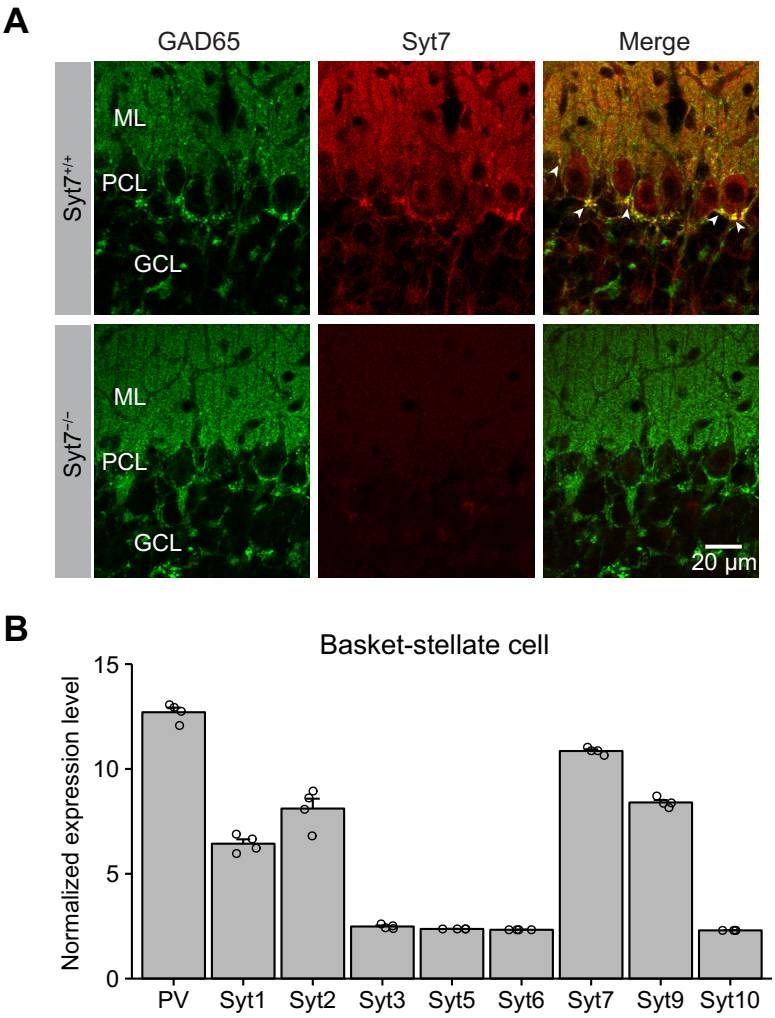

Figure 3-1. Syt7 is highly expressed in presynaptic terminals of cerebellar BCs

(**A**) Light-micrographs of cerebellar cortex, showing immunolabeling for GAD65 (left), Syt7 (middle), and overlay (right) in $Syt7^{+/+}$ (top) and $Syt7^{-/-}$ (bottom) mice; single confocal sections. ML, molecular layer; PCL, Purkinje cell layer; GCL, granule cell layer. Note that Syt7 is highly abundant in GABAergic presynaptic terminals of cerebellar BCs surrounding somata of PCs.

(**B**) Expression level of different synaptotagmin isoforms in cerebellar basket-stellate interneurons. Only Ca^{2+}-binding synaptotagmin isoforms were depicted. Values were obtained by meta-analysis of the data from a previous microarray study (Paul et al., 2012). Expression levels were downloaded from gene expression omnibus (GEO; accession GSE37055; data from four mice) and normalized by GCRMA, as done in the original paper (Paul et al., 2012). Note that Syt7 is the most highly expressed synaptotagmin isoform in basket-stellate interneurons. PV, parvalbumin.

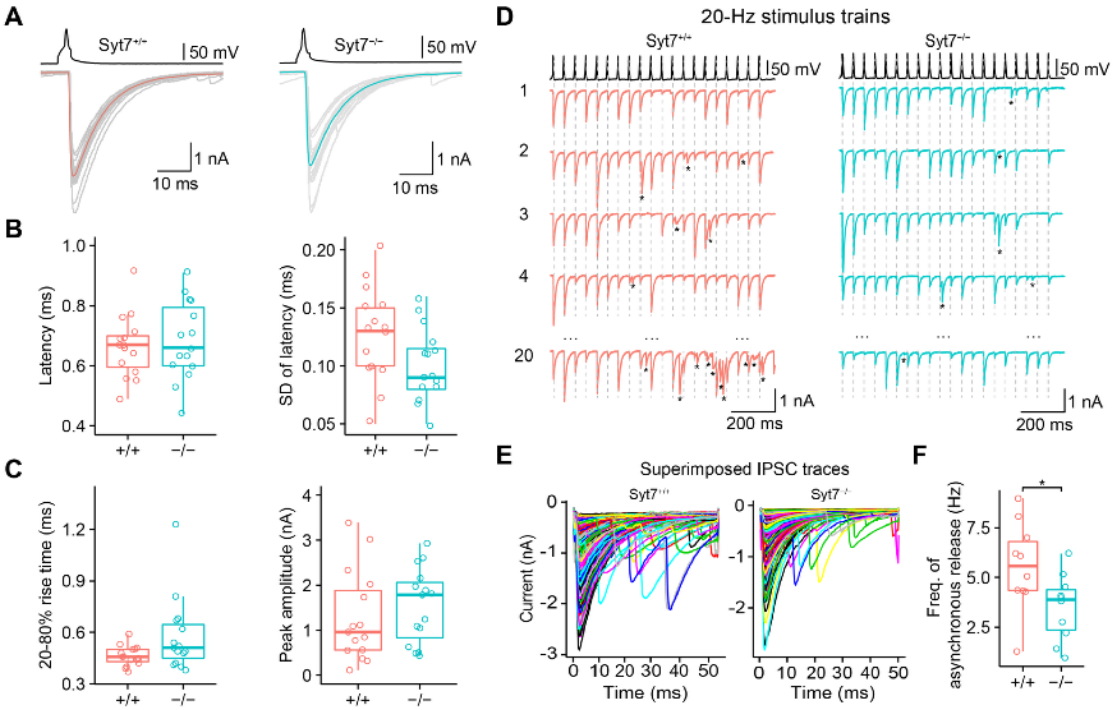

Figure 3-2. Syt7 is a Ca^{2+} sensor for asynchronous, but not synchronous release at BC–PC synapses

(**A**) Evoked IPSCs in $Syt7^{+/+}$ (left) and $Syt7^{-/-}$ (right) mice. Top, presynaptic AP evoked by short current pulses in the presynaptic BC; bottom, IPSCs recorded in the synaptically connected PC (gray traces, individual sweeps; red and cyan traces, average IPSCs).

(**B** and **C**) Box plots of synaptic latency from the peak of the presynaptic AP to the onset of the IPSC (B, left), standard deviation of latency (B, right), 20–80% rise time (C, left), and IPSC peak amplitude (C, right). Data from 15 and 15 pairs, respectively.

(**D**) Synchronous and asynchronous release during 20-Hz stimulation trains in $Syt7^{+/+}$ (left) and $Syt7^{-/-}$ (right) mice. Asterisks represent asynchronous release events, and vertical dashed lines indicate the peaks of the presynaptic APs.

(**E**) Synchronous and asynchronous IPSCs during 20-Hz stimulus trains. Left, superimposed IPSCs shown at expanded time scale (aligned to the peak of the presynaptic AP at t = 0). Individual traces were color coded to enhance visibility.

(**F**) Box plots of asynchronous release frequency. Asynchronous release was quantified in time intervals 15–50 ms after each presynaptic AP. * indicates P = 0.034. Data from 10 and 10 pairs, respectively. In box plots (B, C, and F), horizontal lines represent median; boxes, quartiles; whiskers, most extreme data points ≤1.5 interquartile range from box edges; and single points, data from individual experiments.

2017), we measured synchronous and asynchronous IPSCs during a 20-Hz repetitive stimulation (Arai and Jonas, 2014; **Figure 3-2D**–3-2F). The ideal recording conditions at the BC–PC synapse allowed us to perform direct counting of individual synaptic events. Asynchronous events were counted in a time window of 15–50 ms after each presynaptic AP. Genetic deletion of Syt7 significantly reduced the

Table 3-1. Comparison of basic release properties of $Syt7^{+/+}$ and $Syt7^{-/-}$ synapses

Parameter	$Syt7^{+/+}$	$Syt7^{-/-}$	P
Latency [a]	0.66 ± 0.03 ms (15)	0.68 ± 0.03 ms (15)	0.756
SD of latency [a]	0.13 ± 0.01 ms (15)	0.10 ± 0.03 (15)	0.070
20–80% rise time [a]	0.46 ± 0.02 ms (15)	0.58 ± 0.06 ms (15)	0.089
IPSC peak amplitude [a]	1.28 ± 0.26 nA (15)	1.54 ± 0.21 nA (15)	0.367
IPSC decay time constant [a]	8.45 ± 0.38 ms (15)	9.05 ± 0.48 ms (15)	0.372
IPSC half width [a]	7.40 ± 0.33 (15)	8.68 ± 0.61 (15)	0.120
Miniature IPSC frequency [b]	3.50 ± 0.47 Hz (10)	3.54 ± 0.44 Hz (9)	0.968
Miniature IPSC peak amplitude [b]	129.67 ± 5.38 pA (10)	147.89 ± 12.01 pA (9)	0.842
Frequency of asynchronous release [c]	5.57 ± 0.70 Hz (10)	3.51 ± 0.52 Hz (10)	0.034

Mean ± SEM (number of pairs / experiments).

[a] IPSCs evoked by single AP.

[b] Spontaneous IPSCs recorded in the presence of 1 μM TTX.

[c] IPSCs evoked by 20-Hz train of 20 APs.

frequency of asynchronous release during the train from 5.57 ± 0.70 Hz in Syt7$^{+/+}$ to 3.51 ± 0.52 Hz in Syt7$^{-/-}$ synapses (10 and 10 pairs, respectively; P = 0.034; **Figure 3-2F**). In conclusion, Syt7 contributed to the initiation of asynchronous release during high-frequency stimulus trains, although this function was less prominent at BC–PC synapses than at other previously examined synapses (Wen et al., 2010; Bacaj et al., 2013).

To investigate whether Syt7 contributed to synaptic dynamics (Jackman et al., 2016) or vesicle pool replenishment (Liu et al., 2014), we applied 100-Hz stimulus trains, expected to maximally deplete the vesicle pool (**Figure 3-4; Table 3-2**). Plot

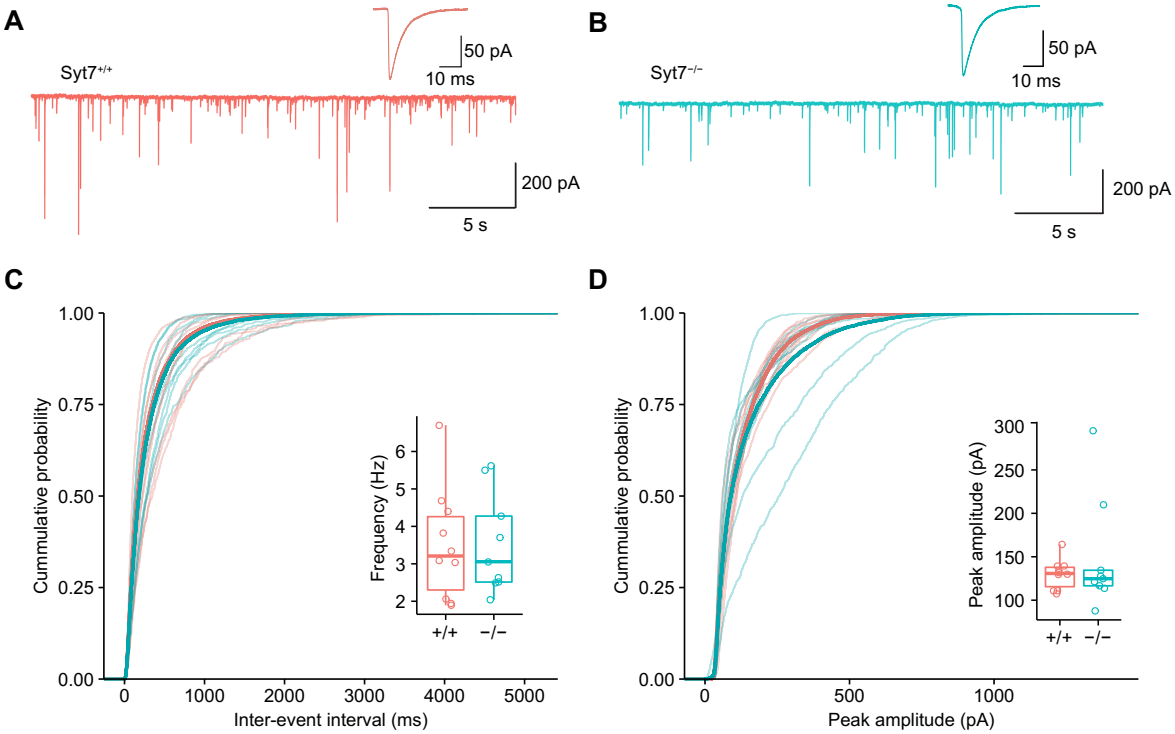

Figure 3-3. Deletion of Syt7 does not affect miniature IPSCs in PCs

(**A** and **B**) Traces of miniature IPSCs at −70 mV in the presence of 1 μM TTX in Syt7$^{+/+}$ (A) and Syt7$^{-/-}$ mice (B). Insets show average miniature IPSCs from 1379 and 667 events, respectively.
(**C** and **D**) Cumulative distributions of miniature IPSC inter-event interval (C) and peak amplitude (D). Thin lines, distributions from individual cells; thick lines, average distributions. Data from 10 and 9 PCs, respectively. In box plots (insets in C and D), horizontal lines represent median; boxes, quartiles; whiskers, most extreme data points ≤1.5 interquartile range from box edges; and single points, data from individual experiments.

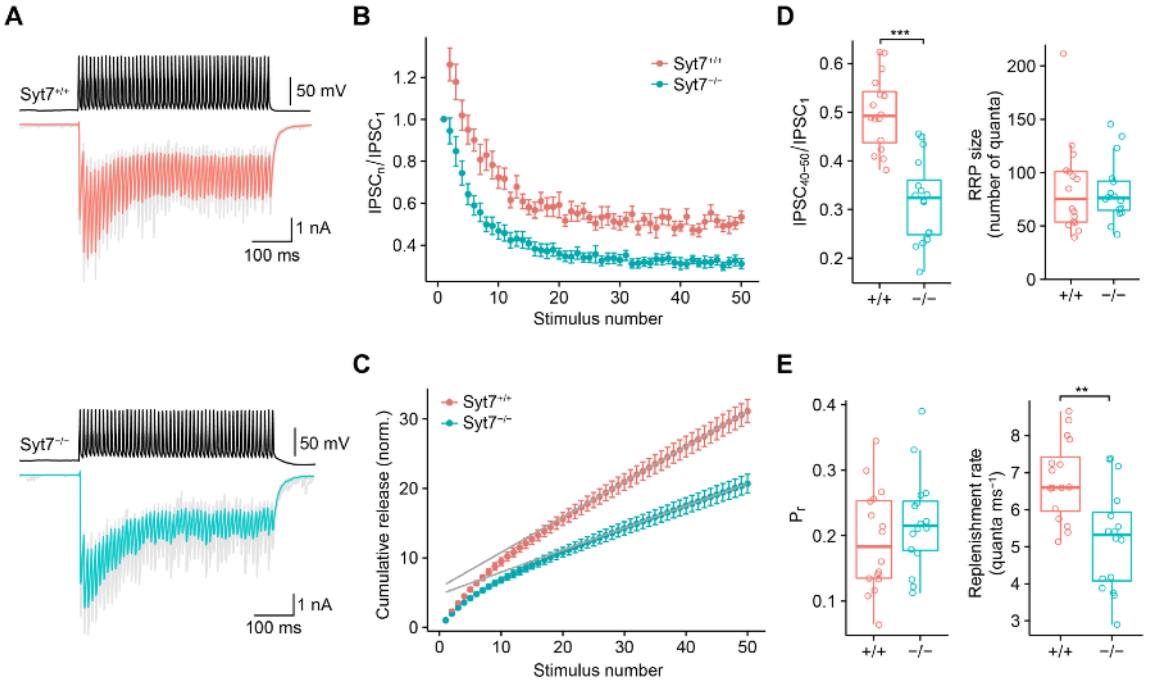

Figure 3-4. Syt7 promotes facilitation and vesicle pool replenishment during stimulus trains at BC–PC synapses

(**A**) IPSCs evoked by a 100-Hz train of 50 APs for Syt7$^{+/+}$ (top) and Syt7$^{-/-}$ (bottom) mice. Upper traces, presynaptic APs evoked by brief current pulses; lower traces, IPSCs (gray traces, individual sweeps; red and cyan traces, average IPSCs).

(**B**) Normalized IPSC peak amplitudes ($IPSC_n$ / $IPSC_1$), plotted against stimulus number (n). Red circles, Syt7$^{+/+}$; cyan circles, Syt7$^{-/-}$ synapses. Data were obtained from 16 pairs in each group.

(**C**) Quantitative analysis of pool size and refilling rate. IPSC peak amplitude was divided by $IPSC_1$, averaged across cells, and cumulatively plotted against stimulus number. The last ten points were fit by linear regression. Size of the RRP was determined from intersection of the regression line with the ordinate, whereas refilling rate was determined from the slope of the line. Release probability was quantified as the ratio of $IPSC_1$ over pool size.

(**D** and **E**) Box plots for $IPSC_{40–50}$ / $IPSC_1$ (D, left), RRP size (D, right), release probability (E, left), and replenishment rate (E, right). *** in (D) indicates $P < 0.001$, and ** in (E) indicates $P = 0.003$.

of normalized IPSC amplitude against stimulus number revealed significant differences between Syt7$^{+/+}$ and Syt7$^{-/-}$ synapses (**Figure 3-4A** and 3-4B). In Syt7$^{+/+}$ synapses, IPSCs showed a slight initial facilitation to 126.1 ± 5.8%, followed by

depression to a steady-state amplitude of 53.0 ± 2.7% of the initial value (16 pairs). In marked contrast, in Syt7$^{-/-}$ synapses, initial facilitation was abolished (94.5 ± 6.1%), and the steady-state IPSC amplitude was markedly reduced to 31.2 ± 2.3% (16 pairs, P < 0.001, **Figure 3-4B**). The effect of genetic deletion of Syt7 was rescued by helper-dependent adenovirus (HdAd)-mediated expression of Syt7, corroborating the validity of the genetic deletion approach (**Figure 3-5**). Interestingly, the steady-state transmission level after HdAd-mediated rescue in Syt7$^{-/-}$ exceeded that in Syt7$^{+/+}$ synapses, suggesting that expression levels of Syt7 after rescue were higher than endogenous levels (**Figure 3-5C–**3-5G). To determine the mechanisms underlying these changes, we computed the cumulative release, plotted it against stimulus number, and fit the data points for the last 10 stimuli by linear regression (Schneggenburger et al., 1999; **Figure 3-4C**) The size of the releasable pool, determined by intersection of the regression line with the ordinate (**Figure 3-4D**), was not significantly different between Syt7$^{+/+}$ and Syt7$^{-/-}$ synapses (85 ± 11 vesicles versus 82 ± 7.0 vesicles; P = 0.88). In contrast, the replenishment rate, determined from the slope of the regression line, was significantly larger in Syt7$^{+/+}$ than in Syt7$^{-/-}$ synapses (6.79 ± 0.26 quanta ms^{-1} versus 5.21 ± 0.34 quanta ms^{-1}; P = 0.003). Taken together, genetic deletion and rescue experiments suggest that Syt7 may regulate both facilitation and pool replenishment during high-frequency stimulation.

Next, we tested whether Syt7 affected the time course of vesicle pool refilling after a train of APs (Liu et al., 2014; **Figure 3-6**). To measure the time course of refilling, a 100-Hz train of 50 stimuli was applied to deplete the pool, followed by a single stimulus at various time points to probe the replenishment of the pool. In Syt7$^{+/+}$ synapses, recovery from depression was fast, with a mean time constant of 3.89 ± 0.59 s (14 pairs; **Figure 3-6C** and 3-6D). In contrast, in Syt7$^{-/-}$ synapses, recovery from depression was substantially prolonged, with a mean time constant of 7.05 ± 1.03 s (15 pairs; P = 0.033; **Figure 3-6C** and 3-6D). These results are consistent with the hypothesis that Syt7 promotes vesicle replenishment during and after high-frequency AP trains.

To examine the frequency-dependence of the effects of Syt7 deletion during repetitive stimulation (Bagnall et al., 2008; Turecek et al., 2016), we examined IPSCs evoked by 10–100 Hz stimulus trains (**Figure 3-7**; **Table 3-2**). Whereas for 10 Hz the extent of steady-state depression was identical between Syt7$^{+/+}$ and Syt7$^{-/-}$

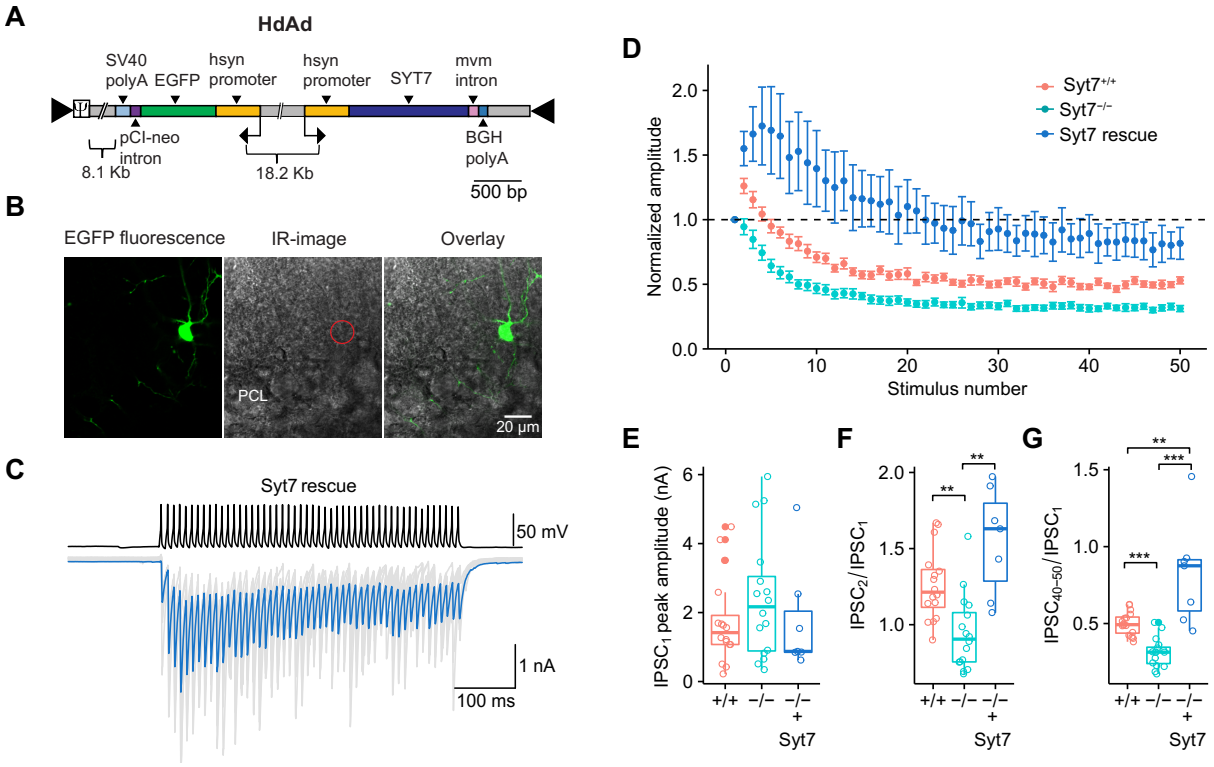

Figure 3-5. HdAd-mediated overexpression of Syt7

(**A**) Schematic illustration of the helper-dependent adenovirus (HdAd) constructs used for rescue experiments. Hsyn, human synapsin promoter; mvm, minute virus of mice intron; SV40 polyA, Simian virus 40 poly A; BGH polyA, bovine growth hormone poly A.

(B) Confocal microscopic image of a cerebellar BC in the molecular layer (left), infrared videomicroscopy light-micrograph (center), and overlay (right). The BC is highly fluorescent, showing successful infection with HdAd.

(**C**) IPSCs evoked by a 100-Hz train of 50 APs in Syt7$^{-/-}$ + HdAd-Syt7 synapses. Upper traces, presynaptic APs evoked by brief current pulses; lower traces, IPSCs (gray traces, individual sweeps; blue trace, average IPSC).

(**D**) Normalized IPSC peak amplitudes ($IPSC_n$ / $IPSC_1$), plotted against stimulus number (n). Red circles, Syt7$^{+/+}$; blue circles, Syt7$^{-/-}$ + HdAd-Syt7. Syt7$^{-/-}$ + HdAd-Syt7 data were obtained from 7 pairs.

(**E–G**) Box plot of IPSC peak amplitude ($IPSC_1$; E), paired-pulse ratio ($IPSC_2$ / $IPSC_1$; F), and normalized steady-state IPSC amplitude ($IPSC_{40–50}$ / $IPSC_1$; G). In box plots, horizontal lines represent median; boxes, quartiles; whiskers, most extreme data points ≤1.5 interquartile range from box edges; and single points, data from individual experiments. Note that overexpression of Syt7 not only rescued the synaptic phenotype, but rather enhanced initial facilitation and steady-state IPSC amplitude values above control values, implying that exogenous Syt7 levels after HdAd infection in Syt7$^{-/-}$ mice were higher than endogenous Syt7 levels in Syt7$^{+/+}$ mice.

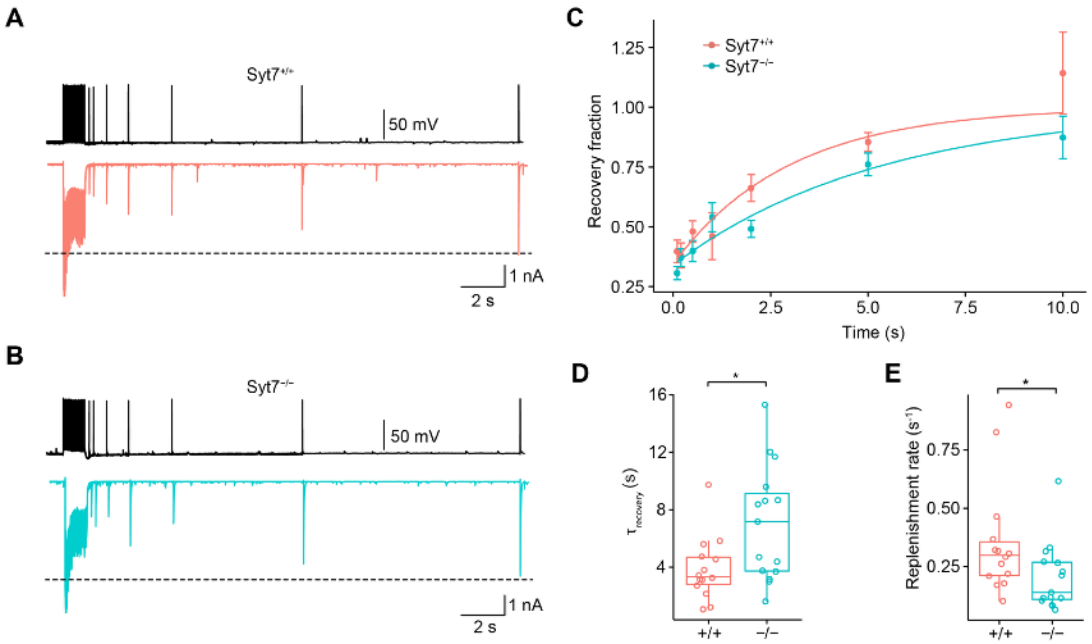

Figure 3-6. Syt7 promotes vesicle pool replenishment after pool depletion

(**A** and **B**) IPSCs evoked by 100-Hz trains of 50 stimuli, followed by single test stimuli at variable time intervals in Syt7$^{+/+}$ (A) and Syt7$^{-/-}$ (B) synapses. Overlay of 7 traces; each trace represents the average from 5 individual sweeps.

(**C**) Plot of peak amplitude of IPSC evoked by the test stimulus, normalized to the amplitude of the first IPSC in the preceding train. Continuous curves represent exponential functions fit to the data points (Syt7$^{+/+}$, red; Syt7$^{-/-}$, cyan). Data were obtained from 14 and 15 pairs, respectively.

(**D**) Box plots for recovery time constant (left) and corresponding replenishment rate (right). * indicates P = 0.033 in both cases.

synapses, the differences between Syt7$^{+/+}$ and Syt7$^{-/-}$ synapses progressively increased for frequencies of 20–100 Hz (P = 0.09, 0.04, 0.003, and <0.001; 10/10, 10/10, 10/10, and 16/16 pairs; **Figure 3-7C**). Linear regression analysis revealed that the ratio $IPSC_{15–20}$ / $IPSC_1$ was not significantly frequency-dependent in Syt7$^{+/+}$ synapses (P = 0.28), but highly frequency-dependent in Syt7$^{-/-}$ synapses (P = 0.005; **Figure 3-7C**). Thus, Syt7 contributed to the frequency-independence of transmitter release at BC–PC synapses during repetitive stimulation (Turecek et al., 2016). To further analyze the functional significance of this property of BC–PC synapses, we quantified the frequency dependence of the inhibitory synaptic charge (Turecek et al., 2016). In Syt7$^{+/+}$ synapses, the charge-frequency relation was linear, whereas in

Table 3-2. Comparison of synaptic dynamics of Syt7$^{+/+}$ and Syt7$^{-/-}$ synapses

Parameter [a]	Syt7$^{+/+}$	Syt7$^{-/-}$	P
$IPSC_2$ / $IPSC_1$ (10 Hz)	0.797 ± 0.037 (10)	0.838 ± 0.031 (10)	0.481
$IPSC_{15–20}$ / $IPSC_1$ (10 Hz)	0.527 ± 0.023 (10)	0.465 ± 0.020 (10)	0.089
$IPSC_2$ / $IPSC_1$ (20 Hz)	1.000 ± 0.087 (10)	0.837 ± 0.032 (10)	0.248
$IPSC_{15–20}$ / $IPSC_1$ (20 Hz)	0.567 ± 0.050 (10)	0.436 ± 0.013 (10)	0.043
$IPSC_2$ / $IPSC_1$ (50 Hz)	1.249 ± 0.063 (10)	0.904 ± 0.045 (10)	0.007
$IPSC_{15–20}$ / $IPSC_1$ (50 Hz)	0.608 ± 0.044 (10)	0.435 ± 0.023 (10)	0.003
$IPSC_2$ / $IPSC_1$ (100 Hz)	1.261 ± 0.058 (16)	0.945 ± 0.061 (16)	<0.001
$IPSC_{15–20}$ / $IPSC_1$ (100 Hz)	0.579 ± 0.030 (16)	0.380 ± 0.028 (16)	<0.001

Mean ± SEM (number of pairs).

[a] IPSCs evoked by trains of APs at indicated frequency

Syt7$^{-/-}$ synapses, a marked sublinearity was apparent (**Figure 3-7D**). Thus, Syt7 linearized the input-output relation of BC–PC synapses.

Our results indicate that Syt7 enhances transmitter release at cerebellar BC-PC synapses during repetitive firing. To find out whether this is a general mechanism that also operates at output synapses of fast-spiking interneurons in other brain areas, we examined the effects of genetic elimination of Syt7 in hippocampal basket cell to granule cell (BC–GC) synapses (Kraushaar and Jonas, 2000; Hefft and Jonas, 2005; **Figure 3-8**). Deletion of Syt7 significantly increased the

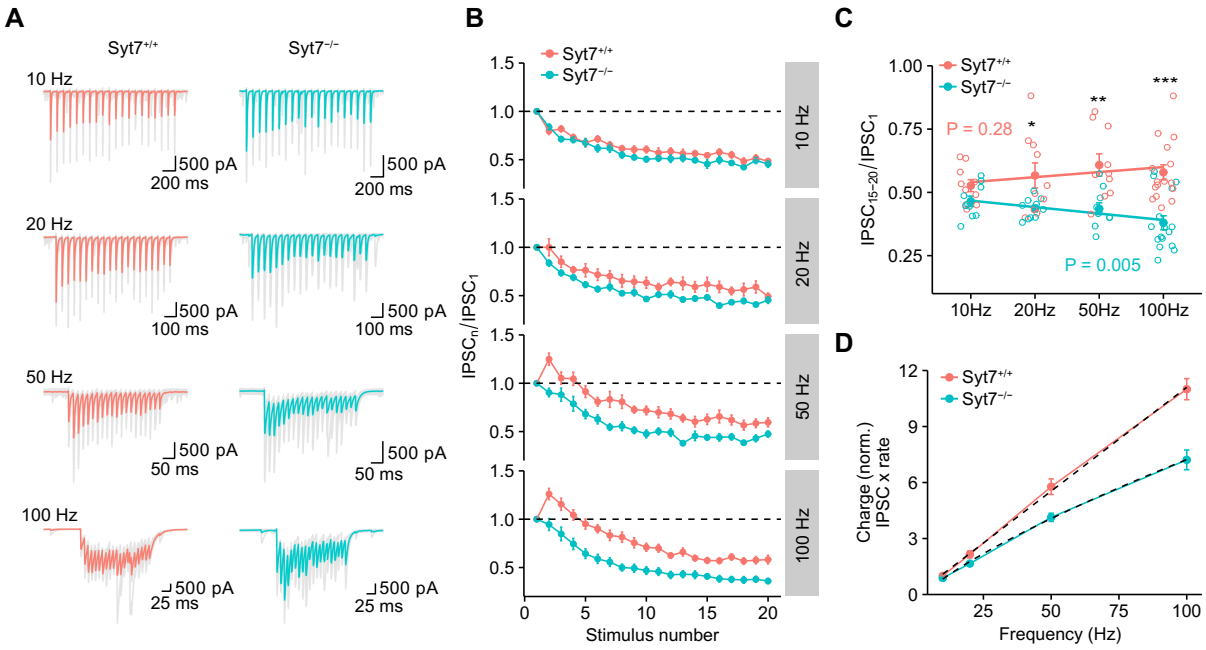

Figure 3-7. Syt7 ensures efficiency of high-frequency synaptic transmission and linearizes the input-output relation of BC–PC synapses

(**A**) IPSCs evoked by trains of 20 APs at different frequencies for Syt7$^{+/+}$ (left) and Syt7$^{-/-}$ synapses (right; gray traces, individual sweeps; red and cyan traces, average IPSCs).

(**B**) Normalized IPSC peak amplitudes ($IPSC_n$ / $IPSC_1$), plotted against stimulus number (n). Red circles, Syt7$^{+/+}$; cyan circles, Syt7$^{-/-}$. Data were obtained from 10 / 10 (10 Hz), 10 / 10 (20 Hz), 10 / 10 (50 Hz), and 16 / 16 pairs (100 Hz; Syt7$^{+/+}$ / Syt7$^{-/-}$).

(**C**) Plot of normalized steady-state IPSC amplitude, as quantified by $IPSC_{15–20}$ / $IPSC_1$, against stimulus frequency. Open circles represent data from individual experiments, filled circles indicate mean ± SEM. Lines represent results from linear regression analysis (Spearman □ = 0.16, P = 0.28 for Syt7$^{+/+}$ synapses; □ = −0.41, P = 0.005 for Syt7$^{-/-}$ synapses). *, **, and *** indicate P = 0.043, 0.003, and < 0.001, respectively. Note that normalized steady-state IPSC amplitude does not show significant frequency dependence in Syt7$^{+/+}$ synapses, but acquires marked frequency dependence in Syt7$^{-/-}$ synapses.

(**D**) Plot of normalized steady-state charge, as quantified by IPSC peak amplitude × stimulation frequency. Dashed lines represent the results from fit with a linear function (Syt7$^{+/+}$) or a power function (Syt7$^{-/-}$). In Syt7$^{+/+}$ synapses, inhibitory charge was linearly dependent on stimulation frequency. In contrast, in Syt7$^{-/-}$ synapses, the dependence was sublinear.

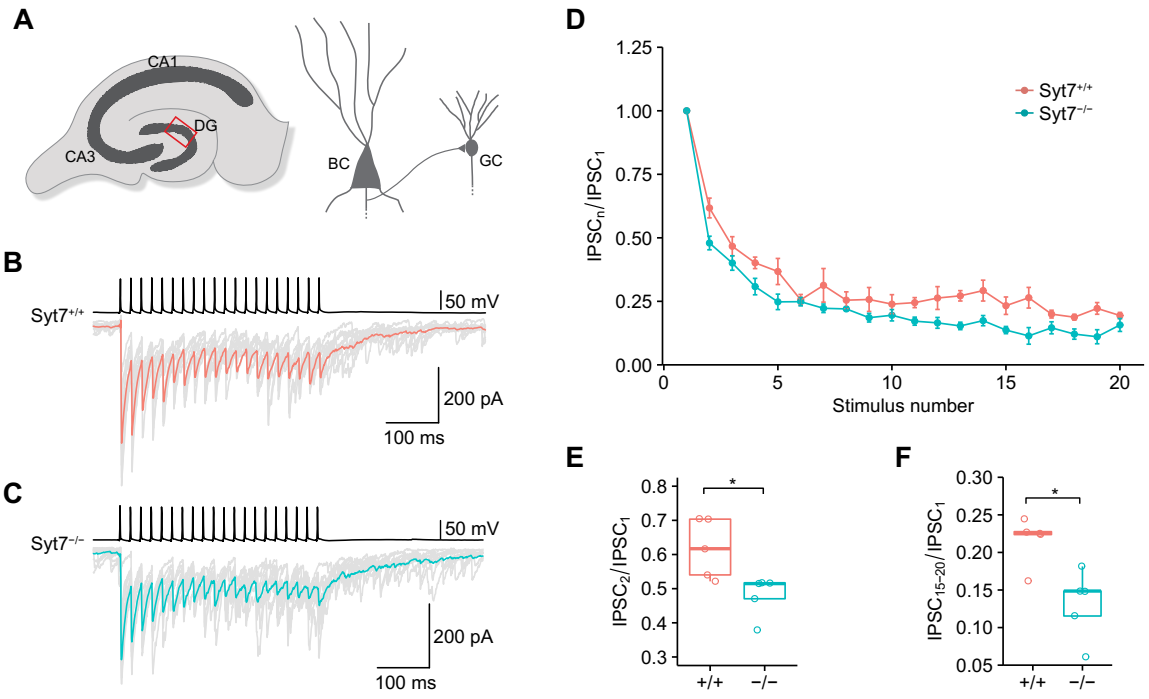

Figure 3-8. Syt7 ensures efficacy of high-frequency synaptic transmission in hippocampal BC–GC synapses

(**A**) Schematic illustration of the recording configuration in hippocampal slices. DG, dentate gyrus; CA3, cornu ammonis 3 subfield; CA1, cornu ammonis 1 subfield.

(**B** and **C**) IPSCs evoked by a 50-Hz train of 20 APs for Syt7$^{+/+}$ (B) and Syt7$^{-/-}$ synapses (C). Upper traces, presynaptic APs evoked by brief current pulses; lower traces, IPSCs (gray traces, individual sweeps; red and cyan traces, average IPSCs).

(**D**) Normalized IPSC peak amplitude, plotted against stimulus number. Red circles, Syt7$^{+/+}$ synapses; cyan circles, Syt7$^{-/-}$ synapses. Data were obtained from 5 pairs in each group.

(**E** and **F**) Box plot of paired-pulse ratio ($IPSC_2$ / $IPSC_1$; E) and normalized steady-state IPSC amplitude ($IPSC_{15–20}$ / $IPSC_1$; F). In box plots, horizontal lines represent median; boxes, quartiles; whiskers, most extreme data points ≤1.5 interquartile range from box edges; and single points, data from individual experiments. All experiments were performed in hippocampal BC–GC synapses. * indicates P = 0.01 in (E) and 0.02 in (F).

extent of depression during trains of 20 APs at 50 Hz ($IPSC_{15–20}$ / $IPSC_1$ = 0.22 ± 0.01 in Syt7$^{+/+}$ versus 0.13 ± 0.02 in Syt7$^{-/-}$ synapses; P = 0.02; 5 pairs in each group; **Figure 3-8**). Thus, Syt7 promoted high-frequency transmission in

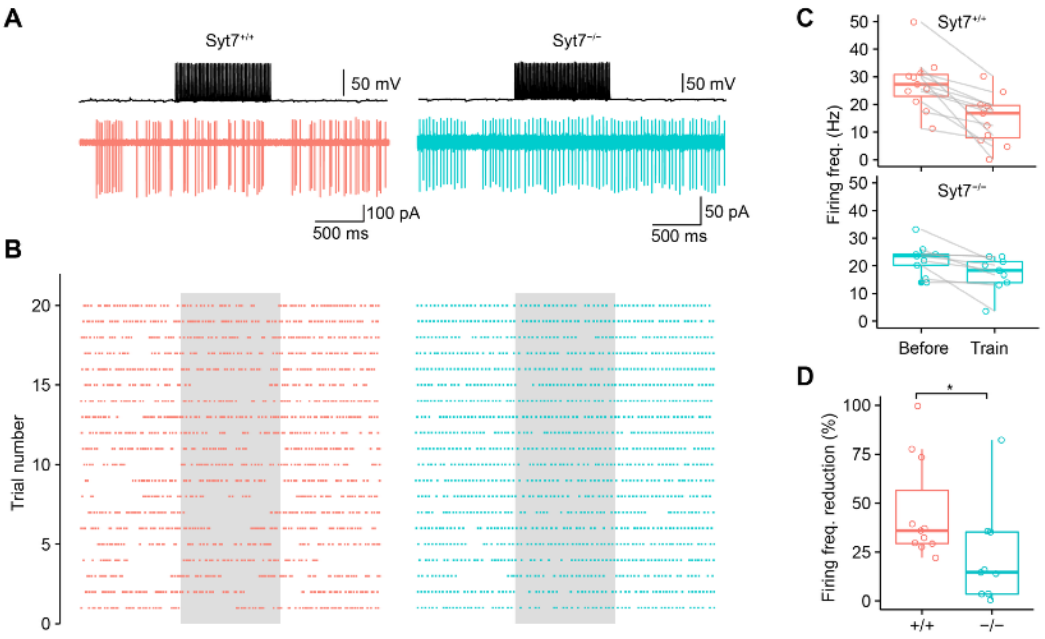

Figure 3-9. Syt7 ensures efficient suppression of PC activity by unitary inhibitory synaptic inputs

(A) Simultaneous paired recording from a presynaptic BC (whole-cell current-clamp configuration, upper trace) and a postsynaptic PC (noninvasive cell-attached voltage-clamp configuration, lower trace) for a $Syt7^{+/+}$ (left) or $Syt7^{-/-}$ synapse (right). Top, presynaptic APs; bottom, postsynaptic action currents during the same period. A 1-s, 50-Hz stimulus train was applied to the presynaptic BC. Note that activation of the unitary BC input suppressed spontaneous activity in PCs, as indicated by a marked reduction in the frequency of action currents.

(**B**) Rasterplot from 20 single trials for a $Syt7^{+/+}$ (left) or $Syt7^{-/-}$ synapse (right). Each point represents an action current in the PC. Gray area indicates time period of BC stimulation. Trial 5 corresponds to traces shown in (A).

(**C**) Box plots of firing frequency in PCs before and during train stimulation of BCs. Lines connect data from the same experiment. Top, $Syt7^{+/+}$; bottom, $Syt7^{-/-}$.

(**D**) Box plot of reduction of firing frequency in PCs by train stimulation of BCs for $Syt7^{+/+}$ (red) and $Syt7^{-/-}$ synapses (cyan). * indicates P = 0.02. In box plots in (C) and (D), horizontal lines represent median; boxes, quartiles; whiskers, most extreme data points ≤1.5 interquartile range from box edges; and single points, data from individual experiments.

hippocampal BC–GC synapses, although the effect was smaller than in cerebellar BC–PC synapses. Therefore, the function of Syt7 is conserved in at least two

different types of rapidly signaling GABAergic synapses.

Our results demonstrate that Syt7 promotes high-frequency transmission at GABAergic interneuron output synapses. Are these effects relevant for the function of principal neuron-interneuron microcircuits? To address this question, we performed paired recordings between cerebellar BCs in the whole-cell current-clamp configuration and PCs in the noninvasive cell-attached configuration (**Figure 3-9**). Presynaptic BCs were activated with a 1-s, 50-Hz stimulation, intended to mimic a high activity level of these neurons under *in vivo* conditions (Jelitai et al., 2016). In the absence of presynaptic stimulation, PCs showed spontaneous firing in both $Syt7^{+/+}$ and $Syt7^{-/-}$ mice (**Figure 3-9A**–3-9C). In $Syt7^{+/+}$ mice, a 1-s, 50−Hz stimulation of a single presynaptic BC caused a reduction of action current frequency in PCs by 45.8 ± 7.7% (11 pairs; **Figure 3-9C** and 3-9D), demonstrating the efficacy of unitary inhibitory synaptic inputs in regulating PC spiking (Häusser and Clark, 1997). In contrast, in slices from $Syt7^{-/-}$ mice, high-frequency stimulation of a single presynaptic BC reduced PC activity by only 22.8.5 ± 8.5% (P = 0.028; 9 pairs; **Figure 3-9C** and 3-9D). Taken together, these results indicate that Syt7 plays a key role to ensure the efficient regulation of PC activity by unitary GABAergic inputs in cerebellar microcircuits.

3.4 Discussion

The role of Syt7 in transmitter release at central synapses has been controversial. Several functions have been proposed, including a trigger function for asynchronous release during stimulus trains (Wen et al., 2010; Bacaj et al., 2013; Luo and Südhof, 2017), an acceleration of vesicle pool replenishment (Liu et al., 2014), and a function as a facilitation sensor (Jackman et al., 2016; Jackman and Regehr, 2017). Our results show that these functions are not mutually exclusive, but coexist at single BC–PC synapses. In combination, these mechanisms ensure efficiency and frequency-independence of inhibitory synaptic transmission at GABAergic synapses. Furthermore, our results suggest that the function of Syt7 is conserved across output synapses of fast-spiking, GABAergic interneurons, at least between cerebellum and hippocampus. Finally, our experiments show that Syt7, at the network level, enables the powerful control of PC activity by single BC synaptic inputs. As PCs represent the sole output from the cerebellum, this puts Syt7 into a strategic position to

regulate the information flow in this motor circuit. Although our conclusions are largely based on a knockout approach and therefore require careful interpretation, the results from the rescue experiments are fully consistent with our hypotheses.

How does a single protein, Syt7, generate three divergent effects at BC–PC synapses? Several models of synaptotagmin action suggest that a single primary mechanism may underlie the three effects. It has been proposed that synaptotagmins reduce the energy level of membrane fusion intermediates (Jackman and Regehr, 2017). In this model, both Syt7 and fast synaptotagmins (Syt1, 2, or 9; Xu et al., 2009) would reduce the activation energy of fusion, Syt7 by a small amount and Syt1, 2, or 9 by a larger amount. In consequence, Syt7 in isolation would trigger asynchronous release, but in conjunction with fast synaptotagmins would promote facilitation, because additive effects on energy barriers cause supralinear effects on vesicle fusion rate (Schotten et al., 2015). In parallel, Syt7 may reduce the activation energy of docking or priming, thus explaining acceleration of vesicle replenishment.

Syt7 could also primarily act as a Ca^{2+} sensor of activity-dependent replenishment, by accelerating vesicle tethering, docking, or priming (Imig et al., 2014; Bacaj et al., 2015). The subcellular localization of Syt7, in plasma membrane and intracellular organelles (Sugita et al., 2001; Liu et al., 2014; Li et al., 2017) might be consistent with these hypothesis. In this model, Syt7 may promote filling of the vesicular pools, leading to an increase in docking site occupancy (Pulido et al., 2015). Accordingly, Syt7 would also enhance both asynchronous release and facilitation. Alternatively, Syt7 could affect replenishment by accelerating endocytosis. Although the kinetics of replenishment may be difficult to reconcile with clathrin-mediated slow endocytosis, it might be compatible with clathrin-independent fast endocytosis (Delvendahl et al., 2016).

Finally, the interrelation of the three effects might be explained by heterogeneity of the vesicular pool. Syt7 could trigger release from a separate slow pool of vesicles (Schonn et al., 2008), whereas Syt1, 2, or 9 would trigger release from a fast pool (Turecek et al., 2016; Chen et al., 2017). If the fast pool shows high release probability, slow recovery, and depression, and the slow pool has low release probability, fast recovery, and facilitation (Sakaba and Neher, 2001; Turecek et al., 2016), Syt7 deletion may slow recovery and reduce facilitation in parallel, as

observed experimentally.

It is well established that Syt7 operates as a Ca^{2+} sensor for asynchronous release at several synapses (Wen et al., 2010; Bacaj et al., 2013; Luo and Südhof, 2017). Our results are consistent with this function, but show that it plays a relatively minor role at the BC–PC synapse. Why is this the case? One important factor that determines the rate of asynchronous release is the coupling distance between Ca^{2+} channels and release sensors (Eggermann et al., 2012). In both cerebellar BC–PC synapses and hippocampal BC–GC synapses, tight, “nanodomain“ coupling governs transmitter release from active zones (Bucurenciu et al., 2008; Arai and Jonas, 2014). Tight coupling is expected to reduce the relative amount of asynchronous release (Bucurenciu et al., 2008; Eggermann et al., 2012). Thus, asynchronous release is small in wild-type synapses, and additional effects of Syt7 elimination are expected to be minimal. Likewise, tight coupling will prevent certain forms of facilitation, e.g. facilitation by saturation of presynaptic buffers (Felmy et al., 2003; Vyleta and Jonas, 2014). In contrast, at synapses with looser coupling (such as hippocampal synapses in culture or the young calyx of Held), asynchronous release and facilitation will be more pronounced, and the effects of Syt7 deletion will be more prominent (Bacaj et al., 2013; Luo and Südhof, 2017).

Our results have major implications for the stability of inhibition in neuronal networks *in vivo*. Fast-spiking, PV^+ interneurons in different brain regions generate APs at high frequency. For example, PV^+ interneurons in the cerebellum fire APs with a frequency of up to 100 Hz during active movement (Jelitai et al., 2016), and PV^+ interneurons in the hippocampal CA1 region generate high-frequency trains of spikes during sharp-wave ripples (Lapray et al., 2012). Under these conditions, PV^+ interneurons need to generate stable and reliable inhibitory output signals. Our results suggest that the expression of Syt7 plays a critical role in maintaining the efficacy of inhibitory synaptic transmission at these synapses. Thus, whereas the fast Ca^{2+} sensor Syt2 is responsible for the speed and temporal precision of transmitter release (Kerr et al., 2008; Chen et al., 2017a), Syt7 plays a critical role in maintaining the efficacy during high-frequency synaptic transmission at cerebellar and hippocampal GABAergic synapses. Whether these results generalize to other fast-signaling synapses throughout the brain remains to be determined.

Chapter 4. General discussion

Fast synaptic transmission is a prominent property of GABAergic interneurons, especially the PV^+ subtype. Several molecular mechanisms have been found contributing to the fast signaling property of PV^+ interneurons, like the expression of Kv3.1 channels (Du et al, 1996), selective usage of the P/Q type Ca^{2+} channels (Hefft and Jonas, 2005; Bucurenciu et al., 2010; Arai and Jonas, 2014), and tight coupling distance between Ca^{2+} channels and release sensors (Hefft and Jonas 2005; Arai and Jonas, 2014). In our study, we first identified that Syt2 is the main Ca^{2+} sensor used by inhibitory BC–PC synapses in the cerebellum (Chen et al., 2017a). Compared with Syt1, Syt2 mediates faster time course and higher temporal precision of inhibitory neurotransmitter release and facilitates vesicle pool refilling. Thus, Syt2 ensures speed and temporal precision of the inhibitory transmitter release. Additionally, we showed that Syt7, another synaptotagmin member, guarantees the efficient inhibitory transmitter release of BC–PC synapses during high activity, through mediating asynchronous release, facilitation and faster vesicle pool refilling rate (Chen et al., 2017b). Working together, Syt2 and Syt7 ensure fast signaling property of the cerebellar BCs, which is critical for controlling the activity of postsynaptic Purkinje cells: the sole projection neuron of the cerebellar cortex.

4.1 Synaptotagmins, why so many?

The mammalian genome encodes 17 synaptotagmins, eight members (Syt1, 2, 3, 5, 6, 7, 9, and 10) among them bind Ca^{2+}, whereas only Syt1, Syt2 and Syt9 have been shown to mediate fast transmitter release (Xu et al., 2007). This raises the important question: “Why so many?” (Südhof, 2002).

For synaptotagmins which mediate fast transmitter release, it’s generally thought Syt1 is highly used in cortical circuits, whereas Syt2 is more prevalent in the caudal brain, like the cerebellum, brainstem and spinal cord (Pang et al., 2006a, 2006b; Mittelsteadt et al., 2009). Syt9 has been reported as the main Ca^{2+} sensor in striatum neurons (Xu et al., 2007). However, the contribution of different synaptotagmins to synaptic transmission cannot be simply split up based on the brain areas. Gene expression analysis indicated that several synaptotagmin members coexist in a synapse (Kerr et al., 2008; Paul et al., 2012; Földy et al., 2016). Genetic deletion of Syt1 dramatically impaired the synchronous release of

some excitatory cortical synapses, whereas the residual component could be mediated by other synaptotagmin isoforms (Bacaj et al., 2013; Liu et al., 2014; Kerr et al., 2008), although part of the increased asynchronous release has been shown to be mediated by Syt7 (Bacaj et al., 2013; Li et al., 2017). For GABAergic interneurons in the hippocampus, Syt1 probably works in concert with other synaptotagmins for transmitter release, since Syt1 deletion only reduced the synchronous release by ~50% (Kerr et al., 2008). Furthermore, the usage of synaptotagmin isoforms also depends on developmental stages. Such as in the calyx of Held, Syt1 is mainly used for transmitter release in newborn mice and then switches to Syt2 at around postnatally one week (Kochubey et al., 2016). Thus, for triggering neurotransmitter release, the most likely scenario should be that several synaptotagmins work in concert. But which synaptotagmin isoform is the main Ca^{2+} sensor depends on the developmental stage, neuron type and brain area.

The function of the remaining isoforms, however, is largely elusive. Syt3, Syt5, Syt6 and Syt7 are widely expressed in the whole brain (Mittelsteadt et al., 2009), but they cannot rescue the fast transmitter release in Syt1-deficient hippocampal neurons in culture (Xu et al., 2007). Among these synaptotagmin members, Syt7 obtained a great deal of attention from neuroscientists (Chen and Jonas, 2017). Compared with Syt1 and Syt2, Syt7 shows several differences. First, Syt7 is expressed in all metazoans, widely expressed in the whole brain without distinct expression pattern (Sugita et al., 2001). Second, *in vitro* assay suggested that Syt7 has the highest Ca^{2+} affinity (Mittelsteadt et al., 2009), but the slowest kinetics of Ca^{2+} binding and unbinding rate (Hui et al, 2005). Third, unlike Syt1 and Syt2, which are mainly present on the synaptic vesicle membrane, Syt7 is abundantly located in the plasma membrane (Li et al., 2017). Three main functions have been proposed of Syt7 for synaptic transmission: triggering asynchronous release (Bacaj et al., 2013; Luo and Südhof, 2017), accelerating vesicle pool replenishment (Liu et al., 2014) and working as a facilitation sensor (Jackman et al., 2016; Turecek et al., 2017). However, Syt7 is highly expressed in fast-spiking interneurons which have an only minimal amount of asynchronous release and mainly show depression rather than facilitation. How could an asynchronous release or a facilitation sensor contributes to inhibitory synaptic transmission? Our study on Syt7 (Chen et al., 2017b) showed that these three functions coexist at the inhibitory BC–PC synapses in the cerebellum,

guaranteeing the frequency-independent release during high activity. Another study working on the inhibitory Purkinje cell to deep cerebellar nucleus synapse obtained a similar result of Syt7. They proposed that Syt7 confers frequency-invariance release by mediating the release of a hidden facilitation pool (Turecek et al., 2017). This has also been proved for another frequency-invariance release synapse, the excitatory vestibular ganglion to the magnocellular medial vestibular nucleus synapse.

Frequency-independent release has been observed at only few synapses before, including vestibular synapses (Bagnall et al., 2008; McElvain et al., 2015), and probably in the chick auditory brainstem (MacLeod et al., 2007). At most depressing synapses, the extent of depression becomes more obvious as the activity increases (Turecek et al., 2016). Since Syt7 has been suggested widely expressed in the whole brain (Sugita et al., 2001), how could it contribute to the frequency-independent release in some synapses but not others? The expression level of Syt7 at different synapses may be important. Research showed that at synapses from the Purkinje cell to the deep cerebellar nuclei, the developmentally upregulated expression of Syt7 induces a more pronounced frequency-independent release in adult mice than in the younger ones (Turecek et al., 2016, 2017). However, the upregulated expression of Syt7 during development may also exist at synapses showing frequency-dependent release (Sugita et al., 2001). Besides, the ratio between the main Ca^{2+} sensor Syt1/2 and Syt7 may contribute, because Syt1/2 and Syt7 could determine the size of the depression vesicle pool, which has a slow refilling rate, and the facilitation vesicle pool, which has a fast refilling rate, respectively. (Turecek et al., 2016, 2017). Finally, an interesting point is that all synapses have been shown to release transmitter in a frequency-independent manner were found in the caudal brain (Bagnall et al., 2008; Turecek et al., 2016, 2017; Chen et al., 2017b) where Syt2 is highly expressed (Pang et al., 2006a; Chen et al., 2017a). Whether Syt7 conveys the frequency independence of release depends on the presence of Syt2 needs to be further examined.

Syt7 is synthesized in a large number of alternatively spliced forms in mouse brain (Sugita et al., 2001). They are mainly classified into three groups: the truncated ones without the C2 domain (Sytβ), the small (Syt7α) and large isoforms (Syt7γ) with the C2 domain but differ in the linker length between the transmembrane domain and C2 domain (Sugita et al., 2001). Quantitative analysis indicated that the proportion of

these three Syt7 mRNAs is approximately α: β: γ = 77: 20: 3 (Fukuda et al., 2002). The Syt7 mutant mouse used in our Syt7 project and many other Syt7 studies was generated by targeting the C2 domain, the critical functional regions responsible for the Ca^{2+}-dependent interactions previously detected in synaptotagmins, of Syt7α isoform (Chapman, 2002; Chakrabati et al., 2003). However, the expression level of other Syt7 isoforms at BC–PC synapse has not been clearly examined. And the function of other Syt7 isoforms for synaptic transmission still needs to be further investigated, since overexpression of the truncated isoform of Syt7 has been shown to prolong endocytosis in cultured hippocampal synapses (Li et al., 2017). The expression level or the function or both of other Syt7 isoforms at the BC–PC synapse could also be a potential mechanism underlying the “over” rescued phenotype we obtained by viral expression of the Syt7α cDNA in Syt7 mutant mice, although we mainly attributed it to the higher expression level of Syt7α isoform after virus injection. Besides, whether there is any compensatory upregulation of other Syt7 isoforms in Syt7 genetic deletion mice still needs to be further tested.

4.2 Synaptotagmin for fast signaling properties of molecular layer cerebellar interneurons

In the cerebellar molecular layer, the inhibitory interneurons have been historically divided into the basket and stellate cells (Sotelo, 2015). Although there are clear location and morphological differences between them (Sultan et al., 1998, Chu et al., 2012), and they target different parts of the Purkinje cell (Palay and Chan-palay, 1974; O’Donoghue et al., 1989; Donato et al., 2008, Huang et al., 2007), several studies showed that they are functionally less distinct (Jörntell and Ekerot, 2003; Ekerot and Jörntell, 2003). Both basket and stellate cells receive input from the parallel fiber and control the activity of postsynaptic Purkinje cells by feedforward inhibition. Our immunochemistry results suggested that Syt1 and Syt2 are highly expressed in the molecular layer without clear overlap (Chen et al., 2017a). Whether Syt1 is only used by excitatory synapses or also used by the output synapse of stellate cells needs to be further investigated, although our feedforward inhibition experiment indicated that Syt2 may mainly be used.

Genetic analysis showed that both Syt1 and Syt2 are highly expressed in basket/stellate cells (Paul et al., 2012), and a study on the calyx of Held has

suggested a developmental switch of the main Ca^{2+} sensor from Syt1 to Syt2 for mediating transmitter release (Kochubey et al, 2016). Our results showed that deletion of Syt2 impaired ~90% of the release at BC–PC synapses in P14–16 old mice. However, whether the residual release is mediated by Syt1 or other synaptotagmin members have not been clearly identified. If both Syt1 and Sy2 work in concert for transmitter release at inhibitory synapses, especially at the hippocampal BC to GC synapse, in which genetic deletion of Syt1 only reduced asynchronous release to ~50% (Kerr et al., 2008), do they trigger release of different vesicles or do they mediate release of the same vesicles collaboratively? The developmental switch of the Ca^{2+} sensor from Syt1 to Syt2 has not been tested at the inhibitory synapses. If there is also a developmental switch of the main Ca^{2+} sensor from Syt1 to Syt2 at the cerebellar basket/stellate output synapses, what is the molecular mechanism mediating this switch? All these questions need to further solved.

Fast transmitter release is the hallmark of PV^{+}-interneurons (Hu et al., 2014). However, how these fast-spiking interneurons keep sufficient release during high activity was not clear. Since most inhibitory synapses show depression in response to train of stimuli, the ability to keep sufficient release during high network activity would be critical for controlling the activity of postsynaptic neurons (Hefft and Jonas, 2005; Arai and Jonas, 2014; Chen et al., 2017a). We found that, different from many other synapses, the BC–PC synapse confers frequency-independent transmitter release during high activity. This property leads to a linear relationship between the activity of BC and the total inhibitory synaptic charge, guaranteeing sufficient inhibitory transmitter release even at high activity. BC–PC synapse may be specialized to precisely fulfill its feedforward inhibition role for controlling the PC activity (Mittmann et al., 2005; Chen et al., 2017b). Considering Syt7 is critical for this frequency-independent release and genetic Syt7 deletion does not significantly affect basic synaptic transmission of BC, some *in vivo* experiments combing behavior tests could be conducted in the future to investigate the physiological function of the frequency−independent release.

4.3 Synaptotagmin for short-term plasticity

Synaptotagmins work as Ca^{2+} sensors and play an important role in short−term plasticity. Genetic deletion of Syt1 or Syt2 switched short-term depression to short−term facilitation in both excitatory (Bacaj et al., 2014; Liu et al., 2014) and inhibitory synapses (Kerr et al., 2008; Chen et al., 2017a). Point mutation of one amino acid in the C2B domain of Syt1, which caused a twofold decrease in overall Ca^{2+} affinity without inducing structural or conformational changes, also switched the short-term depression to short-term facilitation of the hippocampal cultured cells (Fernández-Chacón et al., 2001). Besides, Syt7 has been suggested to work as a facilitation sensor mediating short-term facilitation (Jackman et al., 2016; Turecek et al., 2017). For Syt1 or Syt2 knockout synapse, the facilitation may be mediated by another facilitating Ca^{2+} sensor, but the identity of this sensor needs to be further examined (Chen et al., 2017a). Release probability is another important factor. The release probability was decreased by point mutation of one amino acid in the C2B domain of Syt1, which induced the switch between depression and facilitation (Fernández-Chacón et al., 2001). GABAergic synapse mainly shows short-term depression (Hefft and Jonas, 2005; Sakaba, 2008; Hu et al., 2014; Arai and Jonas, 2014), which has been suggested to work as a low-pass filter (Fortune and Rose, 2000; Hefft and Jonas 2005). Synaptotagmin isoform, however, is also critical for determining the depression level during activity. In Syt2 knockout cerebellar BC–PC synapses, rescued experiments with viral expression of different synaptotagmin isoforms showed that Syt1−rescued synapses displayed a stronger steady−state depression than Syt2−rescued synapses. Further analysis suggested that the stronger depression is due to a slow pool replenishment rate in Syt1−rescued synapses (Chen et al., 2017a). Additionally, research about Syt7 showed that Syt7 conveys frequency-independent release also by promoting the pool replenishment rate in a Ca^{2+}-dependent manner at this synapse (Chen et al., 2017b). However, Syt2 is mainly expressed on the vesicle membrane, while Syt7 is abundantly located in the plasma membrane, what then is the difference between Syt2- and Syt7−mediated replenishment rate during activity? Do Syt2 or Syt7 promotes vesicle pool replenishment through different pathways, or do they mediate the vesicle pool refilling collaboratively?

In Syt1-rescued BC–PC synapses, in which the expression of Syt7 is highly

unaffected, the steady-state depression was similar compared to the Syt7 knockout BC–PC synapses, in which the expression of Syt2 should be unaffected (Chen et al., 2017a; Chen et al., 2017b). Additionally, proteomics analysis showed that Syt2 and Syt7 are linked to the Ca^{2+} channels, but not Syt1 (Müller et al., 2010). These results indicate that Syt2 and Syt7 may highly mediate pool replenishment collaboratively. Syt7 may accelerate pool refilling rate by promoting the reusing of Syt2 when it approximates the plasma membrane during vesicle fusion. Another possibility could be that Syt7 helps to clean the release sites after vesicle fusion, which may promote the priming and docking of vesicles (Jackman and Regehr, 2017). Besides, Syt7 may also contribute to the fast pool refilling by mediating a facilitation pool, which has a faster refilling rate. (Turecek et al., 2016, 2017). Furthermore, considering both Syt2 and Syt7 are connected to the Ca^{2+} channel, they could promote vesicle pool refilling, a Ca^{2+}-dependent process (Sakaba, 2008), by changing kinetics of the Ca^{2+} channel activation and deactivation during activity. However, the possibility that Syt2 and Syt7 mediates vesicle pool replenishment through different pathways still cannot be ruled out.

References:

Adrian, E.D. (1943). Afferent areas in the cerebellum connected with the limbs. Brain *66*, 289–315.

Arai, I., and Jonas, P. (2014). Nanodomain coupling explains Ca^{2+} independence of transmitter release time course at a fast central synapse. Elife *3*, e04057.

Bacaj, T., Wu, D., Burré, J., Malenka, R.C., Liu, X., and Südhof, T.C. (2015). Synaptotagmin-1 and -7 are redundantly essential for maintaining the capacity of the readily-releasable pool of synaptic vesicles. PLoS Biol. *13*, e1002267.

Bacaj, T., Wu, D., Yang, X., Morishita, W., Zhou, P., Xu, W., Malenka, R.C., and Südhof, T.C. (2013). Synaptotagmin-1 and synaptotagmin-7 trigger synchronous and asynchronous phases of neurotransmitter release. Neuron *80*, 947–959.

Bagnall, M.W., McElvain, L.E., Faulstich, M., and du Lac, S. (2008). Frequency–independent synaptic transmission supports a linear vestibular behavior. Neuron *60*, 343–352.

Bao, J., Reim, K., and Sakaba, T. (2010). Target-dependent feedforward inhibition mediated by short-term synaptic plasticity in the cerebellum. J. Neurosci. *30*, 8171–8179.

Bartolini, G., Ciceri, G., and Marín, O. (2013). Integration of GABAergic Interneurons into cortical cell assemblies: lessons from embryos and adults. Neuron *79*, 849–864.

Bastian, A.J., Martin, T. A., Keating, J.G., and Thach, W.T. (1996). Cerebellar ataxia: abnormal control of interaction torques across multiple joints. J. Neurophysiol. *76*, 492–509.

Bucurenciu, I., Bischofberger, J., and Jonas, P. (2010). A small number of open Ca^{2+} channels trigger transmitter release at a central GABAergic synapse. Nat. Neurosci. *13*, 19–21.

Bucurenciu, I., Kulik, A., Schwaller, B., Frotscher, M., and Jonas, P. (2008). Nanodomain coupling between Ca^{2+} channels and Ca^{2+} sensors promotes fast and efficient transmitter release at a cortical GABAergic synapse. Neuron *57*, 536–545.

Burnashev, N., and Rozov, A. (2005). Presynaptic Ca^{2+} dynamics, Ca^{2+} buffers and synaptic efficacy. Cell Calcium *37*, 489–495.

Butt S.J., Stacey J.A., Teramoto Y, and Vagnoni C. (2017) A role for GABAergic interneuron diversity in circuit development and plasticity of the neonatal cerebral cortex. Curr Opin Neurobiol. *43*, 149–155.

Caillard, O., Moreno, H., Schwaller, B., Llano, I., Celio, M.R., and Marty, A. (2000). Role of the calcium-binding protein parvalbumin in short-term synaptic plasticity. Proc. Natl. Acad. Sci. USA *97*, 13372–13377.

Cao P, Yang X and Südhof T.C. (2013). Complexin Activates Exocytosis of Distinct Secretory Vesicles Controlled by Different Synaptotagmins. J. Neurosci. *33*, 1714–1727.

Cardin, J.A., Carlén, M., Meletis, K., Knoblich, U., Zhang, F., Deisseroth, K., Tsai, L.H., and Moore, C.I. (2009). Driving fast-spiking cells induces gamma rhythm and controls sensory responses. Nature *459*, 663–667.

Cattani, A., Solinas, S., and Canuto, C. (2016). A Hybrid Model for the Computationally-Efficient Simulation of the Cerebellar Granular Layer. Front Comput Neurosci. *10*.

Ceccarelli, B., Hurlbut, W.P., and Mauro, A. (1973). Turnover of transmitter and synaptic vesicles at the frog neuromuscular junction. J. Cell Biol. *57*, 499–524

Celio, M.R. (1986). Parvalbumin in Most γ-Aminobutyric Acid-Containing Neurons of the Rat Cerebral Cortex. Science *231*, 995–997.

Chakrabarti, S., Kobayashi, K.S., Flavell, R.A., Marks, C.B., Miyake, K., Liston, D.R., Fowler, K.T., Gorelick, F.S., and Andrews, N.W. (2003). Impaired membrane resealing and autoimmune myositis in synaptotagmin VII-deficient mice. J. Cell Biol. *162*, 543–549.

Chapman, E.R. (2002). Synaptotagmin: a Ca^{2+} sensor that triggers exocytosis? Nat. Rev. Mol. Cell Biol. *3*, 498–508.

Chen, C., and Jonas, P. (2017). Synaptotagmins: That's Why So Many. Neuron *94*, 694–696.

Chen, C., Arai, I., Satterfield, R., Young, S.M. Jr., and Jonas, P. (2017a). Synaptotagmin 2 is the fast Ca^{2+} sensor at a central inhibitory synapse. Cell Rep. *18*, 723–736.

Chen C, Satterfield R, Young SM, and Jonas P. (2017b). Triple function of synaptotagmin 7 ensures efficiency of high-frequency transmission at central GABAergic synapses. Cell Rep. *21,* 2082–2089.

Chen, Z., Cooper, B., Kalla, S., Varoqueaux, F., and Young, S.M. Jr. (2013). The Munc13 proteins differentially regulate readily releasable pool dynamics and calcium-dependent recovery at a central synapse. J. Neurosci. *33*, 8336–8351.

Chen, Z., Das, B., Nakamura, Y., DiGregorio, D.A., and Young, S.M. Jr. (2015). Ca^{2+} channel to synaptic vesicle distance accounts for the readily releasable pool kinetics at a functionally mature auditory synapse. J. Neurosci. *35*, 2083–2100.

Chicka, M.C., Hui, E., Liu, H., and Chapman, E.R. (2008). Synaptotagmin arrests the SNARE complex before triggering fast, efficient membrane fusion in response to Ca^{2+}. Nat. Struct. Mol. Biol. *15*, 827–835.

Christie, J.M., Chiu, D.N., and Jahr, C.E. (2011). Ca^{2+}-dependent enhancement of release by subthreshold somatic depolarization. Nat. Neurosci. *14*, 62–68.

Chu, C.P., Bing, Y.H., Liu, H., and Qiu, D.L. (2012). Roles of molecular layer interneurons in sensory information processing in mouse Cerebellar cortex Crus ii in vivo. PLoS ONE *7*.

Davydova, D., Marini, C., King, C., Klueva, J., Bischof, F., Romorini, S., Montenegro-Venegas, C., Heine, M., Schneider, R., Schröder, M.S., et al. (2014). Bassoon specifically controls presynaptic P/Q-type Ca^{2+} channels via RIM-binding protein. Neuron *82*, 181–194.

DeFelipe, J., López-Cruz, P. L., Benavides-Piccione, R., Bielza, C., Larrañaga, P., Anderson, S., Burkhalter, A., Cauli, B., Fairén, A., Feldmeyer, D., et al., (2013). New insights into the classification and nomenclature of cortical GABAergic interneurons. Nat. Rev. Neurosci. *14*, 202–216.

Delvendahl, I., Vyleta, N.P., von Gersdorff, H., and Hallermann, S. (2016). Fast, temperature-sensitive and clathrin-independent endocytosis at central synapses. Neuron *90*, 492–498.

Dodge, F., and Rahamimoff, R. (1967). Co-operative action of calcium ions in transmitter release at the neuromuscular junction. J. Neurophysiol. *193*, 419–432.

Donato R., Rodrigues R.J., Takahashi M., Tsai M.C., Soto D. (2008). GABA release by basket cells onto Purkinje cells, in rat cerebellar slices, is directly controlled by presynaptic purinergic receptors, modulating Ca^{2+} influx. Cell Calcium *44*, 521–532.

Du, J., Zhang, L., Weiser, M., Rudy, B., and McBain, C.J. (1996). Developmental expression and functional characterization of the potassium-channel subunit Kv3.1b in parvalbumin-containing interneurons of the rat hippocampus. J. Neurosci. *16*, 506–518.

Eccles J.C., Ito M., Szentagothai J. (1967). The Cerebellum as a Neuronal Machine. Berlin: Springer-Verlag.

Eccles J.C., Katz B., Kuffler S.W. (1941). Nature of the “endplate potential” in curarized muscle. J. Neurophysiol. *4*, 362–387

Eggermann, E., and Jonas, P. (2012). How the ‘slow’ Ca^{2+} buffer parvalbumin affects transmitter release in nanodomain coupling regimes. Nat. Neurosci. *15*, 20–22.

Eggermann, E., Bucurenciu, I., Goswami, S.P., and Jonas, P. (2012). Nanodomain coupling between Ca^{2+} channels and sensors of exocytosis at fast mammalian synapses. Nat. Rev. Neurosci. *13*, 7–21.

Ekerot, C.F., and Jörntell, H. (2003). Parallel fiber receptive fields: a key to understanding cerebellar operation and learning. Cerebellum *2*, 101–109.

Felmy, F., Neher, E., and Schneggenburger, R. (2003). Probing the intracellular calcium sensitivity of transmitter release during synaptic facilitation. Neuron *37*, 801–811.

Feng T.P. (1941). The changes in the end- plate potential during and after prolonged stimulation. Chin. J. Physiol. *13*, 79–107

Fernández-Chacón, R., Königstorfer, A., Gerber, S.H., García, J., Matos, M.F., Stevens, C.F., Brose, N., Rizo, J., Rosenmund, C., and Südhof, T.C. (2001). Synaptotagmin I functions as a calcium regulator of release probability. Nature *410*, 41–49.

Fogelson, A.L., and Zucker, R.S. (1985). Presynaptic calcium diffusion from various arrays of single channels. Implications for transmitter release and synaptic facilitation. Biophys J. *48*, 1003–1017.

Földy, C., Darmanis, S., Aoto, J., Malenka, R.C., Quake, S.R., and Südhof, T.C. (2016). Single-cell RNAseq reveals cell adhesion molecule profiles in electrophysiologically defined neurons. Proc. Natl. Acad. Sci. USA *113*, E5222−E5231.

Fortune, E.S., and Rose, G.J. (2000). Short-term synaptic plasticity contributes to the temporal filtering of electrosensory information. J. Neurosci. *20*, 7122–7130.

Fox, M.A., and Sanes, J.R. (2007). Synaptotagmin I and II are present in distinct subsets of central synapses. J. Comp. Neurol. *503*, 280–296.

Fukuda, M., Ogata, Y., Saegusa, C., Kanno, E., and Mikoshiba, K. (2002). Alternative splicing isoforms of synaptotagmin VII in the mouse, rat and human. Biochem. J. *365*, 173–180.

Geppert, M., Goda, Y., Hammer, R.E., Li, C., Rosahl, T.W., Stevens, C.F., and Südhof, T.C. (1994). Synaptotagmin I: a major Ca^{2+} sensor for transmitter release at a central synapse. Cell *79*, 717–727.

Giraudo, C.G., Eng, W.S., Melia, T.J., and Rothman, J.E. (2006). A clamping mechanism involved in SNARE-dependent exocytosis. Science *313*, 676–680.

Goswami, S.P., Bucurenciu, I., and Jonas, P. (2012). Miniature IPSCs in hippocampal granule cells are triggered by N-type Ca^{2+} channels and Ca^{2+} microdomains. J. Neurosci. *32*, 14294–14304.

Guzman, S.J., Schlögl, A., and Schmidt-Hieber, C. (2014). Stimfit: quantifying electrophysiological data with Python. Front. Neuroinform. *8*, 16.

Hanson P.I., Roth R., Morisaki H., Jahn R., and Heuser J.E. (1997). Structure and conformational changes in NSF and its membrane receptor complexes visualized by quick-freeze/deep-etch electron microscopy. Cell *90*, 523–35.

Haucke, V., and De Camilli, P. (1999). AP-2 recruitment to synaptotagmin stimulated by tyrosine-based endocytic motifs. Science *285*, 1268–1271.

Häusser, M., and Clark, B.A. (1997). Tonic synaptic inhibition modulates neuronal output pattern and spatiotemporal synaptic integration. Neuron *19*, 665–678.

Hefft, S., and Jonas, P. (2005). Asynchronous GABA release generates long-lasting inhibition at a hippocampal interneuron–principal neuron synapse. Nat. Neurosci. *8*, 1319–1328.

Herculano-Houzel S. (2010). Coordinated scaling of cortical and cerebellar numbers of neurons. Front Neuroanat. 4: 12.

Herrmann, D.N., Horvath, R., Sowden, J.E., Gonzales, M., Sanchez-Mejias, A., Guan, Z., Whittaker, R.G., Almodovar, J.L., Lane, M., Bansagi, B., et al. (2014). Synaptotagmin 2 mutations cause an autosomal-dominant form of lambert–eaton myasthenic syndrome and nonprogressive motor neuropathy. Am. J. Hum. Genet. *95*, 332–339.

Heuser, J.E. and Reese, T.S. (1973). Evidence for recycling of synaptic vesicle membrane during transmitter release at the frog neuromuscular junction. J. Cell Biol. *57*, 315–344

Hosoi, N., Holt, M., and Sakaba, T. (2009). Calcium dependence of exo- and endocytotic coupling at a glutamatergic synapse. Neuron *63*, 216–229.

Hu, H., Gan, J., and Jonas, P. (2014). Fast-spiking, parvalbumin^{+} GABAergic interneurons: from cellular design to microcircuit function. Science *345*, 1255263.

Huang Z.J., Di Cristo G., and Ango F. (2007). Development of GABA innervation in the cerebral and cerebellar cortices. Nat. Rev. Neurosci. *8,* 673–686.

Hui, E., Bai, J., Wang, P., Sugimori, M., Llinas, R.R., and Chapman, E.R. (2005). Three distinct kinetic groupings of the synaptotagmin family: candidate sensors for rapid and delayed exocytosis. Proc. Natl. Acad. Sci. USA *102*, 5210–5214.

Imig, C., Min, S.W., Krinner, S., Arancillo, M., Rosenmund, C., Südhof, T.C., Rhee, J., Brose, N., and Cooper, B.H. (2014). The morphological and molecular nature of synaptic vesicle priming at presynaptic active zones. Neuron *84*, 416–431.

Jackman, S.L., and Regehr, W.G. (2017). The mechanisms and functions of synaptic facilitation. Neuron *94*, 447–464.

Jackman, S.L., Turecek, J., Belinsky, J.E., and Regehr, W.G. (2016). The calcium sensor synaptotagmin 7 is required for synaptic facilitation. Nature *529*, 88–91.

Jaeger D., and Bower J.M. (1999). Synaptic control of spiking in cerebellar Purkinje cells: dynamic current clamp based on model conductances. J. Neurosci. *19*, 6090–6101.

Jahn, R., Lang, T., and Südhof, T.C. (2003). Membrane fusion. Cell *112*, 519–533.

Jarousse, N., and Kelly, R.B. (2001). The AP2 binding site of synaptotagmin 1 is not an internalization signal but a regulator of endocytosis. J. Cell Biol. *154*, 857–866.

Jelitai, M., Puggioni, P., Ishikawa, T., Rinaldi, A., and Duguid, I. (2016). Dendritic excitation-inhibition balance shapes cerebellar output during motor behaviour. Nat. Commun. *7*, 13722.

Jones, M.V., Jonas, P., Sahara, Y., and Westbrook, G.L. (2001). Microscopic kinetics and energetics distinguish $GABA_A$ receptor agonists from antagonists. Biophys. J. *81*, 2660–2670.

Jörntell, H., and Ekerot, C.F. (2003). Receptive field plasticity profoundly alters the cutaneous parallel fiber synaptic input to cerebellar interneurons in vivo. J. Neurosci. *23*, 9620–9631.

Kaeser, P.S., Deng, L., Wang, Y., Dulubova, I., Liu, X., Rizo, J., and Südhof, T.C. (2011). RIM proteins tether Ca^{2+} channels to presynaptic active zones via a direct PDZ-domain interaction. Cell *144*, 282–295.

Katz B. (1969). The Release of Neural Transmitter Substances. Liverpool: Liverpool Univ. Press.

Kerr, A.M., Reisinger, E., and Jonas, P. (2008). Differential dependence of phasic transmitter release on synaptotagmin 1 at GABAergic and glutamatergic hippocampal synapses. Proc. Natl. Acad. Sci. USA *105*, 15581–15586.

Klausberger, T. and Somogyi, P. (2008) Neuronal diversity and temporal dynamics: the unity of hippocampal circuit operations. Science *321*, 53–57.

Kochubey, O., Babai, N., and Schneggenburger, R. (2016). A synaptotagmin isoform switch during the development of an identified CNS synapse. Neuron *90*, 984–999.

Koh, T.W., and Bellen, H.J. (2003). Synaptotagmin I, a Ca^{2+} sensor for neurotransmitter release. Trends Neurosci. *26*, 413–422.

Kononenko, N.L., and Haucke, V. (2015). Molecular mechanisms of presynaptic membrane retrieval and synaptic vesicle reformation. Neuron *85*, 484–496.

Körber, C., Horstmann, H., Venkataramani, V., Herrmannsdörfer, F., Kremer, T., Kaiser, M., Schwenger, D.B., Ahmed, S., Dean, C., Dresbach, T., et al. (2015). Modulation of Presynaptic Release Probability by the Vertebrate-Specific Protein Mover. Neuron *87*, 521–533.

Kraushaar, U., and Jonas, P. (2000). Efficacy and stability of quantal GABA release at a hippocampal interneuron-principal neuron synapse. J. Neurosci. *20*, 5594–5607.

Kushmerick, C. (2004). Retroinhibition of Presynaptic Ca^{2+} Currents by Endocannabinoids Released via Postsynaptic mGluR Activation at a Calyx Synapse. J. Neurosci. *24*, 5955–5965.

Kushmerick, C. (2006) Physiological temperatures reduce the rate of vesicle pool depletion and short-term depression via an acceleration of vesicle recruitment. J. Neurosci. *26*, 1366–1377

Lapray, D., Lasztoczi, B., Lagler, M., Viney, T.J., Katona, L., Valenti, O., Hartwich, K., Borhegyi, Z., Somogyi, P., and Klausberger, T. (2012). Behavior-dependent specialization of identified hippocampal interneurons. Nat. Neurosci. *15*, 1265−1271.

Li, L., Bischofberger, J., and Jonas, P. (2007). Differential gating and recruitment of P/Q-, N-, and R-type Ca^{2+} channels in hippocampal mossy fiber boutons. J. Neurosci. *27*, 13420–13429.

Li, Y.C., Chanaday, N.L., Xu, W., and Kavalali, E.T. (2017). Synaptotagmin-1- and Synaptotagmin-7-dependent fusion mechanisms target synaptic vesicles to kinetically distinct endocytic pathways. Neuron *93*, 616–631.

Lisberger S.G., and Thach W.T. (2013). “The cerebellum,” in Principles of Neural Science, E. Kandel, J. H. Schwartz, T. M. Jessell, S. Siegelbaum, A. J. Hudspeth, Eds. (McGraw-Hill, New York), pp. 960–979.

Littleton, J.T., Stern, M., Perin, M., and Bellen, H.J. (1994). Calcium dependence of neurotransmitter release and rate of spontaneous vesicle fusions are altered in Drosophila synaptotagmin mutants. Proc. Natl. Acad. Sci. USA *91*, 10888−10892.

Liu, H., Bai, H., Hui, E., Yang, L., Evans, C.S., Wang, Z., Kwon, S.E., and Chapman, E.R. (2014). Synaptotagmin 7 functions as a Ca^{2+}-sensor for synaptic vesicle replenishment. Elife *3*, e01524.

Liu, H., Bai, H., Xue, R., Takahashi, H., Edwardson, J.M., and Chapman, E.R. (2014). Linker mutations reveal the complexity of synaptotagmin 1 action during synaptic transmission. Nat. Neurosci. *17*, 670–677.

Liu, H., Dean, C., Arthur, C.P., Dong, M., and Chapman, E.R. (2009). Autapses and networks of hippocampal neurons exhibit distinct synaptic transmission phenotypes in the absence of synaptotagmin I. J. Neurosci. *29*, 7395–7403.

Luo, F., and Südhof, T.C. (2017). Synaptotagmin-7 mediated asynchronous release boosts high-fidelity synchronous transmission at a central synapse. Neuron *94*, 826–839.

Mackler, J.M., Drummond, J.A., Loewen, C.A., Robinson, I.M., and Reist, N.E. (2002). The C_2B Ca^{2+}-binding motif of synaptotagmin is required for synaptic transmission *in vivo*. Nature *418*, 340–344.

Martina, M., Schultz, J.H., Ehmke, H., Monyer, H., and Jonas, P. (1998). Functional and molecular differences between voltage-gated K^+ channels of fast-spiking interneurons and pyramidal neurons of rat hippocampus. J. Neurosci. *18*, 8111–8125.

Maximov, A., and Südhof, T.C. (2005). Autonomous function of synaptotagmin 1 in triggering synchronous release independent of asynchronous release. Neuron *48*, 547–554.

Maximov, A., Lao, Y., Li, H., Chen, X., Rizo, J., Sørensen, J.B., and Südhof, T.C. Genetic analysis of synaptotagmin-7 function in synaptic vesicle exocytosis. Proc. Natl. Acad. Sci. U S A *105*, 3986–3991.

Mittelsteadt, T., Seifert, G., Alvárez-Barón, E., Steinhäuser, C., Becker, A.J., and Schoch, S. (2009). Differential mRNA expression patterns of the synaptotagmin gene family in the rodent brain. J. Comp. Neurol. *512*, 514–528.

Mittmann, W., Koch, U., and Häusser, M. (2005). Feed-forward inhibition shapes the spike output of cerebellar Purkinje cells. J. Physiol. *563*, 369–378.

Montesinos, M.S., Chen, Z., and Young, S.M. Jr. (2011). pUNISHER: a high-level expression cassette for use with recombinant viral vectors for rapid and long term in vivo neuronal expression in the CNS. J. Neurophysiol. *106*, 3230–3244.

Mueller, V.J. (2004). Monitoring Clathrin-Mediated Endocytosis during Synaptic Activity. J. Neurosci. *24*, 2004–2012.

Mukherjee, K., Yang, X., Gerber, S.H., Kwon, H.B., Ho, A., Castillo, P.E., Liu, X., and Südhof, T.C. (2010). Piccolo and bassoon maintain synaptic vesicle clustering without directly participating in vesicle exocytosis. Proc. Natl. Acad. Sci. USA *107*, 6504–6509.

Müller, C.S., Haupt, A., Bildl, W., Schindler, J., Knaus, H.G., Meissner, M., Rammner, B., Striessnig, J., Flockerzi, V., Fakler, B., and Schulte, U. (2010). Quantitative proteomics of the Cav2 channel nano-environments in the mammalian brain. Proc. Natl. Acad. Sci. USA *107*, 14950–14957.

Nagy, G., Kim, J.H., Pang, Z.P., Matti, U., Rettig, J., Südhof, T.C., and Sørensen, J.B. (2006). Different effects on fast exocytosis induced by synaptotagmin 1 and 2 isoforms and abundance but not by phosphorylation. J. Neurosci. *26*, 632–643.

Neher, E. (2015). Merits and limitations of vesicle pool models in view of heterogeneous populations of synaptic vesicles. Neuron *87*, 1131–1142.

Neher, E., and Augustine, G.J. (1992). Calcium gradients and buffers in bovine chromaffin cells. J. Physiol. *450*, 273–301.

Neher, E., and Sakaba, T. (2008). Multiple Roles of Calcium Ions in the Regulation of Neurotransmitter Release. Neuron *59*, 861–872.

Nishiki, T., and Augustine, G.J. (2004). Dual roles of the C2B domain of synaptotagmin I in synchronizing Ca^{2+}-dependent neurotransmitter release. J. Neurosci. *24*, 8542–8550.

O'Donoghue D.L., King J.S., and Bishop G.A. (2012). Physiological and anatomical studies of the interactions between Purkinje cells and basket cells in the cat's cerebellar cortex: evidence for a unitary relationship. J Neurosci. *9*, 2141–2150.

Palay S.L., and Chan-Palay V. (1974). Cerebellar Cortex, New York: Springer-Verlag.

Palmer, D., and Ng, P. (2003). Improved system for helper-dependent adenoviral vector production. Mol. Ther. *8*, 846–852.

Palmer, M.J., Hull, C., and Vigh, J. (2003). Synaptic cleft acidification and modulation of short-term depression by exocytosed protons in retinal bipolar cells. J. Neurosci. *23*, 11332–11341.

Pang, Z.P., Melicoff, E., Padgett, D., Liu, Y., Teich, A.F., Dickey, B.F., Lin, W., Adachi, R., and Südhof, T.C. (2006a). Synaptotagmin-2 is essential for survival and contributes to Ca^{2+} triggering of neurotransmitter release in central and neuromuscular synapses. J. Neurosci. *26*, 13493–13504.

Pang, Z.P., Sun, J., Rizo, J., Maximov, A., and Südhof, T.C. (2006b). Genetic analysis of synaptotagmin 2 in spontaneous and Ca^{2+}-triggered neurotransmitter release. EMBO J. *25*, 2039–2050.

Paul, A., Cai, Y., Atwal, G.S., and Huang, Z.J. (2012). Developmental coordination of gene expression between synaptic partners during GABAergic circuit assembly in cerebellar cortex. Front Neural Circuits *6*, 37.

Perin, M.S.S., Fried, V.A.A., Mignery, G.A.A., Jahn, R., and Südhof, T.C. (1990). Phospholipid binding by a synaptic vesicle protein homologous to the regulatory region of protein kinase C. Nature *345*, 260–263.

Perin, M.S., Johnston, P.A., Ozcelik, T., Jahn, R., Francke, U., and Südhof, T.C. (1991). Structural and functional conservation of synaptotagmin (p65) in Drosophila and humans. J. Biol. Chem. *266*, 615–622.

Pernía-Andrade, A.J., Goswami, S.P., Stickler, Y., Fröbe, U., Schlögl, A., and Jonas, P. (2012). A deconvolution-based method with high sensitivity and temporal resolution for detection of spontaneous synaptic currents in vitro and in vivo. Biophys. J. *103*, 1429–1439.

Poskanzer, K.E., Marek, K.W., Sweeney, S.T., and Davis, G.W. (2003). Synaptotagmin I is necessary for compensatory synaptic vesicle endocytosis in vivo. Nature *426*, 559–563.

Pouille, F., and Scanziani, M. (2001). Enforcement of temporal fidelity in pyramidal cells by somatic feed-forward inhibition. Science *293*, 1159–1163.

Pulido, C., Trigo, F.F., Llano, I., and Marty, A. (2015). Vesicular release statistics and unitary postsynaptic current at single GABAergic synapses. Neuron *85*, 159−172.

Regehr, W.G. (2012). Short-term presynaptic plasticity. Cold Spring Harb. Perspect. Biol. *4*, 1–19.

Reim K., Mansour M., Varoqueaux F., McMahon H.T., Südhof T.C., Brose N., and Rosenmund C. (2001). Complexins regulate the Ca^{2+}-sensitivity of the synaptic neurotransmitter release machinery. Cell *104*, 71–81.

Rizzoli, S.O., and Betz, W.J. (2005). Synaptic vesicle pools. Nat. Rev. Neurosci. *6*, 57–69.

Roberts WM. (1993). Spatial calcium buffering in saccular hair cells. Nature *363,* 74−76

Rosenmund, C., and Stevens, C.F. (1996). Definition of the readily releasable pool of vesicles at hippocampal synapses. Neuron *16*, 1197–1207.

Roth, A., and Häusser, M. (2001). Compartmental models of rat cerebellar Purkinje cells based on simultaneous somatic and dendritic patch-clamp recordings. J. Physiol. *535*, 445–472.

Rudy, B., and McBain, C.J. (2001). Kv3 channels: Voltage-gated K^+ channels designed for high-frequency repetitive firing. Trends Neurosci. *24*, 517–526.

Sabatini B.L. and Regehr W.G. (1996). Timing of neurotransmission at fast synapses in the mammalian brain. Nature *384*,170–172.

Sakaba T. (2008) Two Ca^{2+}-dependent steps controlling synaptic vesicle fusion and replenishment at the cerebellar basket cell terminal. Neuron *57*, 406–419.

Sakaba, T., and Neher, E. (2001). Calmodulin mediates rapid recruitment of fast−releasing synaptic vesicles at a calyx-type synapse. Neuron *32*, 1119−1131.

Sakaba, T., and Neher, E. (2001). Preferential potentiation of fast-releasing synaptic vesicles by cAMP at the calyx of Held. Proc. Natl. Acad. Sci. USA *98*, 331–336.

Santamaria F., Tripp P.G., and Bower J.M. (2007). Feedforward inhibition controls the spread of granule cell-induced Purkinje cell activity in the cerebellar cortex. J. Neurophysiol. *97,* 248–263.

Scheuss, V., Schneggenburger, R., and Neher, E. (2002). Separation of presynaptic and postsynaptic contributions to depression by covariance analysis of successive EPSCs at the calyx of Held synapse. J. Neurosci. *22*, 728–739.

Schneggenburger, R., and Neher, E. (2005). Presynaptic calcium and control of vesicle fusion. Curr. Opin. Neurobiol. *15*, 266–274.

Schneggenburger, R., Meyer, A.C., and Neher, E. (1999). Released fraction and total size of a pool of immediately available transmitter quanta at a calyx synapse. Neuron *23*, 399–409.

Schneggenburger, R., Sakaba, T., and Neher, E. (2002). Vesicle pools and short−term synaptic depression: Lessons from a large synapse. Trends Neurosci. *25*, 206–212.

Schonn, J.S., Maximov, A., Lao, Y., Südhof, T.C., and Sørensen, J.B. (2008). Synaptotagmin-1 and -7 are functionally overlapping Ca^{2+} sensors for exocytosis in adrenal chromaffin cells. Proc. Natl. Acad. Sci. USA *105*, 3998−4003.

Schotten, S., Meijer, M., Walter, A.M., Huson, V., Mamer, L., Kalogreades, L., ter Veer, M., Ruiter, M., Brose, N., Rosenmund, C., Sørensen, J.B., Verhage, M., and Cornelisse, L.N. (2015). Additive effects on the energy barrier for synaptic

vesicle fusion cause supralinear effects on the vesicle fusion rate. Elife *4*, e05531.

Simon, S.M., and Llinás, R.R. (1985). Compartmentalization of the submembrane calcium activity during calcium influx and its significance in transmitter release. Biophys J. *48*, 485–498.

Smith, S.M., Bergsman, J.B, Harata N.C., Scheller R.H., and Tsien A.R.W. (2004). Recordings from single neocortical nerve terminals reveal a nonselective cation channel activated by decreases in extracellular calcium. Neuron *41*, 243–256

Smith, S.M., Renden, R., and von Gersdorff, H. (2008). Synaptic vesicle endocytosis: fast and slow modes of membrane retrieval. Trends Neurosci. *31*, 559–568.

Sohal VS, Zhang F, Yizhar O, Deisseroth K. Parvalbumin neurons and gamma rhythms enhance cortical circuit performance (2009). Nature, *459*, 698–702.

Sommeijer, J.P., and Levelt, C.N. (2012). Synaptotagmin-2 is a reliable marker for parvalbumin positive inhibitory boutons in the mouse visual cortex. PLoS One *7*, e35323.

Südhof T.C. (2004). The synaptic vesicle cycle. Annu. Rev. Neurosci. *27*, 509–547.

Südhof T.C. (2012). The presynaptic active zone. Neuron *75*, 11–25.

Südhof T.C. (2013). Neurotransmitter release: The last millisecond in the life of a synaptic vesicle. Neuron *80,* 675–690.

Südhof T.C. and Rothman J.E. (2009). Membrane Fusion: Grappling with SNARE and SM Proteins. Science *323,* 474–477.

Südhof, T.C. (2002). Synaptotagmins: why so many? J. Biol. Chem. *277*, 7629−7632.

Sugita, S., Han, W., Butz, S., Liu, X., Fernández-Chacón, R., Lao, Y., and Südhof T.C. (2001). Synaptotagmin VII as a plasma membrane Ca^{2+} sensor in exocytosis. Neuron *30*, 459–473.

Sultan, F. and Bower, J.M. (1998) Quantitative Golgi study of the rat cerebellar molecular layer interneurons using principal component analysis. J. Comp. Neurol. *393*, 353–373

Sotelo, C. (2015). Molecular Layer Interneurons of the Cerebellum: Developmental and Morphological Aspects. Cerebellum *14*, 534–556.

Tricoire, L., Pelkey, K.A., Erkkila, B.E., Jeffries, B.W., Yuan, X., and McBain, C.J. (2011). A Blueprint for the Spatiotemporal Origins of Mouse Hippocampal Interneuron Diversity. J. Neurosci. *31*, 10948–10970.

Turecek, J., Jackman, S.L., and Regehr, W.G. (2016). Synaptic specializations support frequency-independent Purkinje cell output from the cerebellar cortex. Cell Rep. *17*, 3256–3268.

Turecek, J., Jackman, S.L., and Regehr, W.G. (2017). Synaptotagmin 7 confers frequency invariance onto specialized depressing synapses. Nature *551*, 503–506.

von Gersdorff, H. and Matthews, G. (1994). Inhibition of endocytosis by elevated internal calcium in a synaptic terminal. Nature *370*, 652–655

Vyleta, N.P., and Jonas, P. (2014). Loose coupling between Ca^{2+} channels and release sensors at a plastic hippocampal synapse. Science *343*, 665–670.

Wang X.J., and Buzsáki G. (1996). Gamma Oscillation by Synaptic Inhibition in a Hippocampal Interneuronal Network Model. J. Neurosci. *16*, 6402–6413.

Wen, H., Linhoff, M.W., McGinley, M.J., Li, G.L., Corson, G.M., Mandel, G., and Brehm, P. (2010). Distinct roles for two synaptotagmin isoforms in synchronous and asynchronous transmitter release at zebrafish neuromuscular junction. Proc. Natl. Acad. Sci. USA *107*, 13906–13911.

Westbrook, G. (2013). “Seizures and epilepsy,” in Principles of Neural Science, E. Kandel, J. H. Schwartz, T. M. Jessell, S. Siegelbaum, A. J. Hudspeth, Eds. (McGraw-Hill, New York), pp. 1116–1139.

Wu, L.G., and Borst, J.G.G. (1999). The reduced release probability of releasable vesicles during recovery from short-term synaptic depression. Neuron *23*, 821–832.

Wu, L.G., Hamid, E., Shin, W., and Chiang, H.C. (2014). Exocytosis and endocytosis: modes, functions, and coupling mechanisms. Annu. Rev. Physiol. *76*, 301–331.

Wu, L.G., Ryan, T.A., and Lagnado, L. (2007). Modes of Vesicle Retrieval at Ribbon Synapses, Calyx-Type Synapses, and Small Central Synapses. J. Neurosci. *27*, 11793–11802.

Xu, J., Mashimo, T., and Südhof, T.C. (2007). Synaptotagmin-1, -2, and -9: Ca^{2+} sensors for fast release that specify distinct presynaptic properties in subsets of neurons. Neuron *54*, 567–581.

Young, S.M. Jr., and Neher, E. (2009). Synaptotagmin has an essential function in synaptic vesicle positioning for synchronous release in addition to its role as a calcium sensor. Neuron *63*, 482–496.

Zhang, J.Z., Davletov, B.A., Südhof, T.C., and Anderson, R.G. (1994). Synaptotagmin I is a high affinity receptor for clathrin AP-2: implications for membrane recycling. Cell *78*, 751–760.

Zucker, R.S. and Regehr, W.G. (2002) Short-term synaptic plasticity. Annu. Rev. Physiol. *64*, 355–405